

Adaptive Prompt: Unlocking the Power of Visual Prompt Tuning

Minh Le^{◊,*} Anh Nguyen^{◊,*} Huy Nguyen[†] Chau Nguyen[◊] Nhat Ho[†]

The University of Texas at Austin[†]
VinAI Research[◊]

February 5, 2025

Abstract

Visual Prompt Tuning (VPT) has recently emerged as a powerful method for adapting pre-trained vision models to downstream tasks. By introducing learnable prompt tokens as task-specific instructions, VPT effectively guides pre-trained transformer models with minimal overhead. Despite its empirical success, a comprehensive theoretical understanding of VPT remains an active area of research. Building on recent insights into the connection between mixture of experts and prompt-based approaches, we identify a key limitation in VPT: *the restricted functional expressiveness in prompt formulation*. To address this limitation, we propose Visual Adaptive Prompt Tuning (VAPT), a new generation of prompts that redefines prompts as adaptive functions of the input. Our theoretical analysis shows that this simple yet intuitive approach achieves optimal sample efficiency. Empirical results on VTAB-1K and FGVC further demonstrate VAPT’s effectiveness, with performance gains of 7.34% and 1.04% over fully fine-tuning baselines, respectively. Notably, VAPT also surpasses VPT by a substantial margin while using fewer parameters. These results highlight both the effectiveness and efficiency of our method and pave the way for future research to explore the potential of adaptive prompts.

1 Introduction

Foundational vision models have demonstrated remarkable success across a wide range of computer vision tasks [8, 55, 32], primarily by leveraging large-scale pre-training for robust generalization. As a result, fine-tuning these models for specific downstream tasks has become a widely adopted paradigm [26]. However, fully fine-tuning large foundational models can be computationally prohibitive, leading to growing interest in parameter-efficient fine-tuning (PEFT) techniques [2, 76, 25], which update only a small subset of parameters. Among these methods, Visual Prompt Tuning (VPT) [28] has emerged as a simple yet powerful approach that appends learnable *prompt* tokens to the input, serving as task-specific instructions to guide the pre-trained transformer model. Despite VPT’s empirical effectiveness, its theoretical underpinnings remain an active area of research [54, 51, 67]. Recently, [35] uncovered a novel connection between attention mechanisms [64], prompt-based methods, and Mixture of Experts (MoE) models [27, 59], offering fresh insights into the design and optimization of prompt-based approaches. Specifically, they show that *each attention head* in a transformer can be equivalently viewed as *a composition of multiple MoE models* stacked together. This finding implies that, within a pre-trained transformer, each attention head encodes a collection of pre-trained MoE experts whose parameters are embedded in the model’s pre-trained weights.

* Equal contribution

Under this framework, prompt tuning corresponds to fine-tuning these pre-trained MoE models by introducing new, learnable *prompt experts*. These prompt experts collaborate with the pre-trained experts to enable effective task adaptation. This connection paves the way for deeper theoretical investigations and the development of advanced strategies for prompt-based learning [36, 34].

Building on this perspective, we identify a key limitation in the current formulation of VPT. Specifically, while pre-trained experts within attention heads are linear functions of the input features, the newly introduced prompt experts are constant functions that *do not vary with the input*. Since prompt experts must collaborate with the pre-trained ones to achieve optimal downstream performance, we hypothesize that this *restricted functional expressiveness* may inherently limit the efficacy of prompt tuning. This limitation naturally raises an important question about the potential of adaptive prompts, where prompts are modeled as adaptive functions of the input. Although increasing adaptivity may lead to concerns about parameter overhead, we propose a novel formulation that strikes a balance between flexibility and memory efficiency. We refer to this methodology as **Visual Adaptive Prompt Tuning (VAPT)**.

Our design comprises two main components: *token-wise projectors* and a shared *feature projector*, which leverages global information from input features to generate adaptive prompt tokens. Theoretical analysis shows that our formulation achieves *optimal sample efficiency* for prompt estimation. Empirical results further substantiate this claim. For instance, on the Stanford Dogs dataset [31], using only **1%** of the data, while VPT achieves a modest accuracy of **3.6%**, VAPT demonstrates a remarkable improvement with an accuracy of **60.1%**. Moreover, extensive experiments across multiple benchmarks consistently show that VAPT outperforms VPT while *utilizing fewer parameters*, highlighting the effectiveness of its simple yet elegant design. Notably, VAPT also achieves *state-of-the-art performance* compared to other PEFT methods across different pre-trained objectives [4, 20], indicating robustness both theoretically and empirically.

Contribution. The main contributions of this work are summarized as follows: **1.** By leveraging the connection between mixture of experts and prompt-based techniques, we identify a key limitation in the formulation of VPT: the restricted expressiveness of prompts, which remain invariant regardless of the input. **2.** To address this limitation and explore the potential of adaptive prompts, we propose **VAPT**, a novel formulation that balances efficiency and flexibility. **3.** Through theoretical analysis, we demonstrate that our formulation achieves optimal sample efficiency for prompt estimation, establishing a solid foundation for its practical effectiveness. **4.** Extensive experiments demonstrate that VAPT consistently outperforms VPT with fewer parameters, and achieves state-of-the-art results compared to other commonly used PEFT methods.

Organization. The paper proceeds as follows. In Section 2 provides background on visual prompt tuning and mixture of experts. In Section 3, we discuss the connection between VPT and MoE, highlighting the limited expressiveness of the current VPT formulation. Section 4 describes in detail the design of our method to achieve superior performance with fewer parameters. We present our theoretical analysis in Section 5, followed by our empirical results in Section 6. Finally, we conclude the paper and suggest potential directions for future research in Section 7.

Notation. For any $n \in \mathbb{N}$, let $[n] = \{1, 2, \dots, n\}$. For a set S , $|S|$ denotes its cardinality. Given a vector $u = (u_1, u_2, \dots, u_d) \in \mathbb{R}^d$ and $\alpha = (\alpha_1, \alpha_2, \dots, \alpha_d) \in \mathbb{N}^d$, we set $u^\alpha = u_1^{\alpha_1} u_2^{\alpha_2} \dots u_d^{\alpha_d}$, $|u| = u_1 + u_2 + \dots + u_d$ and $\alpha! = \alpha_1! \alpha_2! \dots \alpha_d!$. Moreover, $\|u\|$ denotes the Euclidean norm of u . For two positive sequences $(a_n)_{n \geq 1}$ and $(b_n)_{n \geq 1}$, we write $a_n = \mathcal{O}(b_n)$ or $a_n \lesssim b_n$ if $a_n \leq Cb_n$ for all $n \in \mathbb{N}$ for some constant $C > 0$. The notation $a_n = \mathcal{O}_P(b_n)$ indicates a_n/b_n is stochastically bounded.

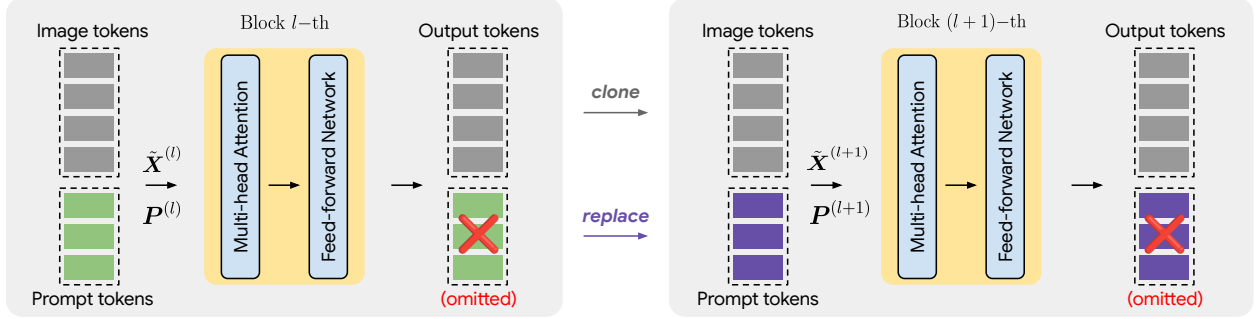


Figure 1: Illustration of the forward propagation of VPT across ViT blocks. Red crosses denote output tokens that are discarded. In each block, the prompt tokens $\mathbf{P}^{(l)}$ are appended to the input $\tilde{\mathbf{X}}^{(l)}$. The output tokens at the prompt positions are then replaced by the prompt tokens $\mathbf{P}^{(l+1)}$ of the next block before being propagated forward.

2 Background

In this section, we first discuss Visual Prompt Tuning in Section 2.1 and then Mixture of Experts model in Section 2.2. Additional related work is provided in Appendix C.

2.1 Visual Prompt Tuning

Vision Transformer (ViT) [8] has been shown to be highly effective as a backbone architecture for various visual recognition tasks. Typically, a ViT consists of L transformer blocks, each containing a *multi-head self-attention* (MSA) layer followed by a *feed-forward network* (FFN). For clarity, we focus on a single transformer block. Let $\tilde{\mathbf{X}}^{(l)} = [\mathbf{x}_1^{(l)}, \dots, \mathbf{x}_N^{(l)}]^\top \in \mathbb{R}^{N \times d}$ be the sequence of input tokens in the l -th ViT block, where $\mathbf{x}_i^{(l)} \in \mathbb{R}^d$ denotes the i -th token, N is the sequence length, and d is the embedding dimension. The MSA layer processes $\mathbf{X}^Q = \mathbf{X}^K = \mathbf{X}^V = \tilde{\mathbf{X}}^{(l)} \in \mathbb{R}^{N \times d}$ as query, key, and value, respectively. Its output can then be written as:

$$\begin{aligned} \text{MSA}(\tilde{\mathbf{X}}^{(l)}) &= \text{Concat}(\mathbf{h}_1, \dots, \mathbf{h}_M) W^O \in \mathbb{R}^{N \times d}, \\ \mathbf{h}_m &= \text{Attention}(\mathbf{X}^Q W_m^Q, \mathbf{X}^K W_m^K, \mathbf{X}^V W_m^V) \in \mathbb{R}^{N \times d_v}, \end{aligned} \quad (1)$$

for $m \in [M]$, where M is the number of attention heads, $W^O \in \mathbb{R}^{Md_v \times d}$, and $W_m^Q \in \mathbb{R}^{d \times d_k}$, $W_m^K \in \mathbb{R}^{d \times d_k}$, $W_m^V \in \mathbb{R}^{d \times d_v}$ are projection matrices with $d_k = d_v = \frac{d}{M}$.

Recently, Visual Prompt Tuning (VPT) [28] has emerged as a promising method for fine-tuning pre-trained vision models. VPT introduces *prompt* parameters, $\mathbf{P}^{(l)} = [\mathbf{p}_1^{(l)}, \dots, \mathbf{p}_{N_p}^{(l)}]^\top \in \mathbb{R}^{N_p \times d}$, which are appended to the input token sequence of ViT block. Here, N_p denotes the prompt length.

The inclusion of these prompts modifies the MSA layer’s output, which can be expressed as follows:

$$\begin{aligned}
\text{MSA}(\tilde{\mathbf{X}}^{(l)}, \mathbf{P}^{(l)}) &= \text{Concat}(\tilde{\mathbf{h}}_1, \dots, \tilde{\mathbf{h}}_M) W^O, \\
\tilde{\mathbf{h}}_m &= \text{Attention} \left(\left[\begin{array}{c} \mathbf{X}^Q \\ \mathbf{P}^{(l)} \end{array} \right] W_m^Q, \left[\begin{array}{c} \mathbf{X}^K \\ \mathbf{P}^{(l)} \end{array} \right] W_m^K, \left[\begin{array}{c} \mathbf{X}^V \\ \mathbf{P}^{(l)} \end{array} \right] W_m^V \right) \\
&= \left[\tilde{\mathbf{h}}_{m,1}, \dots, \tilde{\mathbf{h}}_{m,N+N_p} \right]^\top \in \mathbb{R}^{(N+N_p) \times d_v},
\end{aligned} \tag{2}$$

with $m \in [M]$. During training, only the prompt parameters $\mathbf{P}^{(l)}$ and the classification head are optimized, while the pre-trained ViT parameters, including W_m^Q , W_m^K , W_m^V and W_O , remain frozen. After the MSA layer, each output token is *independently processed* by the pre-trained FFN, with no interaction between tokens. In VPT, the output tokens of each block, where prompts act as queries, are replaced with new trainable prompts $\mathbf{P}^{(l+1)}$ for the subsequent block, as illustrated in Figure 1. Consequently, in equation (2), there is no need to compute $\tilde{\mathbf{h}}_{m,N+1}, \dots, \tilde{\mathbf{h}}_{m,N+N_p}$. Omitting these computations does not affect the output tokens of the current block, and if no new prompts are introduced in the next block, these output tokens can simply be discarded.

2.2 Mixture of Experts

Mixture of Experts (MoE) is a class of statistical machine learning frameworks that combines multiple models, known as experts, to construct more expressive and accurate predictions [27, 30]. An MoE model typically consists of N' *expert functions* $f_i : \mathbb{R}^d \rightarrow \mathbb{R}^{d_v}$ for $i \in [N']$, along with a *gating function* $G : \mathbb{R}^d \rightarrow \mathbb{R}^{N'}$ which assigns weights to the experts based on learned *score functions* $s_i : \mathbb{R}^d \rightarrow \mathbb{R}$. For a given input $\mathbf{h} \in \mathbb{R}^d$, the MoE model generates its output as:

$$\hat{\mathbf{y}} = \sum_{j=1}^{N'} G(\mathbf{h})_j \cdot f_j(\mathbf{h}) = \sum_{j=1}^{N'} \frac{\exp(s_j(\mathbf{h}))}{\sum_{\ell=1}^{N'} \exp(s_\ell(\mathbf{h}))} \cdot f_j(\mathbf{h}),$$

where $G(\mathbf{h}) = \text{softmax}(s_1(\mathbf{h}), \dots, s_{N'}(\mathbf{h}))$. Recent studies have revealed a novel connection between the attention mechanism, prompt-based methods, and MoE frameworks [35, 36]. This connection presents promising opportunities for investigating prompt-based techniques through the lens of mixture of experts.

3 Motivation

Mixture of Experts meets Visual Prompt Tuning. We begin by discussing the connection between VPT and MoE. We adopt the same notation as in Section 2.1. From equation (2), let $\mathbf{X}^{(l)} = \left[\mathbf{x}_1^{(l)\top}, \dots, \mathbf{x}_N^{(l)\top} \right]^\top \in \mathbb{R}^{Nd}$ represent the *concatenation* of all N input image tokens for the MSA layer. For notational simplicity, we omit the superscript (l) in the derivations below. Recent studies [35] have demonstrated that each output vector $\tilde{\mathbf{h}}_{m,i}$ for $i \in [N]$ within the m -th attention head can be *equivalently* expressed as the output of an MoE model, where \mathbf{X} serves as the input. Specifically, we define a set of experts as follows:

$$f_j(\mathbf{X}) = W_m^{V\top} E_j \mathbf{X} = W_m^{V\top} \mathbf{x}_j, \tag{3}$$

$$f_{N+j'}(\mathbf{X}) = W_m^{V\top} \mathbf{p}_{j'}, \tag{4}$$

where $j \in [N]$ and $j' \in [N_p]$. The corresponding score functions are defined as:

$$s_{i,j}(\mathbf{X}) = \frac{\mathbf{X}^\top E_i^\top W_m^Q W_m^K E_j \mathbf{X}}{\sqrt{d_v}} = \frac{\mathbf{x}_i^\top W_m^Q W_m^K \mathbf{x}_j}{\sqrt{d_v}}, \quad (5)$$

$$s_{i,N+j'}(\mathbf{X}) = \frac{\mathbf{X}^\top E_i^\top W_m^Q W_m^K \mathbf{p}_{j'}}{\sqrt{d_v}} = \frac{\mathbf{x}_i^\top W_m^Q W_m^K \mathbf{p}_{j'}}{\sqrt{d_v}}, \quad (6)$$

for $i \in [N]$. Here, $E_j \in \mathbb{R}^{d \times Nd}$ is a standard basis selector such that $E_j \mathbf{X} = \mathbf{x}_j$. Finally, the output of the m -th attention head for the i -th token can be expressed as follows:

$$\tilde{\mathbf{h}}_{m,i} = \sum_{j=1}^N \frac{\exp(s_{i,j}(\mathbf{X}))}{\sum_{k=1}^{N+N_p} \exp(s_{i,k}(\mathbf{X}))} f_j(\mathbf{X}) + \sum_{j'=1}^{N_p} \frac{\exp(s_{i,N+j'}(\mathbf{X}))}{\sum_{k=1}^{N+N_p} \exp(s_{i,k}(\mathbf{X}))} f_{N+j'}(\mathbf{X}). \quad (7)$$

From these formulations, we can see that *each attention head* in ViT implicitly encodes *multiple MoE models* $\tilde{\mathbf{h}}_{m,i}$ for $i \in [N]$. Unlike conventional MoE layers [59], where each expert and its score function operate on a single token embedding \mathbf{x}_i , the expert networks and score functions here *process the entire input sequence \mathbf{X}* . Furthermore, the experts f_1, \dots, f_N and their associated score functions are pre-trained alongside the ViT, as their parameters are already embedded within the pre-trained model (see equation (3) and equation (5)), thereby serving as *pre-trained experts*. Meanwhile, the new *prompt experts* $f_{N+1}, \dots, f_{N+N_p}$, whose learnable parameters are contained in prompts (see equation (4) and equation (6)), are introduced to efficiently adapt the model for downstream tasks. In other words, one can view prompt tuning as an efficient method of fine-tuning these implicitly encoded MoE models by *adding new prompt experts*. These newly introduced prompt experts effectively act as downstream-task experts, enabling the model to specialize in new tasks without retraining the entire network.

Prompts remain invariant to the input. From equation (4), it follows that prompt experts $f_{N+1}, \dots, f_{N+N_p}$, although formally *functions of \mathbf{X}* , are represented by fixed prompt vectors that *remain constant regardless of the input*. In contrast, pre-trained experts f_1, \dots, f_N are linear functions of \mathbf{X} (see equation (3)), making them comparatively more expressive. We hypothesize that this *limited flexibility* may diminish the effectiveness of prompt tuning as a fine-tuning strategy. Supporting this view, prior work [54] demonstrates that prompt tuning can only add a bias term to the output of an attention block, thereby restricting the model’s representational capacity. This observation naturally leads to the following question: *Can the performance of visual prompt tuning be improved by making prompts more flexible and adaptive to the input?* To address this, we propose a novel prompt formulation to enhance their adaptability under varying inputs in Section 4.

The challenge of staying efficient. Despite the limitations noted above, one of the main advantages of the current prompt design in VPT is its simplicity. As indicated by equation (4), each prompt expert requires only d parameters, making it highly *parameter-efficient*. One might consider a naive linear design for a prompt expert $f_{N+j'} : \mathbb{R}^{Nd} \rightarrow \mathbb{R}^{d_v}$, where $f_{N+j'}(\mathbf{X}) = W_{j'}^\top \mathbf{X}$. However, this approach would introduce up to $Nd \times d_v$ parameters, which is Nd_v times larger than the bias-expert formulation and would significantly increase computational costs. Consequently, this highlights the challenge of balancing input adaptability with cost-effectiveness, thereby ensuring that the benefits of a parameter-efficient fine-tuning technique are preserved.

4 VAPT: Visual Adaptive Prompt Tuning

In this section, to explore the potential of adaptive prompts, we introduce our proposed approach, VAPT, which comprises two main modules: token-wise projectors and a feature projector. Detailed descriptions of these modules are provided in Sections 4.1 and 4.2, respectively. An overview of VAPT is shown in Figure 2.

4.1 Aggregating Global Information

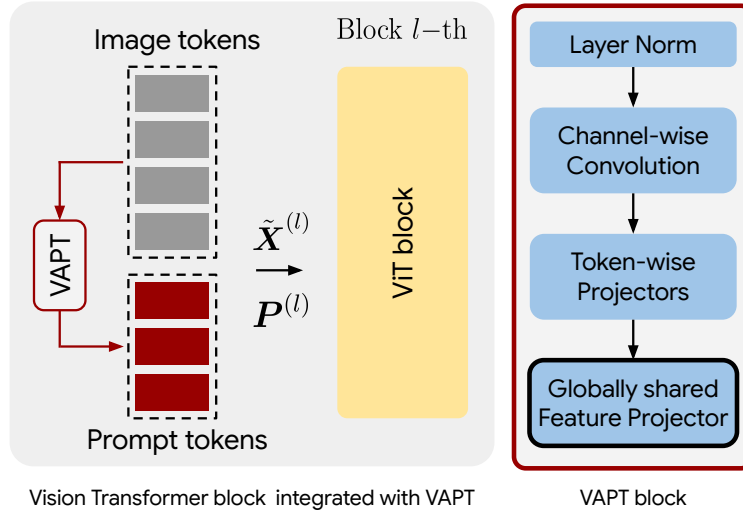


Figure 2: Overview of VAPT. Unlike VPT, where prompt tokens remain constant regardless of the input, our method generates prompt tokens dynamically based on the input via VAPT block.

To rigorously design the formulation of prompts and prompt experts, we first revisit the existing formulation of the input and the pre-trained experts. Specifically, the input $\mathbf{X} = [\mathbf{x}_1^\top, \dots, \mathbf{x}_N^\top]^\top$ is the concatenation of all N feature tokens. These tokens can be reshaped or reordered to form $\mathbf{X}_{\text{img}} \in \mathbb{R}^{H \times W \times d}$, where H and W denote the height and width of the image, respectively, and $N = H \times W$. We refer to \mathbf{X}_{img} as the input *feature map*. Since each token $x_j \in \mathbb{R}^d$ represents a small patch of this feature map, it follows from equation (3) that each pre-trained expert f_j processes the input by *examining each patch independently*, thereby capturing only *local information* within the feature map.

Token-wise Projectors. Because prompt experts will collaborate with these pre-trained experts to facilitate adaptation to downstream tasks, it is naturally desirable for them to specialize in aspects that are *distinct* or *orthogonal* to those captured by pre-trained experts. To accomplish this, we design prompts that extract *global information* from the feature map using *token-wise projectors*, defined as follows:

$$G_{j'}(\mathbf{X}) = \left(\sum_{k=1}^N \alpha_{j',k} E_k \right) \mathbf{X} = \sum_{k=1}^N \alpha_{j',k} \mathbf{x}_k \in \mathbb{R}^d, \quad (8)$$

for $j' \in [N_p]$, where $\alpha_{j',k}$ are learnable weights with $k \in [N]$. These projectors aggregate tokens across spatial locations, enabling communication and global information exchange throughout the feature map.

Channel-wise Convolution. While simple weighted averaging of all feature tokens can be computationally efficient, it may fail to capture important *spatial relationships*. For instance, the adjacency between \mathbf{x}_1 and \mathbf{x}_2 , which correspond to neighboring patches in the feature map, may be overlooked by token-wise projectors. To address this, we introduce a *channel-wise convolution* layer, applied to the input before token-wise projectors. Specifically, let $F = [w_{i,j}]_{i,j=1}^K$ be a kernel of size K . In contrast to a standard convolution kernel, F reuses the *same weights across the channel dimension*, reducing the number of parameters by up to a factor of d (see Figure 3). We show that this channel-wise convolution not only saves parameters but also improves performance in Appendix E.4. Formally, the channel-wise convolution is applied to \mathbf{X}_{img} as follows:

$$\mathbf{X}_{\text{conv}} = F * \mathbf{X}_{\text{img}} \in \mathbb{R}^{H' \times W' \times d}, \quad (9)$$

where $*$ denotes the convolution operation, and $H' = H - K + 1$ and $W' = W - K + 1$ are the output height and width, respectively. By convolving neighboring patches, the channel-wise convolution encodes spatial relationships into the output feature map \mathbf{X}_{conv} . We employ a single channel-wise convolution layer within each ViT block. The resulting feature map \mathbf{X}_{conv} is then flattened to $[\mathbf{x}_1^{\text{conv}}, \dots, \mathbf{x}_{H' \cdot W'}^{\text{conv}}]^{\top} \in \mathbb{R}^{H' \cdot W' \times d}$ before being processed by token-wise projectors. The final aggregated features can be expressed as:

$$G_{j'}(\mathbf{X}_{\text{conv}}) = \sum_{k=1}^{H' \cdot W'} \alpha_{j',k} \mathbf{x}_k^{\text{conv}} = W_{j'} \mathbf{X} \in \mathbb{R}^d \quad (10)$$

for $j' \in [N_p]$. Because the convolution operation can be interpreted as a linear function, these aggregated features can also be expressed as a linear function of \mathbf{X} via $W_{j'} \in \mathbb{R}^{d \times N^d}$. We leverage this aggregated information to construct our adaptive prompts in the next section.

4.2 Adaptive Prompt

Each prompt aggregates its corresponding global feature token through a token-wise projector. To generate the final adaptive prompts, we introduce a *feature projector* implemented as a small MLP $g : \mathbb{R}^d \rightarrow \mathbb{R}^d$, defined as follows:

$$g(\mathbf{x}) = W^{(2)} \sigma(W^{(1)} \mathbf{x}), \quad (11)$$

where $W^{(1)} \in \mathbb{R}^{r \times d}$, $W^{(2)} \in \mathbb{R}^{d \times r}$, $r \ll d$, and $\sigma(\cdot)$ is a non-linear activation function (ReLU in this work). This feature projector is applied to the aggregated features to produce the final adaptive prompt tokens for each input. Formally, the adaptive prompts at each block are given by:

$$\mathbf{P}_{j'}(\mathbf{X}) = g(G_{j'}(\mathbf{X}_{\text{conv}})) = W^{(2)} \sigma(W^{(1)} W_{j'} \mathbf{X}) = W^{(2)} \sigma(W_{j'}^{(1)} \mathbf{X}) \in \mathbb{R}^d, \quad (12)$$

for $j' \in [N_p]$, where $W_{j'}^{(1)} = W^{(1)} W_{j'}$. Our proposed adaptive prompts refine the prompt experts and their associated score functions within the MSA layers as follows:

$$f_{N+j'}(\mathbf{X}) = W_m^{V^{\top}} \mathbf{P}_{j'}(\mathbf{X}), \quad (13)$$

$$s_{i,N+j'}(\mathbf{X}) = \frac{\mathbf{X}^{\top} E_i^{\top} W_m^Q W_m^{K^{\top}} \mathbf{P}_{j'}(\mathbf{X})}{\sqrt{d_v}}, \quad (14)$$

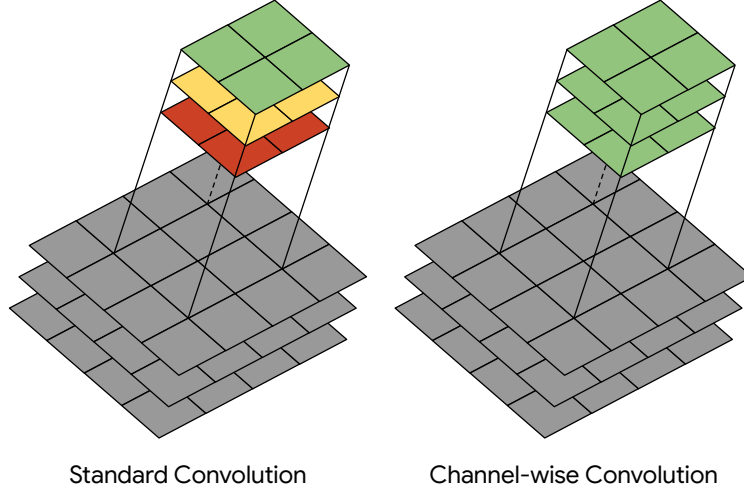


Figure 3: Illustration of channel-wise convolution. In contrast to standard convolution, the same kernel weights are shared across all channels.

where $i \in [N]$ and $j' \in [N_p]$. From equation (13), we can see that prompt experts are now adaptive to the input \mathbf{X} , thereby improving their expressiveness and flexibility. The statistical advantages of our formulation are further analyzed in Section 5.

Efficiency considerations. Following VPT, we insert adaptive prompts into each ViT block. Although the feature projector itself is a lightweight MLP, integrating it separately into every block can still introduce substantial memory overhead. To alleviate this, we employ a single, *shared* feature projector $g(\cdot)$ that is reused across all prompts and ViT blocks. This design substantially reduces overall computational cost while preserving the advantages of the adaptive prompting. Furthermore, to enhance the training of the feature projector, we incorporate a separate LayerNorm [39] before the token-wise projectors in each block.

In terms of parameter complexity, VPT introduces approximately $L \times N_p \times d$ parameters across L ViT blocks. In comparison, the learnable parameters of our proposed method include token-wise projectors, channel-wise convolution layer at each block, and shared feature projector. The total parameter count can be expressed as:

$$\underbrace{L \times N_p \times H' \times W'}_{\text{token-wise projectors}} + \underbrace{L \times K^2}_{\text{convolution}} + \underbrace{2 \times r \times d}_{\text{feature projector}} , \quad (15)$$

where $H' \times W' < N$, and both K and r are small constants. Notably, in most ViT configurations, the number of tokens N is much smaller than the embedding dimension d . (e.g., ViT-B/16 with $N = 196$ and $d = 768$). As a result, our approach can achieve greater parameter efficiency than VPT, as shown in Table 1 and Table 2. Moreover, we show that VAPT only introduces a marginal increase in computational cost, up to 0.6% relative to VPT (see Appendix E.5).

5 Statistical Advantages of VAPT

In this section, we present the theoretical benefits of visual adaptive prompt tuning via its connection to a mixture of experts, as formulated in equation (7). This perspective provides a robust framework for analyzing the convergence behavior of prompt estimation within MoE models [35, 36]. As shown in Section 3, the MoE models $\tilde{\mathbf{h}}_{m,1}, \dots, \tilde{\mathbf{h}}_{m,N}$ in each attention head share a common structure of experts and score functions. Furthermore, as noted in Section 2.1, omitting $\tilde{\mathbf{h}}_{m,N+1}, \dots, \tilde{\mathbf{h}}_{m,N+N_p}$ does not affect the output of the current ViT block. Thus, to simplify our analysis while maintaining rigor, we focus on the first head, namely, $m = 1$, and specifically the first row of the attention matrix in this head, namely, $i = 1$ in equation (7). Under this simplified setting, we consider a regression framework for MoE models as follows.

Problem setup. Assume that the i.i.d. samples of size n : $(\mathbf{X}_1, Y_1), (\mathbf{X}_2, Y_2), \dots, (\mathbf{X}_n, Y_n) \in \mathbb{R}^d \times \mathbb{R}^{d'}$ are generated from the following regression model:

$$Y_i = f_{G_*}(\mathbf{X}_i) + \varepsilon_i, \quad i = 1, 2, \dots, n, \quad (16)$$

where $\varepsilon_1, \varepsilon_2, \dots, \varepsilon_n$ are independent noise variables following Gaussian distributions such that $\mathbb{E}[\varepsilon_i | \mathbf{X}_i] = 0$ and $\text{Var}(\varepsilon_i | \mathbf{X}_i) = \nu^2 I_{d'}$ for all $i \in [n]$. Furthermore, $\mathbf{X}_1, \mathbf{X}_2, \dots, \mathbf{X}_n$ are assumed to be i.i.d. samples from a distribution μ . The ground-truth regression function $f_{G_*}(\cdot)$ is an MoE model of the form

$$\begin{aligned} f_{G_*}(\mathbf{X}) := & \sum_{j=1}^N \frac{\exp(\mathbf{X}^\top A_j^0 \mathbf{X} + a_j^0)}{D_{f,G_*}(\mathbf{X})} \cdot h(\mathbf{X}, \eta_j^0) \\ & + \sum_{j'=1}^L \frac{\exp((BW_{*,2}\sigma(W_{*,1j'}\mathbf{X}))^\top \mathbf{X} + b_{*,j'})}{D_f(\mathbf{X})} \cdot CW_{*,2}\sigma(W_{*,1j'}\mathbf{X}), \end{aligned} \quad (17)$$

where $D_{f,G_*}(\mathbf{X}) = \sum_{k=1}^N \exp(\mathbf{X}^\top A_k^0 \mathbf{X} + a_k^0) + \sum_{j'=1}^L \exp((BW_{*,2}\sigma(W_{*,1j'}\mathbf{X}))^\top \mathbf{X} + b_{*,j'})$. Here, $G_* = \sum_{j'=1}^L \exp(b_{*,j'})\delta_{(W_{*,1j'}, W_{*,2})}$ denotes a true *mixing measure*, which is a weighted sum of Dirac measures δ , associated with unknown parameters $(b_{*,j'}, W_{*,1j'}, W_{*,2})_{j'=1}^L$ in the parameter space $\Theta \subset \mathbb{R} \times \mathbb{R}^{r \times d} \times \mathbb{R}^{d \times r}$. The matrix A_j^0 , the expert parameter η_j^0 , and the bias parameter a_j^0 are known for $j \in [N]$. Finally, the matrices $B \in \mathbb{R}^{d \times d}$ and $C \in \mathbb{R}^{d' \times d}$ are given, which play the role of pre-trained projection matrices in the context of prompt tuning.

Least-square estimator: To estimate those unknown prompt parameters or, equivalently, the ground-truth mixing measure G_* , we use the least square method [62]. In particular, we consider the estimator defined as follows:

$$\hat{G}_n := \arg \min_{G \in \mathcal{G}_{L'}(\Theta)} \sum_{i=1}^n \|Y_i - f_G(\mathbf{X}_i)\|^2, \quad (18)$$

where $\mathcal{G}_{L'}(\Theta) := \{G = \sum_{i=1}^{\ell} \exp(b_i)\delta_{(W_{1,i}, W_2)} : \ell \in [L'], (b_i, W_{1,i}, W_2) \in \Theta\}$ is the set of all mixing measures with at most L' atoms. In practice, the true number of experts L is generally unknown. Therefore, we assume that the number of fitted experts L' is sufficiently large, *i.e.*, $L' > L$. To analyze the convergence rate of prompt estimation, it is essential to define a suitable loss function on the prompt parameters. In this work, we propose a loss function derived from the concept of Voronoi cells [43], which we refer to as the *Voronoi loss function*.

Voronoi loss. Given a mixing measure $G \in \mathcal{G}_{L'}(\Theta)$, we consider a Voronoi cell set $\{\mathcal{V}_j \equiv \mathcal{V}_j(G), j \in [L]\}$ generated by the atoms of G_* , where

$$\mathcal{V}_j := \{i \in [L'] : \|Z_i - Z_{*,j}\| \leq \|Z_i - Z_{*,\ell}\|, \forall \ell \neq j\},$$

where we define $Z_i := (W_{1,i}, W_2)$. The Voronoi loss tailored to the setting in equation (17) is defined as:

$$\begin{aligned} \mathcal{D}_1(G, G_*) := & \sum_{j'=1}^L \left| \sum_{i \in \mathcal{V}_{j'}} \exp(b_i) - \exp(b_{*,j'}) \right| + \sum_{j' \in [L]: |\mathcal{V}_{j'}|=1} \sum_{i \in \mathcal{V}_{j'}} \exp(b_i) (\|\Delta W_{1ij'}\| + \|\Delta W_2\|) \\ & + \sum_{j' \in [L]: |\mathcal{V}_{j'}| > 1} \sum_{i \in \mathcal{V}_{j'}} \exp(b_i) (\|\Delta W_{1ij'}\|^2 + \|\Delta W_2\|^2), \end{aligned}$$

where we denote $\Delta W_{1ij'} := W_{1i} - W_{*,1j'}$ for any i, j' , and $\Delta W_2 := W_2 - W_{*,2}$.

Equipped with this loss function, we wrap up the setting in equation (17) by providing the convergence rate of prompt estimation in Theorem 1. For that purpose, it is necessary to impose some essential assumptions on the activation function σ . However, due to the space limit, we defer those assumptions to the proof of Theorem 1 in Appendix A.1.

Theorem 1. *Given the least square estimator \hat{G}_n defined in equation (18) and assume that the activation function σ satisfies the assumptions (A.1)-(A.3) specified in Appendix A.1, we obtain that*

$$\mathcal{D}_1(\hat{G}_n, G_*) = \mathcal{O}_P([\log(n)/n]^{\frac{1}{2}}).$$

Implication to prompt estimation. Given the formulation of the Voronoi loss function \mathcal{D}_1 , Theorem 1 indicates that the rates for estimating the true parameters $(W_{*,1j}, W_{*,2})$ for indices j such that $|\mathcal{V}_j| = 1$ are of the parametric order $\mathcal{O}_P([\log(n)/n]^{\frac{1}{2}})$. Due to the Lipschitz property of the activation function σ , it directly leads to the rate $\mathcal{O}_P([\log(n)/n]^{\frac{1}{2}})$ for estimating the true prompt $\mathbf{P}_j^*(\mathbf{X}) = W_{*,2}\sigma(W_{*,1j}\mathbf{X})$. On the other hand, for the true parameters $(W_{*,1j}, W_{*,2})$ such that $|\mathcal{V}_j| > 1$, their estimation rates are of the order $\mathcal{O}_P([\log(n)/n]^{1/4})$, which yields the $\mathcal{O}_P([\log(n)/n]^{1/4})$ for estimating the true prompt $\mathbf{P}_j^*(\mathbf{X}) = W_{*,2}\sigma(W_{*,1j}\mathbf{X})$. Finally, all of these rates are optimal, up to the logarithmic factor, which demonstrates the statistical benefits of visual adaptive prompt tuning for the non-linear setting of the activation function σ .

Linear activation setting. For the completeness of the result, we also show that the visual adaptive prompt tuning achieves optimal sample efficiency when the activation function $\sigma(\cdot)$ is linear identity in Appendix B.

6 Experiment

In this section, we compare VAPT with VPT and other widely used PEFT methods. We also examine the robustness of VAPT under different pre-training objectives and present our findings on sample efficiency. For additional results, including ablation studies, computational cost, and interpretative visualizations, please refer to Appendix E.

Table 1: **Overall Comparison for ViT-B/16 Supervised Pre-trained on ImageNet-21K.** Following [28], we report the average accuracy over three runs on FGVC and VTAB-1K, along with the “Number of Wins” $[\cdot]$ compared to full fine-tuning and the “Number of Wins over VPT” $\{\cdot\}$. “Tuned/Total” denotes the average percentage of parameters tuned across 24 tasks, “Scope” specifies the tuning scope, and “Additional parameters” indicates if any parameters beyond the pre-trained backbone and linear head are introduced. **Bold** highlights the best results. Per-task results are in Appendix E.1.

ViT-B/16 [8] (85.8M)	Tuned/ Total (%)	Scope		Extra params	FGVC [5]	VTAB-1K [75] [19]			Mean Total
		Input	Backbone			Natural [7]	Specialized [4]	Structured [8]	
Full [26]	100.00		✓		88.54	75.88	83.36	47.64	65.57
Linear [26]	0.08				79.32 [0]	68.93 [1]	77.16 [1]	26.84 [0]	52.94
Partial-1 [74]	8.34				82.63 [0]	69.44 [2]	78.53 [0]	34.17 [0]	56.52
MLP-3 [3]	1.44			✓	79.80 [0]	67.80 [2]	72.83 [0]	30.62 [0]	53.21
Sidetune [76]	10.08		✓	✓	78.35 [0]	58.21 [0]	68.12 [0]	23.41 [0]	45.65
Bias [56]	0.80		✓		88.41 [3]	73.30 [3]	78.25 [0]	44.09 [2]	62.05
Adapter [2]	1.02		✓	✓	85.46 [1]	70.67 [4]	77.80 [0]	33.09 [0]	62.41
LoRA [25]	0.73		✓	✓	89.46 [3]	78.26 [5]	83.78 [2]	56.20 [7]	72.25
VPT-Shallow [28]	0.16	✓		✓	84.62 [1]	76.81 [4]	79.66 [0]	46.98 [4]	64.85
VPT-Deep [28]	0.73	✓		✓	89.11 [4]	78.48 [6]	82.43 [2]	54.98 [8]	69.43
E2VPT [17]	0.39	✓	✓	✓	89.22 [4]	80.01 [6]	84.43 [3]	57.39 [8]	71.42
VAPT (Ours)	0.36	✓		✓	89.58 [4] {4}	81.43 [6] {7}	85.13 [4] {4}	59.34 [8] {8}	72.91

6.1 Experimental Setup

Datasets. We evaluate our approach on two benchmarks: FGVC and VTAB-1K [75]. FGVC includes five fine-grained classification datasets: CUB [66], Oxford Flowers [50], Stanford Cars [14], Stanford Dogs [31], and NABirds [63], which challenge models to distinguish visually similar classes. VTAB-1K comprises 19 datasets, each with 1,000 training examples, grouped into three categories: *Natural* (images captured by standard cameras), *Specialized* (images collected via specialized equipment), and *Structured* (tasks requiring structural understanding, such as 3D depth prediction).

Baselines. To ensure consistency with prior work [28, 17], we compare VAPT against commonly used PEFT methods. Our experiments include standard Vision Transformer (ViT) [8] architectures with supervised pre-trained on ImageNet-21K [7]. Additionally, we evaluate the performance of VAPT on two self-supervised learning objectives: MAE [20] and MoCo v3 [4].

Training. We perform a grid search on `val` set of each task to determine the optimal learning rate, weight decay, kernel size K , and projector dimension r . We schedule the learning rate with cosine decay and train for 100 epochs. Following [28], we use batch sizes of 64 and 128. Additional details can be found in Appendix D.

6.2 Empirical Results

Overall comparison. In Table 1, we present the average accuracy on VTAB-1K and FGVC, comparing VAPT with full fine-tuning and other widely used PEFT methods. Specifically, Full [26] denotes full fine-tuning, which updates both backbone and classification head, whereas Linear [26], Partial-1 [74] (top layer), and MLP-3 [3] (3 MLP layers) only update partial parameters. Sidetune [76], Bias [56], Adapter [2], and LoRA [25] introduce trainable modules for adaptation. VPT [28] and E2VPT [17] are concurrent visual prompt tuning approaches (see Appendix C). We observe that VAPT outperforms full fine-tuning on across **22 out of 24** tasks. Specifically, it achieves a notable

Table 2: **Comparison of Different Pre-training Objectives.** We consider MAE [20] and MoCo v3 [4] using ViT-B/16 as the backbone. We report the test accuracy on VTAB-1K, as well as the “Number of Wins” $[\cdot]$ relative to full fine-tuning and the “Number of Wins over VPT” $\{\cdot\}$. “Tuned/Total” denotes the average percentage of parameters tuned. **Bold** indicates the best results, excluding full fine-tuning. Per-task results are provided in Appendix E.2.

Pre-trained objectives		MAE [20]						MoCo v3 [4]					
Methods	Params & Data	VTAB-1K [75] [19]			Tuned/Total (%)			VTAB-1K [75] [19]			Tuned/Total (%)		
		Natural [7]	Specialized [4]	Structured [8]	Natural [7]	Specialized [4]	Structured [8]	Natural [7]	Specialized [4]	Structured [8]	Natural [7]	Specialized [4]	Structured [8]
Full [26]	100.00	59.31	79.68	53.82	100.00			71.95	84.72	51.98			
Linear [26]	0.04	18.87 [0]	53.72 [0]	23.70 [0]	0.04	67.46 [4]	81.08 [0]	30.33 [0]					
Partial-1 [74]	8.30	58.44 [5]	78.28 [1]	47.64 [1]	8.30	72.31 [5]	84.58 [2]	47.89 [1]					
Bias [56]	0.16	54.55 [1]	75.68 [1]	47.70 [0]	0.16	72.89 [3]	81.14 [0]	53.43 [4]					
Adapter [2]	0.87	54.90 [3]	75.19 [1]	38.98 [0]	1.12	74.19 [4]	82.66 [1]	47.69 [2]					
VPT-Shallow [28]	0.05	39.96 [1]	69.65 [0]	27.50 [0]	0.06	67.34 [3]	82.26 [0]	37.55 [0]					
VPT-Deep [28]	0.31	36.02 [0]	60.61 [1]	26.57 [0]	0.22	70.27 [4]	83.04 [0]	42.38 [0]					
GateVPT [73]	0.05	47.61 [2]	76.86 [1]	36.80 [1]	0.06	74.84 [4]	83.38 [1]	49.10 [3]					
VAPT (Ours)	0.28	59.23 [5] {7}	80.73 [2] {3}	47.24 [2] {7}	0.27	77.69 [6] {7}	83.95 [2] {3}	60.74 [7] {8}					

1.04% increase in accuracy on FGVC and an substantial **11.70%** improvement on VTAB-1K *Structured*. On VTAB-1K, VAPT yields a **7.34%** average gain over full fine-tuning, while updating only **0.36%** of the backbone parameters. These results underscore both the *effectiveness* and *efficiency* of VAPT as an innovative PEFT method. Additionally, VAPT achieves state-of-the-art performance compared to other PEFT approaches. Among prompt tuning methods, VAPT consistently demonstrates its superiority, surpassing VPT in **23 out of 24 tasks** despite *utilizing fewer parameters*. We attribute these improvements to VAPT’s simple but elegant design, which leverages input information to enhance the expressiveness of prompt experts. These findings highlight the potential of adaptive prompts to improve performance while reducing parameter usage.

Different pre-training methods. In our experiments, we investigate the impact of self-supervised pre-training methods by evaluating two objectives: MAE [20] and MoCo v3 [4], as detailed in Table 2. Previous studies [28, 73] have highlighted the relatively suboptimal performance of VPT when applied to backbones pre-trained using self-supervised objectives. In contrast, VAPT achieves significant performance improvements by effectively leveraging the rich information present in the input features. For example, VAPT demonstrates a remarkable **23.21%** improvement in accuracy under MAE on VTAB-1K *Natural* tasks and an **18.36%** improvement in accuracy under MoCo v3 on VTAB-1K *Structured*. Furthermore, compared to other PEFT methods, VAPT consistently outperforms them, achieving the **highest** “Number of Wins” relative to full fine-tuning, with **9 out of 19** instances under MAE and **15 out of 19** instances under MoCo v3. These results underscore the generality and robustness of our method, both theoretically (see Section 5) and empirically across different pre-training objectives.

Sample efficiency. As discussed in Section 5, our formulation achieves optimal sample efficiency for prompt estimation. To validate these theoretical insights, we systematic experiments on the Stanford Dogs dataset [31]. Following [10], we subsample each class by fraction $f = \{0.01, 0.1, 0.3, 0.5, 1.0\}$ and scaling the number of training epochs by $1/f$ so that the total number of images presented to the model remains constant. The results in Figure 4 and Table 3 show that VAPT consistently outperforms VPT across all training set sizes. Notably, with only 1% of the data, VPT obtains

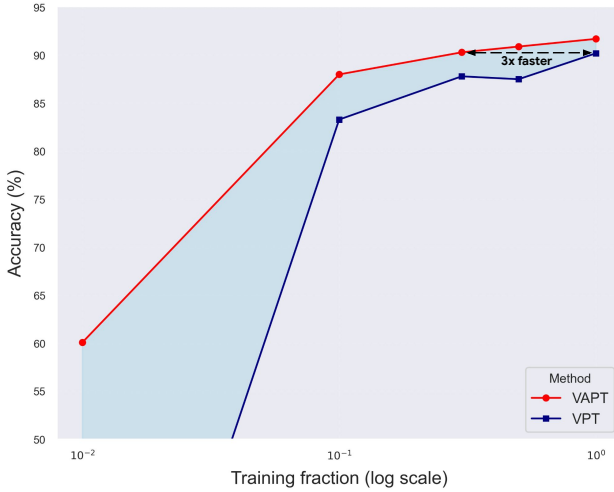


Figure 4: VAPT outperforms the VPT in sample efficiency.

Table 3: Classification accuracy on the Stanford Dogs [31] dataset, where a variable fraction of images per class is retained during training. **Bold** highlights the best results.

Training fraction	VPT	VAPT	Gap
1%	3.6	60.1	56.5%
10%	83.3	88.0	4.7%
30%	87.8	90.3	2.5%
50%	87.5	90.9	3.4%
100%	90.2	91.7	1.5%

a modest accuracy of **3.6%**, whereas VAPT achieves a substantially higher accuracy of **60.1%**. Furthermore, to match the performance of VPT trained on the full dataset, VAPT requires only 30% of the data, yielding an approximate $3\times$ reduction. This highlights the superior sample efficiency of our approach.

7 Conclusion

In this paper, we highlight the restricted functional expressiveness in existing VPT prompt formulations and introduce VAPT, a novel adaptive prompt design. Our approach demonstrates superior performance compared to VPT while using fewer parameters, and achieves optimal sample efficiency both theoretically and empirically. However, our current investigation is limited to implementations on the Vision Transformer architecture and evaluations on classification tasks. Given the promising potential of adaptive prompts, future research could explore alternative designs across different transformer architectures and extend their application to a broader range of tasks. Additionally, future work may investigate the potential synergies between VAPT and VPT through their integration.

Supplement to “Adaptive Prompt: Unlocking the Power of Visual Prompt Tuning”

In this supplementary material, we provide detailed proofs of the main results in Appendix A, along with additional theoretical findings in Appendix B. A discussion of related work can be found in Appendix C. Implementation details of our experiments are described in Appendix D, while additional experimental results are included in Appendix E. Specifically, per task detail results corresponding to the main experiments in Section 6 are reported in Appendix E.1 and Appendix E.2. The performance of VAPT across different backbone scales is evaluated in Appendix E.3. Ablation studies, computational cost analyses, and interpretive visualizations are presented in Appendix E.4, Appendix E.5, and Appendix E.6, respectively.

A Proofs

In this appendix, we provide proofs for key theoretical results for prompt estimation in the main text.

A.1 Proof of Theorem 1

Proposition 1. *Given the least square estimator \hat{G}_n in equation (18), under the $L_2(\mu)$ norm, the estimator $f_{\hat{G}_n}(\cdot)$ converges to the true model $f_{G_*}(\cdot)$ at a parametric rate in the sample size. That is,*

$$\|f_{\hat{G}_n} - f_{G_*}\|_{L_2(\mu)} = \mathcal{O}_P([\log(n)/n]^{\frac{1}{2}}). \quad (19)$$

The proof of Proposition 1 is provided in Appendix A.2. Building on the convergence rate established therein, we now aim to demonstrate the following inequality:

$$\inf_{G \in \mathcal{G}_{L'}(\Theta)} \|f_G - f_{G_*}\|_{L_2(\mu)} / \mathcal{D}_1(G, G_*) > 0. \quad (20)$$

We divide the proof of the above inequality into local and global parts respectively in Appendices A.1.1 and A.1.2. Before going into the proof details, let us introduce some essential assumptions on the activation function σ .

Assumptions. We impose the following assumptions on the activation function σ :

(A.1) (*Identifiability*) If there exist parameters (W_1, W_2) and (W'_1, W'_2) such that $W_2\sigma(W_1\mathbf{X}) = W'_2\sigma(W'_1\mathbf{X})$ for almost surely \mathbf{X} , then we obtain that $(W_1, W_2) = (W'_1, W'_2)$.

(A.2) (*Uniform Lipschitz*) Let $F(\mathbf{X}; W_1, W_2) := \exp((BW_2\sigma(W_1\mathbf{X}))^\top \mathbf{X})CW_2\sigma(W_1\mathbf{X})$. Then, for any $\tau \in \{1, 2\}$, we have

$$\sum_{|\alpha|=\tau} \left| \left(\frac{\partial^{|\alpha|} F}{\partial W_1^{\alpha_1} \partial W_2^{\alpha_2}}(\mathbf{X}; W_1, W_2) - \frac{\partial^{|\alpha|} F}{\partial W'_1^{\alpha_1} \partial W'_2^{\alpha_2}}(\mathbf{X}; W'_1, W'_2) \right) \gamma^\alpha \right| \leq C \|(W_1, W_2) - (W'_1, W'_2)\|^\zeta \|\gamma\|^\tau,$$

for any vector $\gamma \in \mathbb{R}^{2dr}$ and for some positive constants ζ and C which are independent of \mathbf{X} and $(W_1, W_2), (W'_1, W'_2)$. Here, $\alpha = (\alpha_1, \alpha_2) \in \mathbb{N}^{r \times d} \times \mathbb{N}^{d \times r}$.

(A.3) (*Strong identifiability*) The function σ is twice differentiable almost surely and for any natural number ℓ and distinct parameters $\{W_{1,j} : j \in [\ell]\}$, the functions in the set

$$\left\{ \begin{aligned} & \sigma(W_{1,j}\mathbf{X}), \sigma^2(W_{1,j}\mathbf{X})\mathbf{X}^{(u)}, \sigma^{(1)}(W_{1,j}\mathbf{X})\mathbf{X}^{(u)}, \sigma^{(1)}(W_{1,j}\mathbf{X})\sigma(W_{1,j}\mathbf{X})\mathbf{X}^{(u)}\mathbf{X}^{(v)}, \\ & [\sigma^{(1)}(W_{1,j}\mathbf{X})]^2\sigma(W_{1,j}\mathbf{X})\mathbf{X}^{(u)}\mathbf{X}^{(v)}\mathbf{X}^{(w)}, \sigma^{(1)}(W_{1,j}\mathbf{X})\sigma^2(W_{1,j}\mathbf{X})\mathbf{X}^{(u)}\mathbf{X}^{(v)}\mathbf{X}^{(w)}, \\ & [\sigma^{(1)}(W_{1,j}\mathbf{X})]^2\mathbf{X}^{(u)}\mathbf{X}^{(v)}\mathbf{X}^{(w)}, \sigma^{(2)}(W_{1,j}\mathbf{X})\mathbf{X}^{(u)}, \sigma^{(2)}(W_{1,j}\mathbf{X})\mathbf{X}^{(u)}\mathbf{X}^{(v)}, \\ & \sigma^{(2)}(W_{1,j}\mathbf{X})\mathbf{X}^{(u)}\mathbf{X}^{(v)}\mathbf{X}^{(w)} : j \in [\ell], u, v, w \in [d] \end{aligned} \right\}$$

are linearly independent for almost surely \mathbf{X} , where the notations $\sigma^{(1)}$ and $\sigma^{(2)}$ stand for the first and second derivatives of the function σ , which are applied element-wise to the matrices $W_{1,j}\mathbf{X}$.

A.1.1 Local part.

The local part of the inequality (20) corresponds to the following inequality:

$$\lim_{\varepsilon \rightarrow 0} \inf_{G \in \mathcal{G}_{L'}(\Theta) : \mathcal{D}_1(G, G_*) \leq \varepsilon} \frac{\|f_G - f_{G_*}\|_{L_2(\mu)}}{\mathcal{D}_1(G, G_*)} > 0.$$

We assume that the above inequality does not hold. Then, we can find a sequence of measures $G_n := \sum_{j'=1}^{L'} \exp(b_{n,j'})\delta_{(W_{n,1j'}, W_{n,2})}$ in $\mathcal{G}_{L'}(\Theta)$ such that

$$\begin{cases} \mathcal{D}_{1n} := \mathcal{D}_1(G_n, G_*) \rightarrow 0, \\ \|f_{G_n} - f_{G_*}\|_{L_2(\mu)} / \mathcal{D}_{1n} \rightarrow 0. \end{cases}$$

For the sake of the presentation, $\mathcal{V}_j^n := \mathcal{V}_j(G_n)$ is denoted as a Voronoi cell of G_n generated by the j -th components of the true measure G_* . Given that the ensuing arguments are asymptotic, without loss of generality we assume that those Voronoi cells do not depend on the sample size, *i.e.*, we have $\mathcal{V}_j = \mathcal{V}_j^n$ for all n and $1 \leq j \leq L$. Hence, the Voronoi loss \mathcal{D}_{1n} can be rewritten as follows:

$$\begin{aligned} \mathcal{D}_{1n} := & \sum_{j'=1}^L \left| \sum_{i \in \mathcal{V}_{j'}} \exp(b_{n,i}) - \exp(b_{*,j'}) \right| + \sum_{j' \in [L]: |\mathcal{V}_{j'}|=1} \sum_{i \in \mathcal{V}_{j'}} \exp(b_{n,i})(\|\Delta W_{n,1ij'}\| + \|\Delta W_{n,2}\|) \\ & + \sum_{j' \in [L]: |\mathcal{V}_{j'}| > 1} \sum_{i \in \mathcal{V}_{j'}} \exp(b_{n,i})(\|\Delta W_{n,1ij'}\|^2 + \|\Delta W_{n,2}\|^2) \end{aligned}$$

where we define $\Delta W_{n,1ij'} = W_{n,1i} - W_{*,1j'}$ and $\Delta W_{n,2} = W_{n,2} - W_{*,2}$ for all $i \in \mathcal{V}_{j'}$.

From the hypothesis, since $\mathcal{D}_{1n} \rightarrow 0$ as $n \rightarrow \infty$, we have $\sum_{i \in \mathcal{V}_j} \exp(b_{n,i}) \rightarrow \exp(b_{*,j})$, $W_{n,1i} \rightarrow W_{*,1j'}$, and $W_{n,2} \rightarrow W_{*,2}$ for any $i \in \mathcal{V}_j$, $j \in [L]$. Throughout this proof, for the simplicity of the argument we assume without loss of generality that $B = I_d$, $C = I_d$, and $r = 1$ with a note that our techniques can be generalized to the general case of these given matrices. Now, we divide the proof of the local part into three main substeps as follows:

Step 1 - Taylor expansion. We first define the following function:

$$Q_n(\mathbf{X}) := \left[\sum_{j=1}^N \exp(\mathbf{X}^\top A_j^0 \mathbf{X} + a_j^0) + \sum_{j'=1}^L \exp((W_{*,2}\sigma(W_{*,1j'}\mathbf{X}))^\top \mathbf{X} + b_{*,j'}) \right] \cdot [f_{G_n}(\mathbf{X}) - f_{G_*}(\mathbf{X})].$$

Then, we can decompose the function $Q_n(\mathbf{X})$ as follows:

$$\begin{aligned}
Q_n(\mathbf{X}) &= \sum_{j=1}^L \sum_{i \in \mathcal{V}_j} \exp(b_{n,i}) \left[\exp((W_{n,2}\sigma(W_{n,1i}\mathbf{X}))^\top \mathbf{X}) W_{n,2}\sigma(W_{n,1i}\mathbf{X}) \right. \\
&\quad \left. - \exp((W_{*,2}\sigma(W_{*,1j}\mathbf{X}))^\top \mathbf{X}) W_{*,2}\sigma(W_{*,1j}\mathbf{X}) \right] \\
&\quad - \sum_{j=1}^L \sum_{i \in \mathcal{V}_j} \exp(b_{n,i}) \left[\exp((W_{n,2}\sigma(W_{n,1i}\mathbf{X}))^\top \mathbf{X}) - \exp((W_{*,2}\sigma(W_{*,1j}\mathbf{X}))^\top \mathbf{X}) \right] f_{G_n}(\mathbf{X}) \\
&\quad + \sum_{j=1}^L \left(\sum_{i \in \mathcal{V}_j} \exp(b_{n,i}) - \exp(b_{*,j}) \right) \exp((W_{*,2}\sigma(W_{*,1j}\mathbf{X}))^\top \mathbf{X}) \left[W_{*,2}\sigma(W_{*,1j}\mathbf{X}) - f_{G_n}(\mathbf{X}) \right] \\
&:= A_n(\mathbf{X}) - B_n(\mathbf{X}) + C_n(\mathbf{X}). \tag{21}
\end{aligned}$$

Decomposition of the function $A_n(\mathbf{X})$. To streamline the argument, we define the following functions: $\bar{E}(\mathbf{X}; W_1, W_2) := \exp((W_2\sigma(W_1\mathbf{X}))^\top \mathbf{X})$ and $\bar{H}(\mathbf{X}; W_1, W_2) = W_2\sigma(W_1\mathbf{X})$. Furthermore, the product of these functions is defined as $\bar{F}(\mathbf{X}; W_1, W_2) = \bar{E}(\mathbf{X}; W_1, W_2)\bar{H}(\mathbf{X}; W_1, W_2)$. To account for the difference in the number of elements among Voronoi cells, we further decompose the function $A_n(\mathbf{X})$ as follows:

$$\begin{aligned}
A_n(\mathbf{X}) &= \sum_{j:|\mathcal{V}_j|=1} \sum_{i \in \mathcal{V}_j} \exp(b_{n,i}) \left[\bar{F}(\mathbf{X}; W_{n,1i}, W_{n,2}) - \bar{F}(\mathbf{X}; W_{*,1j}, W_{*,2}) \right] \\
&\quad + \sum_{j:|\mathcal{V}_j|>1} \sum_{i \in \mathcal{V}_j} \exp(b_{n,i}) \left[\bar{F}(\mathbf{X}; W_{n,1i}, W_{n,2}) - \bar{F}(\mathbf{X}; W_{*,1j}, W_{*,2}) \right] \\
&:= A_{n,1}(\mathbf{X}) + A_{n,2}(\mathbf{X})
\end{aligned}$$

An application of the first-order Taylor expansion leads to

$$\begin{aligned}
\bar{E}(\mathbf{X}; W_{n,1i}, W_{n,2}) &= \bar{E}(\mathbf{X}; W_{*,1j}, W_{*,2}) + \sum_{|\alpha|=1} (\Delta W_{n,1ij})^{\alpha_1} (\Delta W_{n,2})^{\alpha_2} \frac{\partial^{|\alpha_1|+|\alpha_2|} \bar{E}}{\partial W_1^{\alpha_1} \partial W_2^{\alpha_2}}(\mathbf{X}; W_{*,1j}, W_{*,2}) \\
&\quad + \bar{R}_{ij,1}(\mathbf{X}), \\
\bar{H}(\mathbf{X}; W_{n,1i}, W_{n,2}) &= \bar{H}(\mathbf{X}; W_{*,1j}, W_{*,2}) + \sum_{|\alpha|=1} (\Delta W_{n,1ij})^{\alpha_1} (\Delta W_{n,2})^{\alpha_2} \frac{\partial^{|\alpha_1|+|\alpha_2|} \bar{H}}{\partial W_1^{\alpha_1} \partial W_2^{\alpha_2}}(\mathbf{X}; W_{*,1j}, W_{*,2}) \\
&\quad + \bar{R}_{ij,2}(\mathbf{X}).
\end{aligned}$$

Here, the indices i, j in these equations satisfy that $|\mathcal{V}_j| = 1$, i.e., Voronoi cells with exactly one element and $i \in \mathcal{V}_j$. Furthermore, the functions $\bar{R}_{ij,1}(\mathbf{X})$ and $\bar{R}_{ij,2}(\mathbf{X})$ in these equations correspond

to Taylor remainders when expanding the functions \bar{E} and \bar{H} . Combining the above results leads to

$$\begin{aligned}
A_{n,1}(\mathbf{X}) &= \sum_{j:|\mathcal{V}_j|=1} \sum_{i \in \mathcal{V}_j} \frac{\exp(b_{n,i})}{\alpha!} \sum_{|\alpha|=1} \left\{ (\Delta W_{n,1ij})^{\alpha_1} (\Delta W_{n,2})^{\alpha_2} \frac{\partial^{|\alpha_1|+|\alpha_2|} \bar{E}}{\partial W_1^{\alpha_1} \partial W_2^{\alpha_2}}(\mathbf{X}; W_{*,1j}, W_{*,2}) \bar{H}(\mathbf{X}; W_{*,1j}, W_{*,2}) \right. \\
&\quad \left. + (\Delta W_{n,1ij})^{\alpha_1} (\Delta W_{n,2})^{\alpha_2} \frac{\partial^{|\alpha_1|+|\alpha_2|} \bar{H}}{\partial W_1^{\alpha_1} \partial W_2^{\alpha_2}}(\mathbf{X}; W_{*,1j}, W_{*,2}) \bar{E}(\mathbf{X}; W_{*,1j}, W_{*,2}) \right\} + \tilde{R}_{n,1}(\mathbf{X}) \\
&= \sum_{j:|\mathcal{V}_j|=1} \sum_{|\alpha|=1} \left\{ \bar{M}_{n,j,\alpha_1,\alpha_2} \frac{\partial^{|\alpha_1|+|\alpha_2|} \bar{E}}{\partial W_1^{\alpha_1} \partial W_2^{\alpha_2}}(\mathbf{X}; W_{*,1j}, W_{*,2}) \bar{H}(\mathbf{X}; W_{*,1j}, W_{*,2}) \right. \\
&\quad \left. + \bar{M}_{n,j,\alpha_1,\alpha_2} \frac{\partial^{|\alpha_1|+|\alpha_2|} \bar{H}}{\partial W_1^{\alpha_1} \partial W_2^{\alpha_2}}(\mathbf{X}; W_{*,1j}, W_{*,2}) \bar{E}(\mathbf{X}; W_{*,1j}, W_{*,2}) \right\} + \tilde{R}_{n,1}(\mathbf{X})
\end{aligned}$$

where $\alpha = (\alpha_1, \alpha_2)$. Furthermore, due to the uniform smoothness of the functions \bar{E} and \bar{H} , the function $\tilde{R}_{n,1}(\mathbf{X})$ in that equation satisfies that $\tilde{R}_{n,1}(\mathbf{X})/\mathcal{D}_{1n} \rightarrow 0$ when n approaches infinity. Finally, the terms $M_{n,j,\alpha_1,\alpha_2}$ in that equation admit the following forms:

$$\bar{M}_{n,j,\alpha_1,\alpha_2} = \sum_{i \in \mathcal{V}_j} \frac{\exp(b_{n,i})}{\alpha!} (\Delta W_{n,1ij})^{\alpha_1} (\Delta W_{n,2})^{\alpha_2},$$

for any $|\alpha| = 1$.

We now move to decompose the function $A_{n,2}(\mathbf{X})$. Different from the function $A_{n,1}(\mathbf{X})$ where we utilize only first-order Taylor expansion, to account for more than one element in the Voronoi cells in $A_{n,2}(\mathbf{X})$, we resort to the second-order Taylor expansions to the functions \bar{E} and \bar{H} . In particular, an application of the second-order Taylor expansion leads to

$$\begin{aligned}
A_{n,2}(\mathbf{X}) &= \sum_{j:|\mathcal{V}_j|>1} \sum_{1 \leq |\alpha| \leq 2} \left\{ \bar{M}_{n,j,\alpha_1,\alpha_2} \frac{\partial^{|\alpha_1|+|\alpha_2|} \bar{E}}{\partial W_1^{\alpha_1} \partial W_2^{\alpha_2}}(\mathbf{X}; W_{*,1j}, W_{*,2}) \bar{H}(\mathbf{X}; W_{*,1j}, W_{*,2}) \right. \\
&\quad \left. + \bar{M}_{n,j,\alpha_1,\alpha_2} \frac{\partial^{|\alpha_1|+|\alpha_2|} \bar{H}}{\partial W_1^{\alpha_1} \partial W_2^{\alpha_2}}(\mathbf{X}; W_{*,1j}, W_{*,2}) \bar{E}(\mathbf{X}; W_{*,1j}, W_{*,2}) \right\} \\
&\quad + \sum_{|\alpha|=1, |\beta|=1} \bar{M}_{n,j,\alpha,\beta} \frac{\partial^{|\alpha_1|+|\alpha_2|} \bar{E}}{\partial W_1^{\alpha_1} \partial W_2^{\alpha_2}}(\mathbf{X}; W_{*,1j}, W_{*,2}) \frac{\partial^{|\beta_1|+|\beta_2|} \bar{H}}{\partial W_1^{\beta_1} \partial W_2^{\beta_2}}(\mathbf{X}; W_{*,1j}, W_{*,2}) + \tilde{R}_{n,2}(\mathbf{X})
\end{aligned}$$

where $\alpha = (\alpha_1, \alpha_2)$, $\beta = (\beta_1, \beta_2)$. Furthermore, due to the uniform smoothest of the functions \bar{E} and \bar{H} , the function $\tilde{R}_{n,2}(\mathbf{X})$, which is the combination of Taylor remainders from the second-order Taylor expansion, satisfies that $\tilde{R}_{n,2}(\mathbf{X})/\mathcal{D}_{1n} \rightarrow 0$ when n goes to infinity. Furthermore, the coefficients $\bar{M}_{n,j,\alpha_1,\alpha_2}$ and $\bar{M}_{n,j,\alpha_1,\alpha_2, \beta_1, \beta_2}$ in the above formulation takes the following forms:

$$\bar{M}_{n,j,\alpha_1,\alpha_2} = \sum_{i \in \mathcal{V}_j} \frac{\exp(b_{n,i})}{\alpha!} (\Delta W_{n,1ij})^{\alpha_1} (\Delta W_{n,2})^{\alpha_2},$$

for any index α such that $|\alpha| = 2$ and

$$\bar{M}_{n,j,\alpha_1,\alpha_2, \beta_1, \beta_2} = \sum_{i \in \mathcal{V}_j} \frac{\exp(b_{n,i})}{\alpha! \beta!} (\Delta W_{n,1ij})^{\alpha_1 + \beta_1} (\Delta W_{n,2})^{\alpha_2 + \beta_2},$$

for any coefficients α and β such that $|\alpha| = |\beta| = 1$. Given the formulations of the functions $\bar{E}(\mathbf{X}; W_1, W_2)$ and $\bar{H}(\mathbf{X}; W_1, W_2)$, their partial derivatives take the following forms:

$$\begin{aligned}
\frac{\partial \bar{E}}{\partial W_1^{(u)}}(\mathbf{X}; W_1, W_2) &= \exp((W_2 \sigma(W_1 \mathbf{X}))^\top \mathbf{X}) \mathbf{X}^\top W_2 \sigma^{(1)}(W_1 \mathbf{X}) \mathbf{X}^{(u)}, \\
\frac{\partial \bar{E}}{\partial W_2^{(v)}}(\mathbf{X}; W_1, W_2) &= \exp((W_2 \sigma(W_1 \mathbf{X}))^\top \mathbf{X}) \mathbf{X}^{(v)} \sigma(W_1 \mathbf{X}), \\
\frac{\partial^2 \bar{E}}{\partial W_1^{(u)} \partial W_1^{(v)}}(\mathbf{X}; W_1, W_2) &= \exp((W_2 \sigma(W_1 \mathbf{X}))^\top \mathbf{X}) [\mathbf{X}^\top W_2 \sigma^{(1)}(W_1 \mathbf{X})]^2 \mathbf{X}^{(u)} \mathbf{X}^{(v)} \\
&\quad + \exp((W_2 \sigma(W_1 \mathbf{X}))^\top \mathbf{X}) \mathbf{X}^\top W_2 \sigma^{(2)}(W_1 \mathbf{X}) \mathbf{X}^{(u)} \mathbf{X}^{(v)}, \\
\frac{\partial^2 \bar{E}}{\partial W_2^{(u)} \partial W_2^{(v)}}(\mathbf{X}; W_1, W_2) &= \exp((W_2 \sigma(W_1 \mathbf{X}))^\top \mathbf{X}) \mathbf{X}^{(u)} \mathbf{X}^{(v)} \sigma^2(W_1 \mathbf{X}), \\
\frac{\partial^2 \bar{E}}{\partial W_1^{(u)} \partial W_2^{(v)}}(\mathbf{X}; W_1, W_2) &= \exp((W_2 \sigma(W_1 \mathbf{X}))^\top \mathbf{X}) \mathbf{X}^\top W_2 \sigma^{(1)}(W_1 \mathbf{X}) \mathbf{X}^{(u)} \mathbf{X}^{(v)} \sigma(W_1 \mathbf{X}) \\
&\quad + \exp((W_2 \sigma(W_1 \mathbf{X}))^\top \mathbf{X}) \sigma^{(1)}(W_1 \mathbf{X}) \mathbf{X}^{(u)} \mathbf{X}^{(v)}, \\
\frac{\partial \bar{H}}{\partial W_1^{(u)}}(\mathbf{X}; W_1, W_2) &= W_2 \sigma^{(1)}(W_1 \mathbf{X}) \mathbf{X}^{(u)}, \\
\frac{\partial \bar{H}}{\partial W_2^{(v)}}(\mathbf{X}; W_1, W_2) &= \sigma(W_1 \mathbf{X}) I_d, \\
\frac{\partial^2 \bar{H}}{\partial W_1^{(u)} \partial W_1^{(v)}}(\mathbf{X}; W_1, W_2) &= W_2 \sigma^{(2)}(W_1 \mathbf{X}) \mathbf{X}^{(u)} \mathbf{X}^{(v)}, \\
\frac{\partial^2 \bar{H}}{\partial W_1^{(u)} \partial W_2^{(v)}}(\mathbf{X}; W_1, W_2) &= \sigma^{(2)}(W_1 \mathbf{X}) \mathbf{X}^{(u)} I_d, \\
\frac{\partial^2 \bar{H}}{\partial W_2^{(u)} \partial W_2^{(v)}}(\mathbf{X}; W_1, W_2) &= \mathbf{0}.
\end{aligned}$$

Putting the above formulations together, the functions $A_{n,1}(\mathbf{X})$ and $A_{n,2}(\mathbf{X})$ can be rewritten as

follows:

$$\begin{aligned}
A_{n,1}(\mathbf{X}) &= \sum_{j:|\mathcal{V}_j|=1} \exp((W_{*,2}\sigma(W_{*,1j}\mathbf{X}))^\top \mathbf{X}) [\sigma^{(1)}(W_{*,1j}\mathbf{X})\sigma(W_{*,1j}\mathbf{X})\mathbf{X}^\top L_{n,1,j}\mathbf{X}W_{*,2} \\
&\quad + \sigma^2(W_{*,1j}\mathbf{X})L_{n,2,j}^\top \mathbf{X}W_{*,2} + \sigma^{(1)}(W_{*,1j}\mathbf{X})L_{n,3,j}^\top \mathbf{X}W_{*,2} + \sigma(W_{*,1j}\mathbf{X})L_{n,2,j}^\top] + \bar{R}_{n,1}(\mathbf{X}), \\
A_{n,2}(\mathbf{X}) &= \sum_{j:|\mathcal{V}_j|>1} \exp((W_{*,2}\sigma(W_{*,1j}\mathbf{X}))^\top \mathbf{X}) [\sigma^{(1)}(W_{*,1j}\mathbf{X})\sigma(W_{*,1j}\mathbf{X})\mathbf{X}^\top L_{n,1,j}\mathbf{X}W_{*,2} \\
&\quad + \sigma^2(W_{*,1j}\mathbf{X})L_{n,2,j}^\top \mathbf{X}W_{*,2} + \sigma^{(1)}(W_{*,1j}\mathbf{X})L_{n,3,j}^\top \mathbf{X}W_{*,2} + \sigma(W_{*,1j}\mathbf{X})L_{n,2,j}^\top \\
&\quad + ([\sigma^{(1)}(W_{*,1j}\mathbf{X})]^2\sigma(W_{*,1j}\mathbf{X}) + \sigma^{(2)}(W_{*,1j}\mathbf{X})\sigma(W_{*,1j}\mathbf{X}))\mathbf{X}^\top L_{n,4,j}\mathbf{X}\mathbf{X}^\top W_{*,2}W_{*,2} \\
&\quad + \sigma^2(W_{*,1j}\mathbf{X})\sigma(W_{*,1j}\mathbf{X})\mathbf{X}^\top L_{n,5,j}\mathbf{X}W_{*,2} + \sigma^{(2)}(W_{*,1j}\mathbf{X})\mathbf{X}^\top L_{n,4,j}\mathbf{X}W_{*,2} \\
&\quad + (\sigma^{(1)}(W_{*,1j}\mathbf{X})[\sigma(W_{*,1j}\mathbf{X})]^2\mathbf{X}^\top W_{*,2} + \sigma^{(1)}(W_{*,1j}\mathbf{X})\sigma(W_{*,1j}\mathbf{X}))\mathbf{X}^\top L_{n,6,j}\mathbf{X}W_{*,2} \\
&\quad + \sigma^{(2)}(W_{*,1j}\mathbf{X})\mathbf{X}^\top L_{n,6,j} + [\sigma^{(1)}(W_{*,1j}\mathbf{X})]^2\mathbf{X}^\top L_{n,4,j}\mathbf{X}\mathbf{X}^\top W_{*,2}W_{*,2} \\
&\quad + \sigma^{(1)}(W_{*,1j}\mathbf{X})\sigma(W_{*,1j}\mathbf{X})\mathbf{X}^\top W_{*,2}\mathbf{X}^\top L_{n,6,j} + \sigma^{(1)}(W_{*,1j}\mathbf{X})\sigma(W_{*,1j}\mathbf{X})\mathbf{X}^\top L_{n,6,j}\mathbf{X}W_{*,2} \\
&\quad + [\sigma(W_{*,1j}\mathbf{X})]^2\mathbf{X}^\top L_{n,5,j}] + \bar{R}_{n,2}(\mathbf{X}),
\end{aligned}$$

where the formulations of $L_{n,1,j}, L_{n,2,j}, \dots, L_{n,6,j}$ in these equations are given by:

$$\begin{aligned}
L_{1,n} &:= M_{n,j,e_{1:d},\mathbf{0}_d} W_{*,2}^\top, \quad M_{n,j,e_{1:d},\mathbf{0}_d} := (M_{n,j,e_u,\mathbf{0}_d})_{u=1}^d \\
L_{n,2,j} &:= (M_{n,j,\mathbf{0}_d,e_u})_{u=1}^d, \\
L_{n,3,j} &:= M_{n,j,e_{1:d},\mathbf{0}_d}, \\
L_{n,4,j} &:= (M_{n,j,e_u+e_v,\mathbf{0}_d})_{u,v=1}^d, \\
L_{n,5,j} &:= (M_{n,j,\mathbf{0}_d,e_u+e_v})_{u,v=1}^d, \\
L_{n,6,j} &:= (M_{n,j,e_u,e_v})_{u,v=1}^d,
\end{aligned}$$

Here, for each $1 \leq u \leq d$, e_u denotes the standard basis vector in \mathbb{R}^d with 1 in the u -th position and 0 in all other positions.

Decomposition of the function $B_n(\mathbf{X})$. Similar to our decomposition of the function $A_n(\mathbf{X})$, we also separate the Voronoi cells with exactly one element and with more than one element in the decomposition of the function $B_n(\mathbf{X})$. Therefore, we obtain that

$$\begin{aligned}
B_n(\mathbf{X}) &= \sum_{j:|\mathcal{V}_j|=1} \sum_{i \in \mathcal{V}_j} \exp(b_{n,i}) [\bar{E}(\mathbf{X}; W_{n,1i}, W_{n,2}) - \bar{E}(\mathbf{X}; W_{*,1j}, W_{*,2})] f_{G_n}(\mathbf{X}) \\
&\quad + \sum_{j:|\mathcal{V}_j|>1} \sum_{i \in \mathcal{V}_j} \exp(b_{n,i}) [\bar{E}(\mathbf{X}; W_{n,1i}, W_{n,2}) - \bar{E}(\mathbf{X}; W_{*,1j}, W_{*,2})] f_{G_n}(\mathbf{X}) \\
&:= B_{n,1}(\mathbf{X}) + B_{n,2}(\mathbf{X}).
\end{aligned}$$

For Voronoi cells with exactly one element, we will utilize Taylor expansion up to the first order while for Voronoi cells with more than one element, the second-order Taylor expansion will be employed.

This strategy leads to the following representations:

$$B_{n,1}(\mathbf{X}) = \sum_{j:|\mathcal{V}_j|=1} \sum_{|\alpha|=1} \bar{M}_{n,j,\alpha_1,\alpha_2} \frac{\partial^{|\alpha_1|+|\alpha_2|} \bar{E}}{\partial W_1^{\alpha_1} \partial W_2^{\alpha_2}}(\mathbf{X}; W_{*,1j}, W_{*,2}) f_{G_n}(\mathbf{X}) + \bar{R}_{n,3}(\mathbf{X}),$$

$$B_{n,2}(\mathbf{X}) = \sum_{j:|\mathcal{V}_j|=1} \sum_{1 \leq |\alpha| \leq 2} \bar{M}_{n,j,\alpha_1,\alpha_2} \frac{\partial^{|\alpha_1|+|\alpha_2|} \bar{E}}{\partial W_1^{\alpha_1} \partial W_2^{\alpha_2}}(\mathbf{X}; W_{*,1j}, W_{*,2}) f_{G_n}(\mathbf{X}) + \bar{R}_{n,4}(\mathbf{X}).$$

In these expressions, the functions $\bar{R}_{n,3}(\mathbf{X})$ and $\bar{R}_{n,4}(\mathbf{X})$ correspond to the Taylor remainders. Due to the uniform smoothness of the functions \bar{E} , we obtain that $R_{n,3}(\mathbf{X})/\mathcal{D}_{1n} \rightarrow 0$ and $R_{n,4}(\mathbf{X})/\mathcal{D}_{1n} \rightarrow 0$ as n approaches infinity. By computing the closed-form formulations for the partial derivatives of the function \bar{E} , both the functions $B_{n,1}(\mathbf{X})$ and $B_{n,2}(\mathbf{X})$ can be rewritten as follows:

$$B_{n,1}(\mathbf{X}) = \sum_{j:|\mathcal{V}_j|=1} \exp((W_{*,2}\sigma(W_{*,1j}\mathbf{X}))^\top \mathbf{X}) [\sigma^{(1)}(W_{*,1j}\mathbf{X})\mathbf{X}^\top L_{n,1,j}\mathbf{X} + \sigma(W_{*,1j}\mathbf{X})L_{n,2,j}^\top \mathbf{X}] f_{G_n}(\mathbf{X}) + \bar{R}_{n,3}(\mathbf{X}),$$

$$B_{n,2}(\mathbf{X}) = \sum_{j:|\mathcal{V}_j|>1} \exp((W_{*,2}\sigma(W_{*,1j}\mathbf{X}))^\top \mathbf{X}) [\sigma^{(1)}(W_{*,1j}\mathbf{X})\mathbf{X}^\top L_{n,1,j}\mathbf{X} + \sigma(W_{*,1j}\mathbf{X})L_{n,2,j}^\top \mathbf{X} + ([\sigma^{(1)}(W_{*,1j}\mathbf{X})]^2 + \sigma^{(2)}(W_{*,1j}\mathbf{X}))\mathbf{X}^\top L_{n,4,j}\mathbf{X}\mathbf{X}^\top W_{*,2} + \sigma^2(W_{*,1j}\mathbf{X})\mathbf{X}^\top L_{n,5,j}\mathbf{X} + (\sigma^{(1)}(W_{*,1j}\mathbf{X})\sigma(W_{*,1j}\mathbf{X})\mathbf{X}^\top W_{*,2} + \sigma^{(1)}(W_{*,1j}\mathbf{X}))\mathbf{X}^\top L_{n,6,j}\mathbf{X}] f_{G_n}(\mathbf{X}) + \bar{R}_{n,4}(\mathbf{X}),$$

Plugging all of these results together, the function $Q_n(\mathbf{X})$ can be rewritten as follows:

$$Q_n(\mathbf{X}) = \sum_{j:|\mathcal{V}_j|=1} \exp((W_{*,2}\sigma(W_{*,1j}\mathbf{X}))^\top \mathbf{X}) [\sigma^{(1)}(W_{*,1j}\mathbf{X})\sigma(W_{*,1j}\mathbf{X})\mathbf{X}^\top L_{n,1,j}\mathbf{X}W_{*,2} + \sigma^2(W_{*,1j}\mathbf{X})L_{n,2,j}^\top \mathbf{X}W_{*,2} + \sigma^{(1)}(W_{*,1j}\mathbf{X})L_{n,3,j}^\top \mathbf{X}W_{*,2} + \sigma(W_{*,1j}\mathbf{X})L_{n,2,j}^\top] + \sum_{j:|\mathcal{V}_j|>1} \exp((W_{*,2}\sigma(W_{*,1j}\mathbf{X}))^\top \mathbf{X}) [\sigma^{(1)}(W_{*,1j}\mathbf{X})\sigma(W_{*,1j}\mathbf{X})\mathbf{X}^\top L_{n,1,j}\mathbf{X}W_{*,2} + \sigma^2(W_{*,1j}\mathbf{X})L_{n,2,j}^\top \mathbf{X}W_{*,2} + \sigma^{(1)}(W_{*,1j}\mathbf{X})L_{n,3,j}^\top \mathbf{X}W_{*,2} + \sigma(W_{*,1j}\mathbf{X})L_{n,2,j}^\top + \sigma^2(W_{*,1j}\mathbf{X})L_{n,2,j}^\top \mathbf{X}W_{*,2} + \sigma^{(1)}(W_{*,1j}\mathbf{X})L_{n,3,j}^\top \mathbf{X}W_{*,2} + \sigma(W_{*,1j}\mathbf{X})L_{n,2,j}^\top + ([\sigma^{(1)}(W_{*,1j}\mathbf{X})]^2\sigma(W_{*,1j}\mathbf{X}) + \sigma^{(2)}(W_{*,1j}\mathbf{X})\sigma(W_{*,1j}\mathbf{X}))\mathbf{X}^\top L_{n,4,j}\mathbf{X}\mathbf{X}^\top W_{*,2}W_{*,2} + \sigma^2(W_{*,1j}\mathbf{X})\sigma(W_{*,1j}\mathbf{X})\mathbf{X}^\top L_{n,5,j}\mathbf{X}W_{*,2} + \sigma^{(2)}(W_{*,1j}\mathbf{X})\mathbf{X}^\top L_{n,4,j}\mathbf{X}W_{*,2} + (\sigma^{(1)}(W_{*,1j}\mathbf{X})[\sigma(W_{*,1j}\mathbf{X})]^2\mathbf{X}^\top W_{*,2} + \sigma^{(1)}(W_{*,1j}\mathbf{X})\sigma(W_{*,1j}\mathbf{X}))\mathbf{X}^\top L_{n,6,j}\mathbf{X}W_{*,2} + \sigma^{(2)}(W_{*,1j}\mathbf{X})\mathbf{X}^\top L_{n,6,j} + [\sigma^{(1)}(W_{*,1j}\mathbf{X})]^2\mathbf{X}^\top L_{n,4,j}\mathbf{X}\mathbf{X}^\top W_{*,2}W_{*,2} + \sigma^{(1)}(W_{*,1j}\mathbf{X})\sigma(W_{*,1j}\mathbf{X})\mathbf{X}^\top W_{*,2}\mathbf{X}^\top L_{n,6,j} + \sigma^{(1)}(W_{*,1j}\mathbf{X})\sigma(W_{*,1j}\mathbf{X})\mathbf{X}^\top L_{n,6,j}\mathbf{X}W_{*,2} + [\sigma(W_{*,1j}\mathbf{X})]^2\mathbf{X}^\top L_{n,5,j}]$$

$$\begin{aligned}
& - \sum_{j:|\mathcal{V}_j|=1} \exp((W_{*,2}\sigma(W_{*,1j}\mathbf{X}))^\top \mathbf{X}) [\sigma^{(1)}(W_{*,1j}\mathbf{X})\mathbf{X}^\top L_{n,1,j}\mathbf{X} + \sigma(W_{*,1j}\mathbf{X})L_{n,2,j}^\top \mathbf{X}] f_{G_n}(\mathbf{X}) \\
& - \sum_{j:|\mathcal{V}_j|>1} \exp((W_{*,2}\sigma(W_{*,1j}\mathbf{X}))^\top \mathbf{X}) [\sigma^{(1)}(W_{*,1j}\mathbf{X})\mathbf{X}^\top L_{n,1,j}\mathbf{X} + \sigma(W_{*,1j}\mathbf{X})L_{n,2,j}^\top \mathbf{X} \\
& \quad + ([\sigma^{(1)}(W_{*,1j}\mathbf{X})]^2 + \sigma^{(2)}(W_{*,1j}\mathbf{X}))\mathbf{X}^\top L_{n,4,j}\mathbf{X} \mathbf{X}^\top W_{*,2} + \sigma^2(W_{*,1j}\mathbf{X})\mathbf{X}^\top L_{n,5,j}\mathbf{X} \\
& \quad + (\sigma^{(1)}(W_{*,1j}\mathbf{X})\sigma(W_{*,1j}\mathbf{X})\mathbf{X}^\top W_{*,2} + \sigma^{(1)}(W_{*,1j}\mathbf{X}))\mathbf{X}^\top L_{n,6,j}\mathbf{X}] f_{G_n}(\mathbf{X}) \\
& - \sum_{j=1}^L M_{n,j,\mathbf{0}_d,\mathbf{0}_d} \exp((W_{*,2}\sigma(W_{*,1j}\mathbf{X}))^\top \mathbf{X}) f_{G_n}(\mathbf{X}) \\
& + \sum_{j=1}^L M_{n,j,\mathbf{0}_d,\mathbf{0}_d} \exp((W_{*,2}\sigma(W_{*,1j}\mathbf{X}))^\top \mathbf{X}) \sigma(W_{*,1j}\mathbf{X}) W_{*,2} \\
& + \tilde{R}_{n,1}(\mathbf{X}) + \tilde{R}_{n,2}(\mathbf{X}) - \tilde{R}_{n,3}(\mathbf{X}) - \tilde{R}_{n,4}(\mathbf{X}) \tag{22}
\end{aligned}$$

where the coefficient $\bar{M}_{n,j,\mathbf{0}_d,\mathbf{0}_d} := \sum_{i \in \mathcal{V}_j} \exp(b_{n,i}) - \exp(b_{*,j})$ for any $j \in [L]$.

Step 2 - Non-vanishing coefficients. An important insight from equation (22) is that the ratio $Q_n(\mathbf{X})/\mathcal{D}_{1n}$ can be expressed as a linear combination of the following independent functions:

$$\begin{aligned}
& E(\mathbf{X}; W_{*,1j}, W_{*,2})\sigma(W_{*,1j}\mathbf{X})W_{*,2}, \quad E(\mathbf{X}; W_{*,1j}, W_{*,2})\sigma^{(1)}(W_{*,1j}\mathbf{X})\sigma(W_{*,1j}\mathbf{X})\mathbf{X}^{(u)}\mathbf{X}^{(v)}W_{*,2}, \\
& E(\mathbf{X}; W_{*,1j}, W_{*,2})\sigma^2(W_{*,1j}\mathbf{X})\mathbf{X}^{(u)}W_{*,2}, \quad E(\mathbf{X}; W_{*,1j}, W_{*,2})\sigma^{(1)}(W_{*,1j}\mathbf{X})\mathbf{X}^{(u)}W_{*,2}, \\
& E(\mathbf{X}; W_{*,1j}, W_{*,2})\sigma(W_{*,1j}\mathbf{X})e_u, \quad E(\mathbf{X}; W_{*,1j}, W_{*,2})[\sigma^{(1)}(W_{*,1j}\mathbf{X})]^2\sigma(W_{*,1j}\mathbf{X})\mathbf{X}^{(u)}\mathbf{X}^{(v)}\mathbf{X}^{(w)}W_{*,2}, \\
& E(\mathbf{X}; W_{*,1j}, W_{*,2})\sigma^{(2)}(W_{*,1j}\mathbf{X})\sigma(W_{*,1j}\mathbf{X})\mathbf{X}^{(u)}\mathbf{X}^{(v)}\mathbf{X}^{(w)}W_{*,2}, \quad E(\mathbf{X}; W_{*,1j}, W_{*,2})\sigma^{(2)}(W_{*,1j}\mathbf{X})\mathbf{X}^{(u)}\mathbf{X}^{(v)}W_{*,2}, \\
& E(\mathbf{X}; W_{*,1j}, W_{*,2})\sigma^2(W_{*,1j}\mathbf{X})\sigma(W_{*,1j}\mathbf{X})\mathbf{X}^{(u)}\mathbf{X}^{(v)}W_{*,2}, \\
& E(\mathbf{X}; W_{*,1j}, W_{*,2})\sigma^{(1)}(W_{*,1j}\mathbf{X})[\sigma(W_{*,1j}\mathbf{X})]^2\mathbf{X}^{(u)}\mathbf{X}^{(v)}\mathbf{X}^{(w)}W_{*,2}, \quad E(\mathbf{X}; W_{*,1j}, W_{*,2})\sigma^{(2)}(W_{*,1j}\mathbf{X})\mathbf{X}^{(u)}e_u, \\
& E(\mathbf{X}; W_{*,1j}, W_{*,2})[\sigma^{(1)}(W_{*,1j}\mathbf{X})]^2\mathbf{X}^{(u)}\mathbf{X}^{(v)}\mathbf{X}^{(w)}W_{*,2}, \quad E(\mathbf{X}; W_{*,1j}, W_{*,2})\sigma^{(1)}(W_{*,1j}\mathbf{X})\sigma(W_{*,1j}\mathbf{X})\mathbf{X}^{(u)}\mathbf{X}^{(v)}e_v, \\
& E(\mathbf{X}; W_{*,1j}, W_{*,2})[\sigma(W_{*,1j}\mathbf{X})]^2\mathbf{X}^{(u)}e_u, \\
& E(\mathbf{X}; W_{*,1j}, W_{*,2})\sigma^{(1)}(W_{*,1j}\mathbf{X})\mathbf{X}^{(u)}\mathbf{X}^{(v)}f_{G_n}(\mathbf{X}), \quad E(\mathbf{X}; W_{*,1j}, W_{*,2})\sigma(W_{*,1j}\mathbf{X})\mathbf{X}^{(u)}f_{G_n}(\mathbf{X}), \\
& E(\mathbf{X}; W_{*,1j}, W_{*,2})[\sigma^{(1)}(W_{*,1j}\mathbf{X})]^2\mathbf{X}^{(u)}\mathbf{X}^{(v)}\mathbf{X}^{(w)}f_{G_n}(\mathbf{X}), \quad E(\mathbf{X}; W_{*,1j}, W_{*,2})\sigma^{(2)}(W_{*,1j}\mathbf{X})\mathbf{X}^{(u)}\mathbf{X}^{(v)}\mathbf{X}^{(w)}f_{G_n}(\mathbf{X}), \\
& E(\mathbf{X}; W_{*,1j}, W_{*,2})\sigma^2(W_{*,1j}\mathbf{X})\mathbf{X}^{(u)}\mathbf{X}^{(v)}f_{G_n}(\mathbf{X}), \quad E(\mathbf{X}; W_{*,1j}, W_{*,2})\sigma^{(1)}(W_{*,1j}\mathbf{X})\mathbf{X}^{(u)}\mathbf{X}^{(v)}f_{G_n}(\mathbf{X}), \\
& E(\mathbf{X}; W_{*,1j}, W_{*,2})\sigma^{(1)}(W_{*,1j}\mathbf{X})\sigma(W_{*,1j}\mathbf{X})\mathbf{X}^{(u)}\mathbf{X}^{(v)}\mathbf{X}^{(w)}f_{G_n}(\mathbf{X}), \quad E(\mathbf{X}; W_{*,1j}, W_{*,2})f_{G_n}(\mathbf{X}),
\end{aligned}$$

for any $1 \leq j \leq L$ and $1 \leq u, v, w \leq d$.

We proceed to demonstrate that not all of the coefficients of these linear independent functions go to 0 as n goes to infinity. We prove that claim by contradiction. We assume that all these coefficients go to 0 as n goes to ∞ . From the representation of the ratio $Q_n(\mathbf{X})/\mathcal{D}_{1n}$ in terms of these linear independent functions, we obtain that these ratios $L_{n,1,j}^{(u)}/\mathcal{D}_{1n}$, $L_{n,2,j}^{(u)}/\mathcal{D}_{1n}$, $L_{n,3,j}^{(u)}/\mathcal{D}_{1n}$, $L_{n,4,j}^{(uv)}/\mathcal{D}_{1n}$, $L_{n,5,j}^{(uv)}/\mathcal{D}_{1n}$, $L_{n,6,j}^{(uv)}/\mathcal{D}_{1n}$, and $M_{n,j,\mathbf{0}_d,\mathbf{0}_d}/\mathcal{D}_{1n}$ go to 0 as n approaches infinity for any indices $u, v \in [d]$ and $j \in [L]$.

By first considering the vanishing of the ratio $\bar{M}_{n,j,\mathbf{0}_d,\mathbf{0}_d}/\mathcal{D}_{1n}$ to 0 for any $j \in [L]$ and takes the absolute value of that ratio, we find that

$$\frac{|M_{n,j,\mathbf{0}_d,\mathbf{0}_d}|}{\mathcal{D}_{1n}} = \frac{|\sum_{i \in \mathcal{V}_j} \exp(b_{n,i}) - \exp(b_{*,j})|}{\mathcal{D}_{1n}} \rightarrow 0,$$

By varying the index j from 1 to L in these limits and summing these limits, we find that

$$\frac{\sum_{j=1}^L |\sum_{i \in \mathcal{V}_j} \exp(b_{n,i}) - \exp(b_{*,j})|}{\mathcal{D}_{1n}} \rightarrow 0. \quad (23)$$

Our strategy now is to consider the limits corresponding to Voronoi cells with exactly one element and more than one element separately. In particular, for Voronoi cells with exactly one element, namely, for indices $j \in [L]$ such that their corresponding Voronoi cells have one element, i.e., $|\mathcal{V}_j| = 1$, as the ratio $L_{n,3,j}^{(u)}/\mathcal{D}_{1n}$ approaches 0, we have

$$\frac{\sum_{i \in \mathcal{V}_j} \exp(b_{n,i}) \|\Delta W_{n,1ij}\|_1}{\mathcal{D}_{1n}} = \frac{\sum_{u=1}^d |L_{n,3,j}^{(u)}|}{\mathcal{D}_{1n}} \rightarrow 0.$$

Similarly, $L_{n,2,j}/\mathcal{D}_{1n} \rightarrow 0$ also leads to $\frac{\sum_{i \in \mathcal{V}_j} \exp(b_{n,i}) \|\Delta W_{n,2ij}\|_1}{\mathcal{D}_{1n}} \rightarrow 0$. Combining these results leads to

$$\frac{\sum_{j:|\mathcal{V}_j|=1} \sum_{i \in \mathcal{V}_j} \exp(b_{n,i}) (\|\Delta W_{n,1ij}\|_1 + \|\Delta W_{n,2ij}\|_1)}{\mathcal{D}_{1n}} \rightarrow 0.$$

Due to the equivalence between the ℓ_1 norm and the ℓ_2 norm, we deduce that

$$\frac{\sum_{j:|\mathcal{V}_j|=1} \sum_{i \in \mathcal{V}_j} \exp(b_{n,i}) (\|\Delta W_{n,1ij}\| + \|\Delta W_{n,2ij}\|)}{\mathcal{D}_{1n}} \rightarrow 0. \quad (24)$$

We now move to the Voronoi cells with more than one element, namely, indices $j \in [L]$ such that $|\mathcal{V}_j| > 1$. As the ratios $L_{n,4,j}^{(uu)}/\mathcal{D}_{1n} \rightarrow 0$, we find that

$$\frac{\sum_{u=1}^d L_{n,4,j}^{(uu)}}{\mathcal{D}_{1n}} = \frac{\sum_{i \in \mathcal{V}_j} \exp(b_{n,i}) \|\Delta W_{n,1ij}\|^2}{\mathcal{D}_{1n}} \rightarrow 0.$$

Likewise, as $L_{n,5,j}^{(uu)}/\mathcal{D}_{1n} \rightarrow 0$, we arrive at $\frac{\sum_{i \in \mathcal{V}_j} \exp(b_{n,i}) \|\Delta W_{n,2ij}\|^2}{\mathcal{D}_{1n}} \rightarrow 0$. These results demonstrate that

$$\frac{\sum_{j:|\mathcal{V}_j|>1} \sum_{i \in \mathcal{V}_j} \exp(b_{n,i}) (\|\Delta W_{n,1ij}\|^2 + \|\Delta W_{n,2ij}\|^2)}{\mathcal{D}_{1n}} \rightarrow 0. \quad (25)$$

Combining the results of equations (23), (24), and (25), we achieve that

$$\frac{\mathcal{D}_{1n}}{\mathcal{D}_{1n}} = 1 \rightarrow 0, \text{ as } n \rightarrow \infty,$$

which is a contradiction. As a consequence, at least one of the coefficients of the linear independent functions in the expression of the ratio $Q_n(\mathbf{X})/\mathcal{D}_{1n}$ does not go to 0 as n approaches infinity.

Step 3 - Application of the Fatou's lemma. The idea of this step is to divide all of the coefficients of the linear independent terms in the expression of the ratio $Q_n(\mathbf{X})/\mathcal{D}_{1n}$, namely, the terms $L_{n,1,j}^{(u)}/\mathcal{D}_{1n}$, $L_{n,2,j}^{(u)}/\mathcal{D}_{1n}$, $L_{n,3,j}^{(u)}/\mathcal{D}_{1n}$, $L_{n,4,j}^{(uv)}/\mathcal{D}_{1n}$, $L_{n,5,j}^{(uv)}/\mathcal{D}_{1n}$, $L_{n,6,j}^{(uv)}/\mathcal{D}_{1n}$, and $M_{n,j,\mathbf{0}_d,\mathbf{0}_d}/\mathcal{D}_{1n}$ for all $u, v \in [d]$, by the maximum of their absolute values. In particular, we first denote m_n as the maximum of the absolute values of these coefficients. As not all of these coefficients go to 0, it demonstrates that $1/m_n$ does not go to infinity as $n \rightarrow \infty$.

From the hypothesis, we have $\|f_{G_n} - f_{G_*}\|_{L_2(\mu)}/\mathcal{D}_{1n} \rightarrow 0$ as $n \rightarrow \infty$. As $1/m_n \not\rightarrow \infty$, it follows that $\|f_{G_n} - f_{G_*}\|_{L_2(\mu)}/(m_n \mathcal{D}_{1n}) \rightarrow 0$. An application of the Fatou's lemma leads to

$$\lim_{n \rightarrow \infty} \frac{\|f_{G_n} - f_{G_*}\|_{L_2(\mu)}}{m_n \mathcal{D}_{1n}} \geq \int \liminf_{n \rightarrow \infty} \frac{|f_{G_n}(\mathbf{X}) - f_{G_*}(\mathbf{X})|}{m_n \mathcal{D}_{1n}} d\mu(\mathbf{X}).$$

Combining all of the above results, we obtain that $\liminf_{n \rightarrow \infty} \frac{|f_{G_n}(\mathbf{X}) - f_{G_*}(\mathbf{X})|}{m_n \mathcal{D}_{2n}} = 0$ for almost surely \mathbf{X} . To ease the presentation, we denote the following limits:

$$\frac{L_{n,\tau,j}}{m_n \mathcal{D}_{1n}} \rightarrow \lambda_{\tau,j}, \quad \frac{M_{n,j,\mathbf{0}_d,\mathbf{0}_d}}{\mathcal{D}_{1n}} \rightarrow \lambda_{0,j},$$

for any $1 \leq \tau \leq 6$ and $1 \leq j \leq L$. By the definition of m_n , at least one coefficient in the set $\{\lambda_{0,j}, \lambda_{1,j}, \lambda_{2,j}, \lambda_{3,j}\}_{j:|\mathcal{V}_j|=1}$, $\{\lambda_{0,j}, \lambda_{1,j}, \lambda_{2,j}, \lambda_{3,j}, \lambda_{4,j}, \lambda_{5,j}, \lambda_{6,j}\}_{j:|\mathcal{V}_j|>1}$ must be nonzero. The limit $\liminf_{n \rightarrow \infty} \frac{|f_{G_n}(\mathbf{X}) - f_{G_*}(\mathbf{X})|}{m_n \mathcal{D}_{1n}} = 0$, or equivalently, $\liminf_{n \rightarrow \infty} \frac{|Q_n(\mathbf{X})|}{m_n \mathcal{D}_{1n}} = 0$ leads to

$$\begin{aligned} & \sum_{j:|\mathcal{V}_j|=1} \exp((W_{*,2}\sigma(W_{*,1j}\mathbf{X}))^\top \mathbf{X}) [\sigma^{(1)}(W_{*,1j}\mathbf{X})\sigma(W_{*,1j}\mathbf{X})\mathbf{X}^\top \lambda_{1,j}\mathbf{X}W_{*,2} \\ & \quad + \sigma^2(W_{*,1j}\mathbf{X})\lambda_{2,j}^\top \mathbf{X}W_{*,2} + \sigma^{(1)}(W_{*,1j}\mathbf{X})\lambda_{3,j}^\top \mathbf{X}W_{*,2} + \sigma(W_{*,1j}\mathbf{X})\lambda_{2,j}^\top] \\ & + \sum_{j:|\mathcal{V}_j|>1} \exp((W_{*,2}\sigma(W_{*,1j}\mathbf{X}))^\top \mathbf{X}) [\sigma^{(1)}(W_{*,1j}\mathbf{X})\sigma(W_{*,1j}\mathbf{X})\mathbf{X}^\top \lambda_{1,j}\mathbf{X}W_{*,2} \\ & \quad + \sigma^2(W_{*,1j}\mathbf{X})\lambda_{2,j}^\top \mathbf{X}W_{*,2} + \sigma^{(1)}(W_{*,1j}\mathbf{X})\lambda_{3,j}^\top \mathbf{X}W_{*,2} + \sigma(W_{*,1j}\mathbf{X})\lambda_{2,j}^\top \\ & \quad + ([\sigma^{(1)}(W_{*,1j}\mathbf{X})]^2\sigma(W_{*,1j}\mathbf{X}) + \sigma^{(2)}(W_{*,1j}\mathbf{X})\sigma(W_{*,1j}\mathbf{X}))\mathbf{X}^\top \lambda_{4,j}\mathbf{X}\mathbf{X}^\top W_{*,2}W_{*,2} \\ & \quad + \sigma^2(W_{*,1j}\mathbf{X})\sigma(W_{*,1j}\mathbf{X})\mathbf{X}^\top \lambda_{5,j}\mathbf{X}W_{*,2} + \sigma^{(2)}(W_{*,1j}\mathbf{X})\mathbf{X}^\top \lambda_{4,j}\mathbf{X}W_{*,2} \\ & \quad + (\sigma^{(1)}(W_{*,1j}\mathbf{X})[\sigma(W_{*,1j}\mathbf{X})]^2\mathbf{X}^\top W_{*,2} + \sigma^{(1)}(W_{*,1j}\mathbf{X})\sigma(W_{*,1j}\mathbf{X}))\mathbf{X}^\top \lambda_{6,j}\mathbf{X}W_{*,2} \\ & \quad + \sigma^{(2)}(W_{*,1j}\mathbf{X})\mathbf{X}^\top \lambda_{6,j} + [\sigma^{(1)}(W_{*,1j}\mathbf{X})]^2\mathbf{X}^\top \lambda_{4,j}\mathbf{X}\mathbf{X}^\top W_{*,2}W_{*,2} \\ & \quad + \sigma^{(1)}(W_{*,1j}\mathbf{X})\sigma(W_{*,1j}\mathbf{X})\mathbf{X}^\top W_{*,2}\mathbf{X}^\top \lambda_{6,j} + \sigma^{(1)}(W_{*,1j}\mathbf{X})\sigma(W_{*,1j}\mathbf{X})\mathbf{X}^\top \lambda_{6,j}\mathbf{X}W_{*,2} \\ & \quad + [\sigma(W_{*,1j}\mathbf{X})]^2\mathbf{X}^\top \lambda_{5,j}] \end{aligned}$$

$$\begin{aligned}
& - \sum_{j:|\mathcal{V}_j|=1} \exp((W_{*,2}\sigma(W_{*,1j}\mathbf{X}))^\top \mathbf{X}) [\sigma^{(1)}(W_{*,1j}\mathbf{X})\mathbf{X}^\top \lambda_{1,j}\mathbf{X} + \sigma(W_{*,1j}\mathbf{X})\lambda_{2,j}^\top \mathbf{X}] f_{G_n}(\mathbf{X}) \\
& - \sum_{j:|\mathcal{V}_j|>1} \exp((W_{*,2}\sigma(W_{*,1j}\mathbf{X}))^\top \mathbf{X}) [\sigma^{(1)}(W_{*,1j}\mathbf{X})\mathbf{X}^\top \lambda_{1,j}\mathbf{X} + \sigma(W_{*,1j}\mathbf{X})\lambda_{2,j}^\top \mathbf{X} \\
& \quad + ([\sigma^{(1)}(W_{*,1j}\mathbf{X})]^2 + \sigma^{(2)}(W_{*,1j}\mathbf{X}))\mathbf{X}^\top \lambda_{4,j}\mathbf{X}\mathbf{X}^\top W_{*,2} + \sigma^2(W_{*,1j}\mathbf{X})\mathbf{X}^\top \lambda_{5,j}\mathbf{X} \\
& \quad + (\sigma^{(1)}(W_{*,1j}\mathbf{X})\sigma(W_{*,1j}\mathbf{X})\mathbf{X}^\top W_{*,2} + \sigma^{(1)}(W_{*,1j}\mathbf{X}))\mathbf{X}^\top \lambda_{6,j}\mathbf{X}] f_{G_n}(\mathbf{X}) \\
& - \sum_{j=1}^L \lambda_{0,j} \exp((W_{*,2}\sigma(W_{*,1j}\mathbf{X}))^\top \mathbf{X}) f_{G_n}(\mathbf{X}) \\
& + \sum_{j=1}^L \lambda_{0,j} \exp((W_{*,2}\sigma(W_{*,1j}\mathbf{X}))^\top \mathbf{X}) \sigma(W_{*,1j}\mathbf{X}) W_{*,2} = 0,
\end{aligned} \tag{26}$$

for almost surely \mathbf{X} . However, that equation implies that all the coefficients $\{\lambda_{0,j}, \lambda_{1,j}, \lambda_{2,j}, \lambda_{3,j}\}_{j:|\mathcal{V}_j|=1}$, $\{\lambda_{0,j}, \lambda_{1,j}, \lambda_{2,j}, \lambda_{3,j}, \lambda_{4,j}, \lambda_{5,j}, \lambda_{6,j}\}_{j:|\mathcal{V}_j|>1}$ are 0. It is a contradiction to the hypothesis that at least one coefficient among these coefficients is different from 0.

Consequently, we deduce that

$$\lim_{\varepsilon \rightarrow 0} \inf_{G \in \mathcal{G}_{L'}(\Theta): \mathcal{D}_1(G, G_*) \leq \varepsilon} \|f_G - f_{G_*}\|_{L_2(\mu)} / \mathcal{D}_1(G, G_*) > 0,$$

which suggests that the conclusion of the local part of the inequality (20) is proved.

A.1.2 Global part.

From the result of the local part of the inequality (20), we can find a positive constant ε' such that the following inequality holds:

$$\inf_{G \in \mathcal{G}_{L'}(\Theta): \mathcal{D}_1(G, G_*) \leq \varepsilon'} \|f_G - f_{G_*}\|_{L_2(\mu)} / \mathcal{D}_1(G, G_*) > 0.$$

To obtain the conclusion of the theorem, we only need to demonstrate that

$$\inf_{G \in \mathcal{G}_{L'}(\Theta): \mathcal{D}_1(G, G_*) > \varepsilon'} \|f_G - f_{G_*}\|_{L_2(\mu)} / \mathcal{D}_1(G, G_*) > 0.$$

We prove the claim by contradiction. Indeed, by assuming the claim does not hold, it implies that there exists a sequence of $G'_n := \sum_{j'=1}^{L'} \exp(b_{n,j'}) \delta_{(W_{n,1j'}, W_{n,2})}$ in the set $\mathcal{G}_{L'}(\Theta)$ such that

$$\begin{cases} \mathcal{D}_1(G'_n, G_*) > \varepsilon' \\ \|f_{G'_n} - f_{G_*}\|_{L_2(\mu)} / \mathcal{D}_1(G'_n, G_*) \rightarrow 0, \end{cases}$$

as long as n approaches the infinity. These results prove that $\|f_{G'_n} - f_{G_*}\|_{L_2(\mu)} \rightarrow 0$ as n goes to infinity.

From the hypothesis, the parameter space Θ is compact. Therefore, one of G'_n 's subsequences converges to some mixing measure G' where G' lies in the space $\mathcal{G}_{L'}(\Theta)$. From the hypothesis, we have $\mathcal{D}_1(G'_n, G_*) > \varepsilon'$. By taking the limit of both sides as $n \rightarrow \infty$, we obtain that $\mathcal{D}_1(G', G_*) \geq \varepsilon'$.

An application of the Fatou's lemma leads to the following result:

$$0 = \lim_{n \rightarrow \infty} \|f_{G'_n} - f_{G_*}\|_{L_2(\mu)} \geq \int \liminf_{n \rightarrow \infty} \|f_{G'_n}(\mathbf{X}) - f_{G_*}(\mathbf{X})\|^2 d\mu(\mathbf{X}).$$

This inequality is only possible if $f_{G'} = f_{G_*}$ for almost surely \mathbf{X} .

According to the identifiability of the function $f_G(\mathbf{X})$, that equation only holds when $G' \equiv G_*$. As a consequence, we obtain that $\mathcal{D}_1(G', G_*) = 0$. It contradicts to the assumption that $\mathcal{D}_1(G', G_*) \geq \varepsilon' > 0$. Hence, the proof of the global part is completed. We achieve the conclusion of the theorem.

Proof for the identifiability property. The key claim that we aim to show is that if the equation $f_G(\mathbf{X}) = f_{G_*}(\mathbf{X})$ holds for almost surely \mathbf{X} , we achieve that $G \equiv G_*$, namely, the two mixing measures are identical.

From the hypothesis, as $f_G(\mathbf{X}) = f_{G_*}(\mathbf{X})$ for almost all \mathbf{X} , we achieve that

$$\begin{aligned} & \sum_{j=1}^N \frac{\exp(\mathbf{X}^\top A_j^0 \mathbf{X} + a_j^0))}{D_{f,G}(\mathbf{X})} h(\mathbf{X}, \eta_j^0) + \sum_{j'=1}^{\tilde{L}} \frac{\exp((BW_2 \sigma(W_{1j'} \mathbf{X}))^\top \mathbf{X} + b_{j'})}{D_{f,G}(\mathbf{X})} CW_2 \sigma(W_{1j'} \mathbf{X}) \\ &= \sum_{j=1}^N \frac{\exp(\mathbf{X}^\top A_j^0 \mathbf{X} + a_j^0))}{D_{f,G_*}(\mathbf{X})} h(\mathbf{X}, \eta_j^0) + \sum_{j'=1}^L \frac{\exp((BW_{*,2} \sigma(W_{*,1j'} \mathbf{X}))^\top \mathbf{X} + b_{*,j'})}{D_{f,G_*}(\mathbf{X})} CW_{*,2} \sigma(W_{*,1j'} \mathbf{X}), \end{aligned} \tag{27}$$

where $G = \sum_{j=1}^{\tilde{L}} \exp(b_j) \delta_{(W_{1j}, W_2)}$. Furthermore, we define

$$\begin{aligned} D_{f,G_*}(\mathbf{X}) &= \sum_{k=1}^N \exp(\mathbf{X}^\top A_k^0 \mathbf{X} + a_k^0) + \sum_{j'=1}^L \exp((BW_{*,2} \sigma(W_{*,1j'} \mathbf{X}))^\top \mathbf{X} + b_{*,j'}), \\ D_{f,G}(\mathbf{X}) &= \sum_{k=1}^N \exp(\mathbf{X}^\top A_k^0 \mathbf{X} + a_k^0) + \sum_{j'=1}^{\tilde{L}} \exp((BW_2 \sigma(W_{1j'} \mathbf{X}))^\top \mathbf{X} + b_{j'}). \end{aligned}$$

That equation implies that the number of atoms of G and G_* should be identical, namely, we have $L = \tilde{L}$. Therefore, the following result holds

$$\left\{ \frac{\exp((BW_2 \sigma(W_{1j'} \mathbf{X}))^\top \mathbf{X} + b_{j'})}{D_{f,G}(\mathbf{X})} : j' \in [L] \right\} = \left\{ \frac{\exp((BW_{*,2} \sigma(W_{*,1j'} \mathbf{X}))^\top \mathbf{X} + b_{*,j'})}{D_{f,G_*}(\mathbf{X})} : j' \in [L] \right\},$$

for almost surely \mathbf{X} . By relabelling the indices of these two sets, we can assume without loss of generality that

$$\frac{\exp((BW_2 \sigma(W_{1j'} \mathbf{X}))^\top \mathbf{X} + b_{j'})}{D_{f,G}(\mathbf{X})} = \frac{\exp((BW_{*,2} \sigma(W_{*,1j'} \mathbf{X}))^\top \mathbf{X} + b_{*,j'})}{D_{f,G_*}(\mathbf{X})},$$

for any index $j' \in [L]$ and for almost surely \mathbf{X} . From the invariance to translation property of the

softmax function, the equation (27) becomes

$$\begin{aligned} & \sum_{j=1}^L \exp(b_j) \exp((BW_2 \sigma(W_{1j} \mathbf{X}))^\top \mathbf{X}) CW_2 \sigma(W_{1j} \mathbf{X}) \\ &= \sum_{j'=1}^L \exp(b_{*,j}) \exp((BW_{*,2} \sigma(W_{*,1j'} \mathbf{X}))^\top \mathbf{X}) CW_{*,2} \sigma(W_{*,1j'} \mathbf{X}), \end{aligned} \quad (28)$$

for almost surely \mathbf{X} . This equation suggests that there exists a partition K_1, K_2, \dots, K_m of the set $[L]$ for some m such that we have $\exp(b_{j_1}) = \exp(b_{*,j_2})$ for any $j_1, j_2 \in K_i$ and for any $i \in [m]$. According to that result, the equation (27) can be rewritten as follows:

$$\begin{aligned} & \sum_{i=1}^m \sum_{j_1 \in K_i} \exp(b_{j_1}) \exp((BW_2 \sigma(W_{1j_1} \mathbf{X}))^\top \mathbf{X}) CW_2 \sigma(W_{1j_1} \mathbf{X}) \\ &= \sum_{i=1}^m \sum_{j_2 \in K_i} \exp(b_{*,j_2}) \exp((BW_{*,2} \sigma(W_{*,1j_2} \mathbf{X}))^\top \mathbf{X}) CW_{*,2} \sigma(W_{*,1j_2} \mathbf{X}), \end{aligned}$$

for almost surely \mathbf{X} . That equation proves that

$$\{W_2 \sigma(W_{1j_1} \mathbf{X}) : j_1 \in K_i\} = \{W_{*,2} \sigma(W_{*,1j_2} \mathbf{X}) : j_2 \in K_i\},$$

for any $i \in [m]$. Since the activation function σ is identifiable, that result indicates that

$$\{(W_{1j_1}, W_2) : j_1 \in K_i\} = \{(W_{*,1j_2}, W_2) : j_2 \in K_i\}.$$

As a consequence, we arrive at the following result:

$$\sum_{i=1}^m \sum_{j_1 \in K_i} \exp(b_{j_1}) \delta_{(W_{1j_1}, W_2)} = \sum_{i=1}^m \sum_{j_2 \in K_i} \exp(b_{*,j_2}) \delta_{(W_{*,1j_2}, W_{*,2})}.$$

It is equivalent to $G \equiv G_*$. As a consequence, we obtain the conclusion of the identifiability property of the function f_G .

A.2 Proof of Proposition 1

Recall that $(\mathbf{X}_1, Y_1), (\mathbf{X}_2, Y_2), \dots, (\mathbf{X}_n, Y_n) \in \mathbb{R}^d \times \mathbb{R}^{d'}$ follow the regression model:

$$Y_i = f_{G_*}(\mathbf{X}_i) + \varepsilon_i, \quad i = 1, 2, \dots, n,$$

where the independent Gaussian noises $\varepsilon_1, \dots, \varepsilon_n$ are satisfy that $\mathbb{E}[\varepsilon_i | \mathbf{X}_i] = 0$ and $\text{Var}(\varepsilon_i | \mathbf{X}_i) = \sigma^2 I_{d'}$ for all $i \in [n]$. The true regression function takes the following form:

$$\begin{aligned} f_{G_*}(\mathbf{X}) := & \sum_{j=1}^N \frac{\exp(\mathbf{X}^\top A_j^0 \mathbf{X} + a_j^0)}{D_f(\mathbf{X})} \cdot h(\mathbf{X}, \eta_j^0) \\ & + \sum_{j'=1}^L \frac{\exp((BW_{*,2}^{(2)} \sigma(W_{*,1j'}^{(1)} \mathbf{X}))^\top \mathbf{X} + b_{*,j'}))}{D_f(\mathbf{X})} \cdot CW_{*,2}^{(2)} \sigma(W_{*,1j'}^{(1)} \mathbf{X}) \end{aligned}$$

where $D_f(\mathbf{X}) := \sum_{k=1}^N \exp(\mathbf{X}^\top A_k^0 \mathbf{X} + a_k^0) + \sum_{j'=1}^L \exp((BW_*^{(2)} \sigma(W_{*,j'}^{(1)} \mathbf{X}))^\top \mathbf{X} + b_{*,j'})$. The least square estimator \widehat{G}_n is defined as

$$\widehat{G}_n := \arg \min_{G \in \mathcal{G}_{L'}(\Theta)} \sum_{i=1}^n \|Y_i - f_G(\mathbf{X}_i)\|^2,$$

From the assumption that $\varepsilon_i | \mathbf{X}_i \sim \mathcal{N}(\mathbf{0}_d, \sigma^2 I_{d'})$, it indicates that the least square estimator \widehat{G}_n is indeed a maximum likelihood estimator, which is given by:

$$\widehat{G}_n \in \arg \max_{G \in \mathcal{G}_{L'}(\Theta)} \frac{1}{n} \sum_{i=1}^n \log(p(Y_i | f_G(\mathbf{X}_i), \sigma^2 I_{d'})),$$

where $p(Y_i | f_G(\mathbf{X}_i), \sigma^2 I_{d'})$ is the multivariate Gaussian distribution with mean $f_G(\mathbf{X})$ and covariance matrix $\sigma^2 I_{d'}$. From the result of Theorem 7.4 in [62], we obtain that

$$h(p(Y | f_{\widehat{G}_n}(\mathbf{X}), \sigma^2 I_{d'}), p(Y | f_{G_*}(\mathbf{X}), \sigma^2 I_{d'})) = \mathcal{O}_P(\sqrt{\log(n)/n}).$$

Given the close-form expression for the Hellinger distance between two multivariate Gaussian distributions, we have

$$h^2(p(Y | f_{\widehat{G}_n}(\mathbf{X}), \sigma^2 I_{d'}), p(Y | f_{G_*}(\mathbf{X}), \sigma^2 I_{d'})) = 1 - \exp \left\{ -\frac{1}{8\sigma^2} \|f_{\widehat{G}_n}(\mathbf{X}) - f_{G_*}(\mathbf{X})\|^2 \right\}.$$

Putting the above results together leads to

$$1 - \exp \left\{ -\frac{1}{8\sigma^2} \|f_{\widehat{G}_n}(\mathbf{X}) - f_{G_*}(\mathbf{X})\|^2 \right\} = \mathcal{O}_P(\log(n)/n).$$

Hence, for sufficiently large n , for some universal constant C the above inequality leads to

$$\begin{aligned} \|f_{\widehat{G}_n}(\mathbf{X}) - f_{G_*}(\mathbf{X})\|^2 &\leq 8\sigma^2 \log \left(\frac{1}{1 - C \log(n)/n} \right) \\ &= 8\sigma^2 \log \left(1 + \frac{C \log(n)/n}{1 - C \log(n)/n} \right) \\ &\leq 8\sigma^2 \cdot \frac{C \log(n)/n}{1 - C \log(n)/n} \\ &\leq 16\sigma^2 C \log(n)/n. \end{aligned}$$

It is equivalent to

$$\|f_{\widehat{G}_n}(\mathbf{X}) - f_{G_*}(\mathbf{X})\| = \mathcal{O}_P(\sqrt{\log(n)/n}).$$

As a consequence, we achieve that

$$\|f_{\widehat{G}_n} - f_{G_*}\|_{L_2(\mu)} = \left(\int_{\mathcal{X}} \|f_{\widehat{G}_n}(\mathbf{X}) - f_{G_*}(\mathbf{X})\|^2 d\mu(\mathbf{X}) \right)^{1/2} = \mathcal{O}_P(\sqrt{\log(n)/n}).$$

The proof of the proposition is completed.

B Additional Theoretical Results for Visual Adaptive Prompt Tuning

Thus far, in Section 5, we provide theoretical benefits of visual adaptive prompt tuning when the function σ in equation (12) is nonlinear. In this appendix, we demonstrate that the visual adaptive prompt tuning also has appealing theoretical properties when that function σ is linear.

Similar to the setting considered in Section 5, we provide a theoretical guarantee for the linear setting of the visual adaptive prompt tuning via the regression framework. For empirical results, please refer to Appendix E.4.

Problem setup. We assume that the i.i.d. samples of size n : $(\mathbf{X}_1, Y_1), (\mathbf{X}_2, Y_2), \dots, (\mathbf{X}_n, Y_n) \in \mathbb{R}^d \times \mathbb{R}^{d'}$ are generated from the model:

$$Y_i = f_{\tilde{G}_*}(\mathbf{X}_i) + \varepsilon_i, \quad i = 1, 2, \dots, n, \quad (29)$$

where $\varepsilon_1, \dots, \varepsilon_n$ are independent Gaussian noise variables such that $\mathbb{E}[\varepsilon_i | \mathbf{X}_i] = 0$ and $\text{Var}(\varepsilon_i | \mathbf{X}_i) = \nu^2 I_{d'}$ for all $1 \leq i \leq n$. Additionally, we assume that $\mathbf{X}_1, \mathbf{X}_2, \dots, \mathbf{X}_n$ are i.i.d. samples from some probability distribution μ . The regression function $f_{\tilde{G}_*}(\cdot)$ in equation (29) then takes the form of a prefix MoE model with N pre-trained experts and L unknown experts,

$$\begin{aligned} f_{\tilde{G}_*}(\mathbf{X}) := & \sum_{j=1}^N \frac{\exp(\mathbf{X}^\top A_j^0 \mathbf{X} + a_j^0)}{\tilde{D}_f(\mathbf{X})} \cdot h(\mathbf{X}, \eta_j^0) \\ & + \sum_{j'=1}^L \frac{\exp((BW_{*,2}W_{*,1j'}\mathbf{X})^\top \mathbf{X} + b_{*,j'})}{\tilde{D}_f(\mathbf{X})} \cdot CW_{*,2}W_{*,1j'}\mathbf{X}, \end{aligned} \quad (30)$$

where $\tilde{D}_{f,\tilde{G}_*}(\mathbf{X}) := \sum_{k=1}^N \exp(\mathbf{X}^\top A_k^0 \mathbf{X} + a_k^0) + \sum_{j'=1}^L \exp((BW_{*,2}W_{*,1j'}\mathbf{X})^\top \mathbf{X} + b_{*,j'})$, while $\tilde{G}_* := \sum_{j'=1}^L \exp(b_{*,j'}) \delta_{W_{*,2}W_{*,1j'}}$ denotes a *mixing measure*, i.e., a weighted sum of Dirac measures δ , associated with unknown parameters $(b_{*,j'}, W_{*,2}W_{*,1j'})_{j'=1}^L$ in the parameter space $\Theta \subset \mathbb{R} \times \mathbb{R}^{d \times d}$. At the same time, the values of the matrix A_j^0 , the expert parameter η_j^0 , and the bias parameter a_j^0 are known for all $1 \leq j \leq N$. Additionally, the matrices $B \in \mathbb{R}^{d \times d}$ and $C \in \mathbb{R}^{d' \times d}$ are given.

Least square estimator. In particular, we take into account the estimator

$$\tilde{G}_n := \arg \min_{G \in \mathcal{G}_{L'}(\Theta)} \sum_{i=1}^n \left(Y_i - f_G(\mathbf{X}_i) \right)^2, \quad (31)$$

Voronoi loss. The Voronoi loss tailored to the setting in equation (30) is defined as

$$\begin{aligned} \mathcal{D}_2(G, \tilde{G}_*) := & \sum_{j'=1}^L \left| \sum_{i \in \mathcal{V}_{j'}} \exp(b_i) - \exp(b_{*,j'}) \right| + \sum_{j' \in [L]: |\mathcal{V}_{j'}|=1} \sum_{i \in \mathcal{V}_{j'}} \exp(b_i) \|\Delta W_2 W_{1ij'}\| \\ & + \sum_{j' \in [L]: |\mathcal{V}_{j'}| > 1} \sum_{i \in \mathcal{V}_{j'}} \exp(b_i) \|\Delta W_2 W_{1ij'}\|^2, \end{aligned}$$

where we denote $\Delta W_2 W_{1ij'} := W_2 W_{1i} - W_{*,2} W_{*,1j'}$ for any i, j' . Equipped with this loss function, we wrap up the setting in equation (30) by providing the convergence rate of prompt estimation in Theorem 2.

Theorem 2. Given the least square estimator \tilde{G}_n defined in equation (31), we have that

$$\mathcal{D}_2(\tilde{G}_n, \tilde{G}_*) = \mathcal{O}_P([\log(n)/n]^{\frac{1}{2}}).$$

Proof of Theorem 2. Based on the convergence rate of regression function estimation presented in Proposition 1, our objective is to establish the following inequality:

$$\inf_{G \in \mathcal{G}_{L'}(\Theta)} \|f_G - f_{G_*}\|_{L_2(\mu)} / \mathcal{D}_2(G, G_*) > 0. \quad (32)$$

We partition the proof of the above inequality into local and global parts.

B.0.1 Local part.

The local part of the inequality (32) corresponds to the following inequality:

$$\lim_{\varepsilon \rightarrow 0} \inf_{G \in \mathcal{G}_{L'}(\Theta): \mathcal{D}_2(G, \tilde{G}_*) \leq \varepsilon} \frac{\|f_G - f_{\tilde{G}_*}\|_{L_2(\mu)}}{\mathcal{D}_2(G, \tilde{G}_*)} > 0.$$

We assume that the above inequality does not hold. Then, we can find a sequence of measures $G_n := \sum_{j'=1}^{L'} \exp(b_{n,j'}) \delta_{W_{n,2}W_{n,1j'}}$ in $\mathcal{G}_{L'}(\Theta)$ such that as $n \rightarrow \infty$, we have

$$\begin{cases} \mathcal{D}_{2n} := \mathcal{D}_2(G_n, \tilde{G}_*) \rightarrow 0, \\ \|f_{G_n} - f_{\tilde{G}_*}\|_{L_2(\mu)} / \mathcal{D}_{2n} \rightarrow 0. \end{cases}$$

Similar to the proof of Theorem 1, for the sake of the presentation, $\mathcal{V}_j^n := \mathcal{V}_j(G_n)$ is denoted as a Voronoi cell of G_n generated by the j -th components of the true measure \tilde{G}_* . Given that the ensuing arguments are asymptotic, without loss of generality we assume that those Voronoi cells do not depend on the sample size, *i.e.*, we have $\mathcal{V}_j = \mathcal{V}_j^n$ for all n and $1 \leq j \leq L$. Therefore, the Voronoi loss \mathcal{D}_{2n} can be rewritten as follows:

$$\begin{aligned} \mathcal{D}_{2n} := & \sum_{j'=1}^L \left| \sum_{i \in \mathcal{V}_{j'}} \exp(b_{n,i}) - \exp(b_{*,j'}) \right| + \sum_{j' \in [L]: |\mathcal{V}_{j'}|=1} \sum_{i \in \mathcal{V}_{j'}} \exp(b_{n,i}) \|\Delta W_{n,2}W_{n,1ij'}\| \\ & + \sum_{j' \in [L]: |\mathcal{V}_{j'}| > 1} \sum_{i \in \mathcal{V}_{j'}} \exp(b_{n,i}) \|\Delta W_{n,2}W_{n,1ij'}\|^2, \end{aligned}$$

where we define $\Delta W_{n,2}W_{n,1ij'} := W_{n,2}W_{n,1i} - W_{*,2}W_{*,1j'}$ for all $i \in \mathcal{V}_{j'}$.

From the hypothesis, since $\mathcal{D}_{2n} \rightarrow 0$ as n approaches ∞ , we find that $\sum_{i \in \mathcal{V}_j} \exp(b_{n,i}) \rightarrow \exp(b_{*,j})$ and $W_{n,2}W_{n,1i} \rightarrow W_{*,2}W_{*,1j'}$ for any $i \in \mathcal{V}_j$ and $j \in [L]$. Throughout this proof, we assume WLOG that $B = Id_d$, $C = Id_d$ and $r = 1$ for simplicity with a note that our techniques can totally be generalized to the general case. We partition the proof of the local part into three steps, as detailed below:

Step 1 - Taylor expansion. We first define the following function:

$$Q_n(\mathbf{X}) := \left[\sum_{j=1}^N \exp(\mathbf{X}^\top A_j^0 \mathbf{X} + a_j^0) + \sum_{j'=1}^L \exp((W_{*,2}W_{*,1j'} \mathbf{X})^\top \mathbf{X} + b_{*,j'}) \right] \cdot [f_{G_n}(\mathbf{X}) - f_{\tilde{G}_*}(\mathbf{X})].$$

Then, we can decompose the function $Q_n(\mathbf{X})$ as follows:

$$\begin{aligned}
Q_n(\mathbf{X}) &= \sum_{j=1}^L \sum_{i \in \mathcal{V}_j} \exp(b_{n,i}) \left[\exp((W_{n,2}W_{n,1i}\mathbf{X})^\top \mathbf{X}) W_{n,2}W_{n,1i}\mathbf{X} - \exp((W_{*,2}W_{*,1j}\mathbf{X})^\top \mathbf{X}) W_{*,2}W_{*,1j}\mathbf{X} \right] \\
&\quad - \sum_{j=1}^L \sum_{i \in \mathcal{V}_j} \exp(b_{n,i}) \left[\exp((W_{n,2}W_{n,1i}\mathbf{X})^\top \mathbf{X}) - \exp((W_{*,2}W_{*,1j}\mathbf{X})^\top \mathbf{X}) \right] f_{G_n}(\mathbf{X}) \\
&\quad + \sum_{j=1}^L \left(\sum_{i \in \mathcal{V}_j} \exp(b_{n,i}) - \exp(b_{*,j}) \right) \exp((W_{*,2}W_{*,1j}\mathbf{X})^\top \mathbf{X}) \left[W_{*,2}W_{*,1j}\mathbf{X} - f_{G_n}(\mathbf{X}) \right] \\
&:= \tilde{A}_n(\mathbf{X}) - \tilde{B}_n(\mathbf{X}) + \tilde{C}_n(\mathbf{X}).
\end{aligned} \tag{33}$$

Decomposition of the function $\tilde{A}_n(\mathbf{X})$. To streamline the argument, we define the following functions: $\tilde{E}(\mathbf{X}; W_2W_1) := \exp((W_2W_1\mathbf{X})^\top \mathbf{X})$ and $\tilde{H}(\mathbf{X}; W_2W_1) = W_2W_1\mathbf{X}$. The product of the functions \tilde{E} and \tilde{H} is defined as $\tilde{F}(\mathbf{X}; W_2W_1) = \tilde{E}(\mathbf{X}; W_2W_1)\tilde{H}(\mathbf{X}; W_2W_1)$. To account for the difference in the number of elements among Voronoi cells, we further decompose the function $A_n(\mathbf{X})$ as follows:

$$\begin{aligned}
\tilde{A}_n(\mathbf{X}) &= \sum_{j:|\mathcal{V}_j|=1} \sum_{i \in \mathcal{V}_j} \exp(b_{n,i}) \left[\tilde{F}(\mathbf{X}; W_{n,2}W_{n,1i}) - \tilde{F}(\mathbf{X}; W_{*,2}W_{*,1j}) \right] \\
&\quad + \sum_{j:|\mathcal{V}_j|>1} \sum_{i \in \mathcal{V}_j} \exp(b_{n,i}) \left[\tilde{F}(\mathbf{X}; W_{n,2}W_{n,1i}) - \tilde{F}(\mathbf{X}; W_{*,2}W_{*,1j}) \right] \\
&:= \tilde{A}_{n,1}(\mathbf{X}) + \tilde{A}_{n,2}(\mathbf{X})
\end{aligned}$$

An application of the first-order Taylor expansion to the function \tilde{E} and \tilde{H} leads to

$$\begin{aligned}
\tilde{E}(\mathbf{X}; W_{n,2}W_{n,1i}) &= \tilde{E}(\mathbf{X}; W_{*,2}W_{*,1j}) + \sum_{|\alpha|=1} (\Delta W_{n,2}W_{n,1ij})^\alpha \frac{\partial^{|\alpha|} \tilde{E}}{\partial (W_2W_1)^\alpha}(\mathbf{X}; W_{*,2}W_{*,1j}) + \tilde{R}_{ij,1}(\mathbf{X}), \\
\tilde{H}(\mathbf{X}; W_{n,2}W_{n,1i}) &= \tilde{H}(\mathbf{X}; W_{*,2}W_{*,1j}) + \sum_{|\alpha|=1} (\Delta W_{n,2}W_{n,1ij})^\alpha \frac{\partial^{|\alpha|} \tilde{H}}{\partial (W_2W_1)^\alpha}(\mathbf{X}; W_{*,2}W_{*,1j}) + \tilde{R}_{ij,2}(\mathbf{X}),
\end{aligned}$$

Here, the indices i, j in these equations satisfy that $|\mathcal{V}_j| = 1$, i.e., Voronoi cells with exactly one element and $i \in \mathcal{V}_j$. Furthermore, the functions $\tilde{R}_{ij,1}(\mathbf{X})$ and $\tilde{R}_{ij,2}(\mathbf{X})$ in these equations correspond to Taylor remainders when expanding the functions \tilde{E} and \tilde{H} . Putting the above results together leads to

$$\begin{aligned}
\tilde{A}_{n,1}(\mathbf{X}) &= \sum_{j:|\mathcal{V}_j|=1} \sum_{i \in \mathcal{V}_j} \frac{\exp(b_{n,i})}{\alpha!} \sum_{|\alpha|=1} \left\{ (\Delta W_{n,2}W_{n,1ij})^\alpha \frac{\partial^{|\alpha|} \tilde{E}}{\partial (W_2W_1)^\alpha}(\mathbf{X}; W_{*,2}W_{*,1j}) \tilde{H}(\mathbf{X}; W_{*,2}W_{*,1j}) \right. \\
&\quad \left. + (\Delta W_{n,2}W_{n,1ij})^\alpha \frac{\partial^{|\alpha|} \tilde{H}}{\partial (W_2W_1)^\alpha}(\mathbf{X}; W_{*,2}W_{*,1j}) \tilde{E}(\mathbf{X}; W_{*,2}W_{*,1j}) \right\} + \hat{R}_{n,1}(\mathbf{X}) \\
&= \sum_{j:|\mathcal{V}_j|=1} \sum_{|\alpha|=1} \left\{ \tilde{M}_{n,j,\alpha} \frac{\partial^{|\alpha|} \tilde{E}}{\partial (W_2W_1)^\alpha}(\mathbf{X}; W_{*,2}W_{*,1j}) \tilde{H}(\mathbf{X}; W_{*,2}W_{*,1j}) \right. \\
&\quad \left. + \tilde{M}_{n,j,\alpha} \frac{\partial^{|\alpha|} \tilde{H}}{\partial (W_2W_1)^\alpha}(\mathbf{X}; W_{*,2}W_{*,1j}) \tilde{E}(\mathbf{X}; W_{*,2}W_{*,1j}) \right\} + \hat{R}_{n,1}(\mathbf{X})
\end{aligned}$$

where $\alpha = (\alpha_1, \alpha_2)$. Furthermore, due to the uniform smoothness of the functions \tilde{E} and \tilde{H} , the function $\hat{R}_{n,1}(\mathbf{X})$ in that equation satisfies that $\hat{R}_{n,1}(\mathbf{X})/\mathcal{D}_{2n} \rightarrow 0$ when n approaches infinity. Finally, the terms $\tilde{M}_{n,j,\alpha}$ in that equation admit the following forms:

$$\tilde{M}_{n,j,\alpha} = \sum_{i \in \mathcal{V}_j} \frac{\exp(b_{n,i})}{\alpha!} (\Delta W_{n,2} W_{n,1ij})^\alpha,$$

for any $|\alpha| = 1$.

We now move to decompose the function $\tilde{A}_{n,2}(\mathbf{X})$. Different from the function $\tilde{A}_{n,1}(\mathbf{X})$ where we utilize only first-order Taylor expansion, to account for more than one element in the Voronoi cells in $\tilde{A}_{n,2}(\mathbf{X})$, we resort to the second-order Taylor expansions to the functions \tilde{E} and \tilde{H} . In particular, an application of the second-order Taylor expansion leads to

$$\begin{aligned} \tilde{A}_{n,2}(\mathbf{X}) = & \sum_{j:|\mathcal{V}_j|>1} \sum_{1 \leq |\alpha| \leq 2} \left\{ \tilde{M}_{n,j,\alpha} \frac{\partial^{|\alpha|} \tilde{E}}{\partial(W_2 W_1)^\alpha}(\mathbf{X}; W_{*,2} W_{*,1j}) \tilde{H}(\mathbf{X}; W_{*,2} W_{*,1j}) \right. \\ & + \tilde{M}_{n,j,\alpha} \frac{\partial^{|\alpha|} \tilde{H}}{\partial(W_2 W_1)^\alpha}(\mathbf{X}; W_{*,2} W_{*,1j}) \tilde{E}(\mathbf{X}; W_{*,2} W_{*,1j}) \Big\} \\ & + \sum_{|\alpha|=1, |\beta|=1} \tilde{M}_{n,j,\alpha,\beta} \frac{\partial^{|\alpha|} \tilde{E}}{\partial(W_2 W_1)^\alpha}(\mathbf{X}; W_{*,2} W_{*,1j}) \frac{\partial^{|\beta|} \tilde{H}}{\partial(W_2 W_1)^\beta}(\mathbf{X}; W_{*,2} W_{*,1j}) + \hat{R}_{n,2}(\mathbf{X}) \end{aligned}$$

where $\alpha = (\alpha_1, \alpha_2)$, $\beta = (\beta_1, \beta_2)$. Furthermore, due to the uniform smoothest of the functions \tilde{E} and \tilde{H} , the function $\hat{R}_{n,2}(\mathbf{X})$, which is the combination of Taylor remainders from the second-order Taylor expansion, satisfies that $\hat{R}_{n,2}(\mathbf{X})/\mathcal{D}_{2n} \rightarrow 0$ when n goes to infinity. Furthermore, the coefficients $\tilde{M}_{n,j,\alpha}$ and $\tilde{M}_{n,j,\alpha,\beta}$ in the above formulation takes the following forms:

$$\tilde{M}_{n,j,\alpha} = \sum_{i \in \mathcal{V}_j} \frac{\exp(b_{n,i})}{\alpha!} (\Delta W_{n,2} W_{n,1ij})^\alpha,$$

for any coefficient $\alpha = (\alpha_1, \alpha_2)$ such that $|\alpha| = 2$ and

$$\tilde{M}_{n,j,\alpha,\beta} = \sum_{i \in \mathcal{V}_j} \frac{\exp(b_{n,i})}{\alpha! \beta!} (\Delta W_{n,2} W_{n,1ij})^{\alpha+\beta},$$

for any coefficients $\alpha = (\alpha_1, \alpha_2)$ and $\beta = (\beta_1, \beta_2)$ such that $|\alpha| = |\beta| = 1$. Given the formulations of the functions $\tilde{E}(\mathbf{X}; W_1, W_2)$ and $\tilde{H}(\mathbf{X}; W_1, W_2)$, their partial derivatives take the

$$\begin{aligned} \frac{\partial \tilde{E}}{\partial(W_2 W_1)^{(u_1 v_1)}}(\mathbf{X}; W_2 W_1) &= \mathbf{X}^{(u_1)} \mathbf{X}^{(v_1)} \exp((W_2 W_1 \mathbf{X})^\top \mathbf{X}) \\ \frac{\partial^2 \tilde{E}}{\partial(W_2 W_1)^{(u_1 v_1)} \partial(W_2 W_1)^{(u_2 v_2)}}(\mathbf{X}; W_2 W_1) &= \mathbf{X}^{(u_1)} \mathbf{X}^{(v_1)} \mathbf{X}^{(u_2)} \mathbf{X}^{(v_2)} \exp((W_2 W_1 \mathbf{X})^\top \mathbf{X}), \\ \frac{\partial \tilde{H}}{\partial(W_2 W_1)^{(u_1 v_1)}}(\mathbf{X}; W_2 W_1) &= \mathbf{X}^{(v_1)} e_{u_1}, \\ \frac{\partial^2 \tilde{H}}{\partial(W_2 W_1)^{(u_1 v_1)} \partial(W_2 W_1)^{(u_2 v_2)}}(\mathbf{X}; W_2 W_1) &= \mathbf{0}_d. \end{aligned}$$

Putting the above formulations together, the functions $\tilde{A}_{n,1}(\mathbf{X})$ and $\tilde{A}_{n,2}(\mathbf{X})$ can be rewritten as follows:

$$\begin{aligned}\tilde{A}_{n,1}(\mathbf{X}) &= \sum_{j:|\mathcal{V}_j|=1} \exp((W_{*,2}W_{*,1j}\mathbf{X})^\top \mathbf{X}) \left[\sum_{u_1,v_1=1}^d M_{n,j,e_{u_1v_1}} \mathbf{X}^{(u_1)} \mathbf{X}^{(v_1)} W_{*,2}W_{*,1j} \mathbf{X} \right. \\ &\quad \left. + \sum_{u_1,v_1=1}^d M_{n,j,e_{u_1v_1}} \mathbf{X}^{(v_1)} e_{u_1} \right] + \hat{R}_{n,1}(\mathbf{X}), \\ \tilde{A}_{n,2}(\mathbf{X}) &= \sum_{j:|\mathcal{V}_j|>1} \exp((W_{*,2}W_{*,1j}\mathbf{X})^\top \mathbf{X}) \left[\sum_{u_1,v_1=1}^d M_{n,j,e_{u_1v_1}} \mathbf{X}^{(u_1)} \mathbf{X}^{(v_1)} W_{*,2}W_{*,1j} \mathbf{X} \right. \\ &\quad + \sum_{u_1,v_1=1}^d M_{n,j,e_{u_1v_1}} \mathbf{X}^{(v_1)} e_{u_1} + \sum_{u_1,v_1=1}^d \sum_{u_2,v_2=1}^d M_{n,j,e_{u_1v_1}+e_{u_2v_2}} \mathbf{X}^{(u_1)} \mathbf{X}^{(v_1)} \mathbf{X}^{(u_2)} \mathbf{X}^{(v_2)} W_{*,2}W_{*,1j} \mathbf{X} \\ &\quad \left. + \sum_{u_1,v_1=1}^d \sum_{u_2,v_2=1}^d M_{n,j,e_{u_1v_1},e_{u_2v_2}} \mathbf{X}^{(u_1)} \mathbf{X}^{(v_1)} \mathbf{X}^{(v_2)} e_{u_2} \right] + \hat{R}_{n,2}(\mathbf{X})\end{aligned}$$

Here, we denote e_u is the standard basis vector in \mathbb{R}^d with 1 in the u -th position and 0 in all other positions for any $1 \leq u \leq d$, while e_{uv} stands for the matrix in $\mathbb{R}^{d \times d}$ with its uv -th entry is 1 while other entries are zero.

Decomposition of the function $\tilde{B}_n(\mathbf{X})$. Similar to our decomposition of the function $\tilde{A}_n(\mathbf{X})$, we also separate the Voronoi cells with exactly one element and with more than one element in the decomposition of the function $\tilde{B}_n(\mathbf{X})$. Therefore, we obtain that

$$\begin{aligned}\tilde{B}_n(\mathbf{X}) &= \sum_{j:|\mathcal{V}_j|=1} \sum_{i \in \mathcal{V}_j} \exp(b_{n,i}) \left[\tilde{E}(\mathbf{X}; W_{n,2}W_{n,1i}) - \tilde{E}(\mathbf{X}; W_{*,2}W_{*,1j}) \right] f_{G_n}(\mathbf{X}) \\ &\quad + \sum_{j:|\mathcal{V}_j|>1} \sum_{i \in \mathcal{V}_j} \exp(b_{n,i}) \left[\tilde{E}(\mathbf{X}; W_{n,2}W_{n,1i}) - \tilde{E}(\mathbf{X}; W_{*,2}W_{*,1j}) \right] f_{G_n}(\mathbf{X}) \\ &:= \tilde{B}_{n,1}(\mathbf{X}) + \tilde{B}_{n,2}(\mathbf{X}).\end{aligned}$$

For Voronoi cells with exactly one element, we will utilize Taylor expansion up to the first order while for Voronoi cells with more than one element, the second-order Taylor expansion will be employed. This strategy leads to the following representations:

$$\begin{aligned}\tilde{B}_{n,1}(\mathbf{X}) &= \sum_{j:|\mathcal{V}_j|=1} \sum_{|\alpha|=1} \tilde{M}_{n,j,\alpha} \frac{\partial^{|\alpha|} \tilde{E}}{\partial (W_2 W_1)^\alpha}(\mathbf{X}; W_{*,2}W_{*,1j}) f_{G_n}(\mathbf{X}) + \tilde{R}_{n,3}(\mathbf{X}), \\ \tilde{B}_{n,2}(\mathbf{X}) &= \sum_{j:|\mathcal{V}_j|=1} \sum_{1 \leq |\alpha| \leq 2} \tilde{M}_{n,j,\alpha} \frac{\partial^{|\alpha|} \tilde{E}}{\partial (W_2 W_1)^\alpha}(\mathbf{X}; W_{*,2}W_{*,1j}) f_{G_n}(\mathbf{X}) + \tilde{R}_{n,4}(\mathbf{X}).\end{aligned}$$

In these expressions, the functions $\tilde{R}_{n,3}(\mathbf{X})$ and $\tilde{R}_{n,4}(\mathbf{X})$ correspond to the Taylor remainders. Due to the uniform smoothness of the functions \tilde{E} , we obtain that $\tilde{R}_{n,3}(\mathbf{X})/\mathcal{D}_{2n} \rightarrow 0$ and $\tilde{R}_{n,4}(\mathbf{X})/\mathcal{D}_{2n} \rightarrow 0$

as n approaches infinity. By computing the closed-form formulations for the partial derivatives of the function \tilde{E} , both the functions $\tilde{B}_{n,1}(\mathbf{X})$ and $\tilde{B}_{n,2}(\mathbf{X})$ can be rewritten as follows:

$$\begin{aligned}\tilde{B}_{n,1}(\mathbf{X}) &= \sum_{j:|\mathcal{V}_j|=1} \exp((W_{*,2}W_{*,1j}\mathbf{X})^\top \mathbf{X}) \left[\sum_{u_1,v_1=1}^d \tilde{M}_{n,j,e_{u_1v_1}} \mathbf{X}^{(u_1)} \mathbf{X}^{(v_1)} \right] f_{G_n}(\mathbf{X}) + \tilde{R}_{n,3}(\mathbf{X}), \\ \tilde{B}_{n,2}(\mathbf{X}) &= \sum_{j:|\mathcal{V}_j|>1} \exp((W_{*,2}W_{*,1j}\mathbf{X})^\top \mathbf{X}) \left[\sum_{u_1,v_1=1}^d \tilde{M}_{n,j,e_{u_1v_1}} \mathbf{X}^{(u_1)} \mathbf{X}^{(v_1)} \right. \\ &\quad \left. + \sum_{u_1,v_1=1}^d \sum_{u_2,v_2=1}^d \tilde{M}_{n,j,e_{u_1v_1}} \mathbf{X}^{(u_1)} \mathbf{X}^{(v_1)} \mathbf{X}^{(u_2)} \mathbf{X}^{(v_2)} \right] f_{G_n}(\mathbf{X}) + \tilde{R}_{n,4}(\mathbf{X}),\end{aligned}$$

Plugging all of these results together, the function $Q_n(\mathbf{X})$ can be rewritten as follows:

$$\begin{aligned}Q_n(\mathbf{X}) &= \sum_{j:|\mathcal{V}_j|=1} \exp((W_{*,2}W_{*,1j}\mathbf{X})^\top \mathbf{X}) \left[\sum_{u_1,v_1=1}^d \tilde{M}_{n,j,e_{u_1v_1}} \mathbf{X}^{(u_1)} \mathbf{X}^{(v_1)} W_{*,2}W_{*,1j}\mathbf{X} + \sum_{u_1,v_1=1}^d \tilde{M}_{n,j,e_{u_1v_1}} \mathbf{X}^{(v_1)} e_{u_1} \right] \\ &\quad + \sum_{j:|\mathcal{V}_j|>1} \exp((W_{*,2}W_{*,1j}\mathbf{X})^\top \mathbf{X}) \left[\sum_{u_1,v_1=1}^d \tilde{M}_{n,j,e_{u_1v_1}} \mathbf{X}^{(u_1)} \mathbf{X}^{(v_1)} W_{*,2}W_{*,1j}\mathbf{X} + \sum_{u_1,v_1=1}^d \tilde{M}_{n,j,e_{u_1v_1}} \mathbf{X}^{(v_1)} e_{u_1} \right. \\ &\quad \left. + \sum_{u_1,v_1=1}^d \sum_{u_2,v_2=1}^d \tilde{M}_{n,j,e_{u_1v_1}+e_{u_2v_2}} \mathbf{X}^{(u_1)} \mathbf{X}^{(v_1)} \mathbf{X}^{(u_2)} \mathbf{X}^{(v_2)} W_{*,2}W_{*,1j}\mathbf{X} \right. \\ &\quad \left. + \sum_{u_1,v_1=1}^d \sum_{u_2,v_2=1}^d \tilde{M}_{n,j,e_{u_1v_1},e_{u_2v_2}} \mathbf{X}^{(u_1)} \mathbf{X}^{(v_1)} \mathbf{X}^{(v_2)} e_{u_2} \right] \\ &\quad - \sum_{j:|\mathcal{V}_j|=1} \exp((W_{*,2}W_{*,1j}\mathbf{X})^\top \mathbf{X}) \left[\sum_{u_1,v_1=1}^d \tilde{M}_{n,j,e_{u_1v_1}} \mathbf{X}^{(u_1)} \mathbf{X}^{(v_1)} \right] f_{G_n}(\mathbf{X}) \\ &\quad - \sum_{j:|\mathcal{V}_j|>1} \exp((W_{*,2j}W_{*,1j}\mathbf{X})^\top \mathbf{X}) \left[\sum_{u_1,v_1=1}^d \tilde{M}_{n,j,e_{u_1v_1}} \mathbf{X}^{(u_1)} \mathbf{X}^{(v_1)} \right. \\ &\quad \left. + \sum_{u_1,v_1=1}^d \sum_{u_2,v_2=1}^d \tilde{M}_{n,j,e_{u_1v_1}} \mathbf{X}^{(u_1)} \mathbf{X}^{(v_1)} \mathbf{X}^{(u_2)} \mathbf{X}^{(v_2)} \right] f_{G_n}(\mathbf{X}) \\ &\quad - \sum_{j=1}^L \tilde{N}_{n,j} \exp((W_{*,2}W_{*,1j}\mathbf{X})^\top \mathbf{X}) f_{G_n}(\mathbf{X}) \\ &\quad + \sum_{j=1}^L \tilde{N}_{n,j} \exp((W_{*,2}W_{*,1j}\mathbf{X})^\top \mathbf{X}) W_{*,2}W_{*,1j}\mathbf{X} \\ &\quad + \hat{R}_{n,1}(\mathbf{X}) + \hat{R}_{n,2}(\mathbf{X}) - \tilde{R}_{n,3}(\mathbf{X}) - \tilde{R}_{n,4}(\mathbf{X})\end{aligned}\tag{34}$$

where $\tilde{N}_{n,j} := \sum_{i \in \mathcal{V}_j} \exp(b_{n,i}) - \exp(b_{*,j})$ for any $j \in [L]$.

Step 2 - Non-vanishing coefficients. An important insight from equation (34) is that the ratio $Q_n(\mathbf{X})/\mathcal{D}_{1n}$ can be expressed as a linear combination of the following independent functions:

$$\begin{aligned} & E(\mathbf{X}; W_{*,2}W_{*,1j})\mathbf{X}^{(u_1)}\mathbf{X}^{(v_1)}W_{*,2}W_{*,1j}\mathbf{X}, \quad E(\mathbf{X}; W_{*,2}W_{*,1j})\mathbf{X}^{(v_1)}e_{u_1}, \\ & E(\mathbf{X}; W_{*,2}W_{*,1j})\mathbf{X}^{(u_1)}\mathbf{X}^{(v_1)}\mathbf{X}^{(u_2)}W_{*,2}W_{*,1j}\mathbf{X}, \quad E(\mathbf{X}; W_{*,2}W_{*,1j})\mathbf{X}^{(u_1)}\mathbf{X}^{(v_1)}\mathbf{X}^{(v_2)}e_{u_2}, \\ & E(\mathbf{X}; W_{*,2}W_{*,1j})\mathbf{X}^{(u_1)}\mathbf{X}^{(v_1)}f_{G_n}(\mathbf{X}), \quad E(\mathbf{X}; W_{*,2}W_{*,1j})\mathbf{X}^{(u_1)}\mathbf{X}^{(v_1)}\mathbf{X}^{(u_2)}\mathbf{X}^{(v_2)}f_{G_n}(\mathbf{X}), \\ & E(\mathbf{X}; W_{*,2}W_{*,1j})f_{G_n}(\mathbf{X}), \quad E(\mathbf{X}; W_{*,2}W_{*,1j})W_{*,2j}W_{*,1j}\mathbf{X}, \end{aligned}$$

for any $1 \leq j \leq L$ and $1 \leq u, v, w \leq d$.

We proceed to demonstrate that not all of the coefficients of these linear independent functions go to 0 as n goes to infinity. We prove that claim by contradiction. We assume that all these coefficients go to 0 as n goes to ∞ . From the representation of the ratio $Q_n(\mathbf{X})/\mathcal{D}_{2n}$ in terms of these linear independent functions, we obtain that these ratios $\tilde{M}_{n,j,\alpha}/\mathcal{D}_{2n}$, $\tilde{M}_{n,j,\alpha,\beta}/\mathcal{D}_{2n}$, and $\tilde{N}_{n,j}/\mathcal{D}_{2n}$ approach 0 as $n \rightarrow \infty$, for all $\alpha, \beta \in \mathbb{N}^{d \times d}$ such that $1 \leq |\alpha| + |\beta| \leq 2$.

By first considering the vanishing of the ratio $\tilde{N}_{n,j}/\mathcal{D}_{2n} \rightarrow 0$, we find that

$$\frac{|\sum_{i \in \mathcal{V}_j} \exp(b_{n,i}) - \exp(b_{*,j})|}{\mathcal{D}_{2n}} = \frac{|\tilde{N}_{n,j}|}{\mathcal{D}_{2n}} \rightarrow 0,$$

for any $1 \leq j \leq L$. By varying the index j from 1 to L in these limits and summing these limits, we find that

$$\frac{\sum_{j=1}^L |\sum_{i \in \mathcal{V}_j} \exp(b_{n,i}) - \exp(b_{*,j})|}{\mathcal{D}_{2n}} \rightarrow 0. \quad (35)$$

Our strategy now is to consider the limits corresponding to Voronoi cells with exactly one element and more than one element separately. In particular, for Voronoi cells with exactly one element, namely, for indices $j \in [L]$ such that their corresponding Voronoi cells have one element, i.e., $|\mathcal{V}_j| = 1$, as the ratio $\tilde{M}_{n,j,e_{uv}}/\mathcal{D}_{2n} \rightarrow 0$, we have

$$\frac{\sum_{i \in \mathcal{V}_j} \exp(b_{n,i}) \|\Delta W_{n,2}W_{n,1ij}\|_1}{\mathcal{D}_{2n}} = \frac{\sum_{u,v=1}^d |\tilde{M}_{n,j,e_{uv}}|}{\mathcal{D}_{2n}} \rightarrow 0.$$

Due to the equivalence between the ℓ_1 norm and the ℓ_2 norm, we deduce that

$$\frac{\sum_{j:|\mathcal{V}_j|=1} \sum_{i \in \mathcal{V}_j} \exp(b_{n,i}) \|\Delta W_{n,2}W_{n,1ij}\|}{\mathcal{D}_{2n}} \rightarrow 0. \quad (36)$$

We now move to the Voronoi cells with more than one element, namely, indices $j \in [L]$ such that $|\mathcal{V}_j| > 1$. As the ratio $\tilde{M}_{n,j,2e_{uv}}/\mathcal{D}_{2n} \rightarrow 0$, we obtain that

$$\frac{\sum_{i \in \mathcal{V}_j} \exp(b_{n,i}) \|\Delta W_{n,2}W_{n,1ij}\|^2}{\mathcal{D}_{2n}} = \frac{\sum_{u,v=1}^d \tilde{M}_{n,j,2e_{uv}}}{\mathcal{D}_{2n}} \rightarrow 0. \quad (37)$$

Combining all the results in equations (35), (36), and (37), we obtain that

$$\frac{\mathcal{D}_{2n}}{\mathcal{D}_{2n}} = 1 \rightarrow 0, \text{ as } n \rightarrow \infty,$$

which is a contradiction. As a consequence, at least one of the coefficients of the linear independent functions in the expression of the ratio $Q_n(\mathbf{X})/\mathcal{D}_{2n}$ does not go to 0 as n approaches infinity.

Step 3 - Application of Fatou's lemma. The idea of this step is to divide all of the coefficients of the linear independent terms in the expression of the ratio $Q_n(\mathbf{X})/\mathcal{D}_{2n}$, namely, the terms $\tilde{M}_{n,j,\alpha}/\mathcal{D}_{2n}$, $\tilde{M}_{n,j,\alpha,\beta}/\mathcal{D}_{2n}$, and $\tilde{N}_{n,j}/\mathcal{D}_{2n}$ for all $\alpha, \beta \in \mathbb{N}^{d \times d}$ such that $1 \leq |\alpha| + |\beta| \leq 2$, by the maximum of their absolute values. In particular, we first denote m_n as the maximum of the absolute values of those coefficients. As not all of these coefficients go to 0, it demonstrates that $1/m_n$ does not go to infinity as $n \rightarrow \infty$.

From the hypothesis, we have $\|f_{G_n} - f_{\tilde{G}_*}\|_{L_2(\mu)}/\mathcal{D}_{2n} \rightarrow 0$ as $n \rightarrow \infty$. Since $1/m_n \not\rightarrow \infty$, it follows that $\|f_{G_n} - f_{\tilde{G}_*}\|_{L_2(\mu)}/(m_n \mathcal{D}_{2n}) \rightarrow 0$. An application of the Fatou's lemma leads to

$$0 = \lim_{n \rightarrow \infty} \frac{\|f_{G_n} - f_{\tilde{G}_*}\|_{L_2(\mu)}}{m_n \mathcal{D}_{2n}} \geq \int \liminf_{n \rightarrow \infty} \frac{|f_{G_n}(\mathbf{X}) - f_{\tilde{G}_*}(\mathbf{X})|}{m_n \mathcal{D}_{2n}} d\mu(\mathbf{X}) \geq 0.$$

Combining all of the above results, we obtain that $\liminf_{n \rightarrow \infty} \frac{|f_{G_n}(\mathbf{X}) - f_{\tilde{G}_*}(\mathbf{X})|}{m_n \mathcal{D}_{2n}} = 0$ for almost surely \mathbf{X} . To ease the presentation, we denote the following limits:

$$\frac{\tilde{M}_{n,j,\alpha}}{m_n \mathcal{D}_{2n}} \rightarrow \lambda_{j,\alpha}, \quad \frac{\tilde{M}_{n,j,\alpha,\beta}}{m_n \mathcal{D}_{2n}} \rightarrow \xi_{j,\alpha,\beta}, \quad \frac{\tilde{N}_{n,j}}{m_n \mathcal{D}_{2n}} \rightarrow \tau_j,$$

for any $1 \leq j \leq L$ and $\alpha, \beta \in \mathbb{N}^{d \times d}$ such that $1 \leq |\alpha| + |\beta| \leq 2$. By the definition of m_n , at least one coefficient in the set $\{\lambda_{j,\alpha}, \xi_{j,\alpha,\beta}, \tau_j : j \in [L], \alpha, \beta \in \mathbb{N}^{d \times d} : 1 \leq |\alpha| + |\beta| \leq 2\}$ must be nonzero.

Then, the equation $\liminf_{n \rightarrow \infty} \frac{|f_{G_n}(\mathbf{X}) - f_{\tilde{G}_*}(\mathbf{X})|}{m_n \mathcal{D}_{2n}} = 0$, or equivalently, $\liminf_{n \rightarrow \infty} \frac{|Q_n(\mathbf{X})|}{m_n \mathcal{D}_{2n}} = 0$

leads to

$$\begin{aligned}
& \sum_{j:|\mathcal{V}_j|=1} \exp((W_{*,2}W_{*,1j}\mathbf{X})^\top \mathbf{X}) \left[\sum_{u_1,v_1=1}^d \lambda_{j,e_{u_1v_1}} \mathbf{X}^{(u_1)} \mathbf{X}^{(v_1)} W_{*,2}W_{*,1j}\mathbf{X} + \sum_{u_1,v_1=1}^d \lambda_{j,e_{u_1v_1}} \mathbf{X}^{(v_1)} e_{u_1} \right] \\
& + \sum_{j:|\mathcal{V}_j|>1} \exp((W_{*,2}W_{*,1j}\mathbf{X})^\top \mathbf{X}) \left[\sum_{u_1,v_1=1}^d \lambda_{j,e_{u_1v_1}} \mathbf{X}^{(u_1)} \mathbf{X}^{(v_1)} W_{*,2}W_{*,1j}\mathbf{X} + \sum_{u_1,v_1=1}^d \lambda_{j,e_{u_1v_1}} \mathbf{X}^{(v_1)} e_{u_1} \right. \\
& \quad + \sum_{u_1,v_1=1}^d \sum_{u_2,v_2=1}^d \lambda_{j,e_{u_1v_1}+e_{u_2v_2}} \mathbf{X}^{(u_1)} \mathbf{X}^{(v_1)} \mathbf{X}^{(u_2)} \mathbf{X}^{(v_2)} W_{*,2}W_{*,1j}\mathbf{X} \\
& \quad \left. + \sum_{u_1,v_1=1}^d \sum_{u_2,v_2=1}^d \xi_{j,e_{u_1v_1},e_{u_2v_2}} \mathbf{X}^{(u_1)} \mathbf{X}^{(v_1)} \mathbf{X}^{(v_2)} e_{u_2} \right] \\
& - \sum_{j:|\mathcal{V}_j|=1} \exp((W_{*,2}W_{*,1j}\mathbf{X})^\top \mathbf{X}) \left[\sum_{u_1,v_1=1}^d \lambda_{j,e_{u_1v_1}} \mathbf{X}^{(u_1)} \mathbf{X}^{(v_1)} \right] f_{\tilde{G}_*}(\mathbf{X}) \\
& - \sum_{j:|\mathcal{V}_j|>1} \exp((W_{*,2}W_{*,1j}\mathbf{X})^\top \mathbf{X}) \left[\sum_{u_1,v_1=1}^d \lambda_{j,e_{u_1v_1}} \mathbf{X}^{(u_1)} \mathbf{X}^{(v_1)} \right. \\
& \quad \left. + \sum_{u_1,v_1=1}^d \sum_{u_2,v_2=1}^d \xi_{j,e_{u_1v_1},e_{u_2v_2}} \mathbf{X}^{(u_1)} \mathbf{X}^{(v_1)} \mathbf{X}^{(u_2)} \mathbf{X}^{(v_2)} \right] f_{\tilde{G}_*}(\mathbf{X}) \\
& - \sum_{j=1}^L \tau_j \exp((W_{*,2}W_{*,1j}\mathbf{X})^\top \mathbf{X}) f_{G_*}(\mathbf{X}) \\
& + \sum_{j=1}^L \tau_j \exp((W_{*,2}W_{*,1j}\mathbf{X})^\top \mathbf{X}) W_{*,2}W_{*,1j}\mathbf{X} = 0, \tag{38}
\end{aligned}$$

for almost surely \mathbf{X} . However, the new equation implies that all the coefficients $\{\lambda_{j,\alpha}, \xi_{j,\alpha,\beta}, \tau_j : j \in [L], \alpha, \beta \in \mathbb{N}^{d \times d} : 1 \leq |\alpha| + |\beta| \leq 2\}$ are 0, which is a contradiction.

As a consequence, we obtain

$$\lim_{\varepsilon \rightarrow 0} \inf_{G \in \mathcal{G}_{L'}(\Theta) : \mathcal{D}_2(G, \tilde{G}_*) \leq \varepsilon} \|f_G - f_{\tilde{G}_*}\|_{L_2(\mu)} / \mathcal{D}_2(G, \tilde{G}_*) > 0,$$

which suggests that the conclusion of the local part of the inequality (32) is proved.

B.0.2 Global part.

From the result of the local part of the inequality (32), we can find a positive constant ε' such that the following inequality holds:

$$\inf_{G \in \mathcal{G}_{L'}(\Theta) : \mathcal{D}_2(G, \tilde{G}_*) \leq \varepsilon'} \|f_G - f_{\tilde{G}_*}\|_{L_2(\mu)} / \mathcal{D}_2(G, \tilde{G}_*) > 0.$$

To obtain the conclusion of the theorem, we only need to demonstrate that

$$\inf_{G \in \mathcal{G}_{L'}(\Theta) : \mathcal{D}_2(G, \tilde{G}_*) > \varepsilon'} \|f_G - f_{\tilde{G}_*}\|_{L_2(\mu)} / \mathcal{D}_2(G, \tilde{G}_*) > 0.$$

We prove the claim by contradiction. Indeed, by assuming the claim does not hold, it implies that there exists a sequence of $G'_n := \sum_{j'=1}^{L'} \exp(b_{n,j'}) \delta_{W_{n,1j'} W_{n,2}}$ in the set $\mathcal{G}_{L'}(\Theta)$ such that

$$\begin{cases} \mathcal{D}_2(G'_n, \tilde{G}_*) > \varepsilon' \\ \|f_{G'_n} - f_{\tilde{G}_*}\|_{L_2(\mu)} / \mathcal{D}_2(G'_n, \tilde{G}_*) \rightarrow 0, \end{cases}$$

as long as n approaches the infinity. These results prove that $\|f_{G'_n} - f_{\tilde{G}_*}\|_{L_2(\mu)} \rightarrow 0$ as n goes to infinity.

From the hypothesis, the parameter space Θ is compact. Therefore, one of G'_n 's subsequences converges to some mixing measure G' where G' lies in the space $\mathcal{G}_{L'}(\Theta)$. From the hypothesis, we have $\mathcal{D}_2(G'_n, \tilde{G}_*) > \varepsilon'$. By taking the limit of both sides as $n \rightarrow \infty$, we obtain that $\mathcal{D}_2(G', \tilde{G}_*) \geq \varepsilon'$. An application of the Fatou's lemma leads to the following result:

$$0 = \lim_{n \rightarrow \infty} \|f_{G'_n} - f_{\tilde{G}_*}\|_{L_2(\mu)} \geq \int \liminf_{n \rightarrow \infty} \|f_{G'_n}(\mathbf{X}) - f_{\tilde{G}_*}(\mathbf{X})\|^2 d\mu(\mathbf{X}).$$

This inequality is only possible if $f_{G'} = f_{\tilde{G}_*}$ for almost surely \mathbf{X} .

According to the identifiability of the function $f_G(\mathbf{X})$, that equation only holds when $G' \equiv \tilde{G}_*$. As a consequence, we obtain that $\mathcal{D}_2(G', \tilde{G}_*) = 0$. It contradicts to the assumption that $\mathcal{D}_1(G', \tilde{G}_*) \geq \varepsilon' > 0$. Hence, the proof of the global part is completed. We achieve the conclusion of the theorem.

Proof for the identifiability property. The key claim that we aim to show is that if the equation $f_G(\mathbf{X}) = f_{\tilde{G}_*}(\mathbf{X})$ for almost every \mathbf{X} , then we achieve that $G \equiv \tilde{G}_*$, namely, the two mixing measures are identical.

From the hypothesis, as $f_G(\mathbf{X}) = f_{G_*}(\mathbf{X})$ for almost all \mathbf{X} , we achieve that

$$\begin{aligned} & \sum_{j=1}^N \frac{\exp(\mathbf{X}^\top A_j^0 \mathbf{X} + a_j^0))}{\tilde{D}_{f,G}(\mathbf{X})} h(\mathbf{X}, \eta_j^0) + \sum_{j'=1}^{\tilde{L}} \frac{\exp((BW_2 W_{1j'} \mathbf{X})^\top \mathbf{X} + b_{j'}))}{\tilde{D}_{f,G}(\mathbf{X})} CW_2 W_{1j'} \mathbf{X} \\ &= \sum_{j=1}^N \frac{\exp(\mathbf{X}^\top A_j^0 \mathbf{X} + a_j^0))}{\tilde{D}_{f,\tilde{G}_*}(\mathbf{X})} h(\mathbf{X}, \eta_j^0) + \sum_{j'=1}^L \frac{\exp((BW_{*,2} W_{*,1j'} \mathbf{X})^\top \mathbf{X} + b_{*,j'}))}{\tilde{D}_{f,\tilde{G}_*}(\mathbf{X})} CW_{*,2} W_{*,1j'} \mathbf{X}, \end{aligned} \quad (39)$$

where $G = \sum_{j=1}^{\tilde{L}} \exp(b_j) \delta_{W_2 W_{1j}}$. Furthermore, we define

$$\begin{aligned} \tilde{D}_{f,\tilde{G}_*}(\mathbf{X}) &= \sum_{k=1}^N \exp(\mathbf{X}^\top A_k^0 \mathbf{X} + a_k^0) + \sum_{j'=1}^L \exp((BW_{*,2} W_{*,1j'} \mathbf{X})^\top \mathbf{X} + b_{*,j'}), \\ \tilde{D}_{f,G}(\mathbf{X}) &= \sum_{k=1}^N \exp(\mathbf{X}^\top A_k^0 \mathbf{X} + a_k^0) + \sum_{j'=1}^{\tilde{L}} \exp((BW_2 W_{1j'} \mathbf{X})^\top \mathbf{X} + b_{j'}). \end{aligned}$$

That equation implies that the number of atoms of G and \tilde{G}_* should be identical, namely, we have $L = \tilde{L}$. Therefore, the following result holds

$$\left\{ \frac{\exp((BW_2 W_{1j'} \mathbf{X})^\top \mathbf{X} + b_{j'}))}{\tilde{D}_{f,G}(\mathbf{X})} : j' \in [L] \right\} = \left\{ \frac{\exp((BW_{*,2} W_{*,1j'} \mathbf{X})^\top \mathbf{X} + b_{*,j'}))}{\tilde{D}_{f,\tilde{G}_*}(\mathbf{X})} : j' \in [L] \right\},$$

for almost surely \mathbf{X} . By relabelling the indices of these two sets, we can assume without loss of generality that

$$\frac{\exp((BW_2W_{1j'}\mathbf{X})^\top\mathbf{X} + b_{j'})}{\tilde{D}_{f,G}(\mathbf{X})} = \frac{\exp((BW_{*,2}W_{*,1j'}\mathbf{X})^\top\mathbf{X} + b_{*,j'})}{\tilde{D}_{f,\tilde{G}_*}(\mathbf{X})},$$

for any index $j' \in [L]$ and for almost surely \mathbf{X} . From the invariance to translation property of the softmax function, the equation (39) becomes

$$\begin{aligned} & \sum_{j=1}^L \exp(b_j) \exp((BW_2W_{1j}\mathbf{X})^\top\mathbf{X}) CW_2W_{1j}\mathbf{X} \\ &= \sum_{j'=1}^L \exp(b_{*,j}) \exp((BW_{*,2}W_{*,1j'}\mathbf{X})^\top\mathbf{X}) CW_{*,2}W_{*,1j'}\mathbf{X}, \end{aligned} \quad (40)$$

for almost surely \mathbf{X} . This equation suggests that there exists a partition K_1, K_2, \dots, K_m of the set $[L]$ for some m such that we have $\exp(b_{j_1}) = \exp(b_{*,j_2})$ for any $j_1, j_2 \in K_i$ and for any $i \in [m]$. According to that result, the equation (40) can be rewritten as follows:

$$\begin{aligned} & \sum_{i=1}^m \sum_{j_1 \in K_i} \exp(b_{j_1}) \exp((BW_2W_{1j_1}\mathbf{X})^\top\mathbf{X}) CW_2W_{1j_1}\mathbf{X} \\ &= \sum_{i=1}^m \sum_{j_2 \in K_i} \exp(b_{*,j_2}) \exp((BW_{*,2}W_{*,1j_2}\mathbf{X})^\top\mathbf{X}) CW_{*,2}W_{*,1j_2}\mathbf{X}, \end{aligned}$$

for almost surely \mathbf{X} . That equation proves that

$$\{W_2W_{1j_1}\mathbf{X} : j_1 \in K_i\} = \{W_{*,2}W_{*,1j_2}\mathbf{X} : j_2 \in K_i\},$$

for any $i \in [m]$. That result indicates that

$$\{W_2W_{1j_1} : j_1 \in K_i\} = \{W_{*,2}W_{*,1j_2} : j_2 \in K_i\}.$$

As a consequence, we arrive at the following result:

$$\sum_{i=1}^m \sum_{j_1 \in K_i} \exp(b_{j_1}) \delta_{W_2W_{1j_1}} = \sum_{i=1}^m \sum_{j_2 \in K_i} \exp(b_{*,j_2}) \delta_{W_{*,2}W_{*,1j_2}}.$$

It is equivalent to $G \equiv \tilde{G}_*$. As a consequence, we obtain the conclusion of the identifiability property of the function f_G . \square

C Related Work

Mixture of Experts. Building on classical mixture models with adaptive gating mechanism [27, 30, 70], the MoE model has been extensively studied and refined over the years. Notably, subsequent works [11, 59] introduced the MoE layer as an efficient tool for scaling model capacity. Unlike traditional models applying uniform parameters to all inputs, the MoE layer specific parameter

subsets for each input, creating a sparsely activated layer that enables significant capacity growth without proportional computational cost [12, 77]. This efficiency and scalability have driven its adoption across diverse domains and tasks [57, 9, 60].

Theory of Mixture of Experts. Although MoEs have been widely used to scale up large models, their theoretical foundations remain under active development. For example, [23] focused on input-free gating Gaussian MoEs and showed that under maximum likelihood estimation, the experts’ convergence rates depend on the algebraic independence of the expert functions. Next, [49, 46] established convergence rates for both density and parameter estimation in Softmax gating Gaussian MoEs, linking these rates to the solvability of polynomial systems under Voronoi-based loss functions. More recently, [47, 48] employed least squares estimation to identify conditions under which expert functions are identifiable. Under these conditions, the resulting estimation rates improve substantially.

Parameter-Efficient Fine-Tuning. Fine-tuning pre-trained foundational models [8, 41, 32] has become a widely adopted strategy for tackling downstream tasks [69]. While effective, full fine-tuning is *resource-intensive*, requiring updates to all network parameters and the storage of a separate fine-tuned model for each task [18]. To address these challenges, researchers have increasingly focused on parameter-efficient fine-tuning (PEFT) methods. These methods can be categorized into *partial tuning*, *extra module*, and *prompt tuning*. Partial tuning freezes most of the backbone, fine-tuning only a subset, such as linear heads or a few layers [42, 4, 20]. Extra module methods add trainable parameters to the backbone, such as side structures [76], residual MLP modules in Transformer layers [24, 2], or low-rank weight updates [25]. Despite their promise, partial tuning and extra module methods often face limitations that restrict their applicability. First, they may fail to achieve performance comparable to full fine-tuning [42, 4, 28, 21]. Second, some methods rely on specific architectural modifications [56, 2, 76], limiting their generalizability across different backbone architectures.

Prompting Methods. Prompt tuning [40], initially proposed for language tasks, offers a simpler yet effective alternative by introducing learnable parameters to the *input sequence* of backbone models, updating only these parameters during fine-tuning [40, 28, 36, 34]. Despite its simplicity, prompt tuning has demonstrated significant performance gains. Recently, visual prompt tuning has emerged as a promising paradigm in PEFT techniques for computer vision. Current advancements in visual prompt tuning focus on engineering improvements, such as minimizing parameter usage [17] and broadening applicability to diverse tasks [71, 61, 72]. However, the theoretical foundations of prompt-based methods remain under-explored. For instance, [19] investigate the relationship between prompt tuning and adapter methods, while [35] analyze these techniques within the context of mixture of experts models. Furthermore, [54] highlight the limitations of prompting, showing that it cannot alter relative attention patterns and instead biases attention layer outputs in a fixed direction.

D Implementation Details

Datasets specifications. Table 4 provides a summary of the statistics and details of the classification datasets evaluated in the paper. Figure 5 presents image examples from all 24 datasets. Following [28], each FGVC dataset is randomly split into 90% `train` and 10% `val`, with the `val` set used for hyperparameter tuning. For VTAB-1K, we use an 800-200 split for tuning and train on all available data for the final evaluation.

Table 4: Specifications of the datasets used in our experiments, including 24 datasets from two benchmarks: FGVC and VTAB-1K [75].

Dataset	Description	# Classes	Train	Val	Test
Fine-grained visual recognition tasks (FGVC)					
CUB-200-2011 [66]	Fine-grained bird species recognition	200	5,394	600	5,794
NABirds [63]	Fine-grained bird species recognition	55	21,536	2,393	24,633
Oxford Flowers [50]	Fine-grained flower species recognition	102	1,020	1,020	6,149
Stanford Dogs [31]	Fine-grained dog species recognition	120	10,800	1,200	8,580
Stanford Cars [14]	Fine-grained car recognition	196	7,329	815	8,041
Visual Task Adaptation Benchmark (VTAB-1K)					
CIFAR-100 [33]		100			10,000
Caltech101 [13]		102			6,084
DTD [6]		47			1,880
Flowers102 [50]	Natural	102	800/1000	200	6,149
Pets [52]		37			3,669
SVHN [45]		10			26,032
Sun397 [68]		397			21,750
Patch Camelyon [65]		2			32,768
EuroSAT [22]	Specialized	10	800/1000	200	5,400
Resisc45 [5]		45			6,300
Retinopathy [16]		5			42,670
Clevr/count [29]		8			15,000
Clevr/distance [29]		6			15,000
DMLab [1]		6			22,735
KITTI/distance [15]	Structured	4	800/1000	200	711
dSprites/loc [44]		16			73,728
dSprites/ori [44]		16			73,728
SmallNORB/azi [38]		18			12,150
SmallNORB/ele [38]		9			12,150

Pre-trained backbones specifications. This study explores two primary groups of Vision Transformer (ViT) models. The first group comprises conventional ViT architectures [8], including ViT-Base, ViT-Large, and ViT-Huge, pre-trained on the large-scale ImageNet-21K [7] dataset. The second group focuses on self-supervised models, specifically Masked Autoencoders (MAE) [20] and Momentum Contrast v3 (MoCo v3) [4], both pre-trained using ImageNet-1K. Unless otherwise specified, we use ViT-B/16 with supervised pre-training on ImageNet-21K by default.

Augmentation. During training, we employ standard image augmentation techniques. For the five FGVC datasets, images are normalized using ImageNet mean and standard deviation, followed by random resized cropping to 224×224 and random horizontal flipping. For the VTAB-1k, images are directly resized to 224×224 .

Hyperparameters. We use `val` set of each dataset to find best prompt length N_p , kernel size K and hidden dimension r of the feature projector. Following [28], the search range for N_p is $\{1, 5, 10, 50, 100, 200\}$. Given the relatively small resolution of our feature map \mathbf{X}_{img} (e.g., 14×14 for ViT), the kernel size K is selected from $\{2, 3, 4\}$. For the hidden dimension r , we explore the range $\{4, 8, 16, 32, 64, 128, 256\}$. To identify the optimal learning rate and weight decay, we perform a grid search, consistent with [42, 28]. The learning rate is searched within $\{50, 25, 10, 5, 2.5, 1, 0.5, 0.25, 0.1, 0.05\}$, while the weight decay is chosen from $\{0.01, 0.001, 0.0001, 0.0\}$. We adopt the batch size settings of [28], using 64 and 128. The models are optimized with SGD for

100 epochs, employing a cosine decay learning rate schedule with 10 warmup epochs.

Reproducibility. Our method, VAPT, is implemented in PyTorch [53]. All experimental workflows, including training and evaluation, were conducted on NVIDIA A100-40GB GPUs. The entire implementation will be made openly available to ensure reproducibility and facilitate future research.

E Additional Experiments

E.1 Per-task Results for VTAB-1K and FGVC

Table 5: **VTAB-1K Natural Per-Task Results for ViT-B/16 Supervised Pre-trained on ImageNet-21K.** “Number of Wins” in [·] denotes comparisons relative to full fine-tuning. “Tuned/Total” is the percentage of parameters tuned for each task. The highest accuracy among all approaches except Full is highlighted in **bold**.

ViT-B/16 [8] (85.8M)	VTAB-1K [75] <i>Natural</i> [7]							Mean
	CIFAR-100	Caltech101	DTD	Flowers102	Pets	SVHN	Sun397	
Full [26]	68.9	87.7	64.3	97.2	86.9	87.4	38.8	75.88
Linear [26]	63.4	85.0	63.2	97.0	86.3	36.6	51.0	68.93 [1]
Partial-1 [74]	66.8	85.9	62.5	97.3	85.5	37.6	50.6	69.44 [2]
MLP-2 [3]	63.2	84.8	60.5	97.6	85.9	34.1	47.8	67.70 [2]
MLP-3 [3]	63.8	84.7	62.3	97.4	84.7	32.5	49.2	67.80 [2]
MLP-5 [3]	59.3	84.4	59.9	96.1	84.4	30.9	46.8	65.98 [1]
MLP-9 [3]	53.1	80.5	53.9	95.1	82.6	24.4	43.7	61.90 [1]
Sidetune [76]	60.7	60.8	53.6	95.5	66.7	34.9	35.3	58.21 [0]
Bias [56]	72.8	87.0	59.2	97.5	85.3	59.9	51.4	73.30 [3]
Adapter-256 [2]	74.1	86.1	63.2	97.7	87.0	34.6	50.8	70.50 [4]
Adapter-64 [2]	74.2	85.8	62.7	97.6	87.2	36.3	50.9	70.65 [4]
Adapter-8 [2]	74.2	85.7	62.7	97.8	87.2	36.4	50.7	70.67 [4]
VPT-Shallow [28]	77.7	86.9	62.6	97.5	87.3	74.5	51.2	76.81 [4]
- Tuned / Total (%)	0.18	0.10	0.04	0.27	0.08	0.19	0.36	0.17
VPT-Deep [28]	78.8	90.8	65.8	98.0	88.3	78.1	49.6	78.48 [6]
- Tuned / Total (%)	0.20	0.20	0.15	0.10	0.04	0.54	0.41	0.23
E2VPT [17]	78.6	89.4	67.8	98.2	88.5	85.3	52.3	80.01 [6]
- Tuned / Total (%)	0.22	0.19	0.12	0.11	0.05	0.24	0.43	0.19
VAPT (Ours)	80.8 ± (0.15)	91.9 ± (0.46)	69.7 ± (0.63)	98.8 ± (0.05)	89.2 ± (0.05)	86.7 ± (0.42)	52.9 ± (0.15)	81.43 [6]
- Tuned / Total (%)	0.15	0.16	0.11	0.13	0.07	0.20	0.42	0.18

Table 5, Table 6, Table 7, and Table 8 provide per-task results across 24 classification tasks evaluated in Table 1. All results are averaged of three runs using different initialization seeds, with standard deviation error bars included. Compared to VPT and other commonly used PEFT methods, VAPT demonstrates consistently superior performance across a variety of downstream tasks while utilizing fewer parameters.

E.2 Per-task Results on MAE and MoCo v3

Tables 9, 10, and 11 provide per-task results for MAE [20], as summarized in Table 2. Similarly, Tables 12, 13, and 14 present per-task results for MoCo v3 [4], corresponding to the overview in Table 2.

Table 6: **VTAB-1K Specialized Per-Task Results for ViT-B/16 Supervised Pre-trained on ImageNet-21K.** “Number of Wins” in [·] denotes comparisons relative to full fine-tuning. “Tuned/Total” is the percentage of parameters tuned for each task. The highest accuracy among all approaches except Full is highlighted in **bold**.

ViT-B/16 [8] (85.8M)	VTAB-1K [75] Specialized [4]				Mean
	Patch Camelyon	EuroSAT	Resisc45	Retinopathy	
Full [26]	79.7	95.7	84.2	73.9	83.36
Linear [26]	78.5	87.5	68.6	74.0	77.16 [1]
Partial-1 [74]	78.6	89.8	72.5	73.3	78.53 [0]
MLP-2 [3]	74.3	88.8	67.1	73.2	75.86 [0]
MLP-3 [3]	77.0	88.0	70.2	56.1	72.83 [0]
MLP-5 [3]	73.7	87.2	64.8	71.5	74.31 [0]
MLP-9 [3]	78.5	83.0	60.2	72.3	73.49 [0]
Sidetune [76]	58.5	87.7	65.2	61.0	68.12 [0]
Bias [56]	78.7	91.6	72.9	69.8	78.25 [0]
Adapter-256 [2]	76.3	88.0	73.1	70.5	76.98 [0]
Adapter-64 [2]	76.3	87.5	73.7	70.9	77.10 [0]
Adapter-8 [2]	76.9	89.2	73.5	71.6	77.80 [0]
VPT-Shallow [28]	78.2	92.0	75.6	72.9	79.66 [0]
- Tuned / Total (%)	0.01	0.05	0.09	0.01	0.04
VPT-Deep [28]	81.8	96.1	83.4	68.4	82.43 [2]
- Tuned / Total (%)	1.06	1.07	0.15	0.02	0.57
E2VPT [17]	82.5	96.8	84.8	73.6	84.43 [3]
- Tuned / Total (%)	0.20	0.29	0.12	0.07	0.17
VAPT (Ours)	84.4 ± (0.72)	96.5 ± (0.09)	85.1 ± (0.46)	74.5 ± (0.32)	85.13 [4]
- Tuned / Total (%)	0.30	0.35	0.09	0.06	0.20

E.3 Different Backbone Scales

In Figure 6, we compare VAPT and VPT on the CUB-200-2011 dataset [66] under varying scales of the pre-trained backbone (ViT-Base, ViT-Large, and ViT-Huge). The results demonstrate that VAPT consistently surpasses VPT as the model size increases. Notably, with the ViT-Huge backbone, VAPT achieves up to a 1.3% improvement over VPT. These findings highlights the scalability and effectiveness of VAPT compared to VPT as model size grows.

E.4 Ablation Study

Impact of different components. We conducted ablation studies on the VTAB-1K benchmark [75] to evaluate the individual contributions of each component in VAPT. The results, presented in Table 15, show that incorporating the channel-wise convolution layer increases the overall average performance by 0.97%. This improvement highlights the benefit of explicitly encoding spatial relationships in the feature map before it is processed by the token-wise projectors. Furthermore, the channel-wise convolution layer reduces the overall parameter count by downsampling the feature map from $H \times W$ to $H' \times W'$, where $H' = H - K + 1$ and $W' = W - K + 1$. Consequently, the dimensionality for each token-wise projector is also reduced, leading to fewer parameters. When the feature projector is removed, performance decreases; for instance, in VTAB-1K *Natural*, the performance drops from 81.43% to 79.43%. This highlights the importance of the feature projector.

Table 7: **VTAB-1K Structured** Per-Task Results for ViT-B/16 Supervised Pre-trained on ImageNet-21K. “Number of Wins” in [·] denotes comparisons relative to full fine-tuning. “Tuned/Total” is the percentage of parameters tuned for each task. The highest accuracy among all approaches except Full is highlighted in **bold**.

ViT-B/16 [8] (85.8M)	Clevr/ count	Clevr/ distance	DMLab	KITTI/ distance	dSprites/ location	dSprites/ orientation	SmallNORB/ azimuth	SmallNORB/ elevation	Mean
Full [26]	56.3	58.6	41.7	65.5	57.5	46.7	25.7	29.1	47.64
Linear [26]	34.3	30.6	33.2	55.4	12.5	20.0	9.6	19.2	26.84 [0]
Partial-1 [74]	41.5	34.3	33.9	61.0	31.3	32.8	16.3	22.4	34.17 [0]
MLP-2 [3]	45.2	31.6	31.8	55.7	30.9	24.6	16.6	23.3	32.47 [0]
MLP-3 [3]	47.8	32.8	32.3	58.1	12.9	21.2	15.2	24.8	30.62 [0]
MLP-5 [3]	50.8	32.3	31.5	56.4	7.5	20.8	14.4	20.4	29.23 [0]
MLP-9 [3]	47.5	27.9	28.9	54.0	6.2	17.7	10.8	16.2	26.15 [0]
Sidetune [76]	27.6	22.6	31.3	51.7	8.2	14.4	9.8	21.8	23.41 [0]
Bias [56]	61.5	55.6	32.4	55.9	66.6	40.0	15.7	25.1	44.09 [2]
Adapter-256 [2]	45.7	37.4	31.2	53.2	30.3	25.4	13.8	22.1	32.39 [0]
Adapter-64 [2]	42.9	39.9	30.4	54.5	31.9	25.6	13.5	21.4	32.51 [0]
Adapter-8 [2]	45.2	41.8	31.1	56.4	30.4	24.6	13.2	22.0	33.09 [0]
VPT-Shallow [28]	50.5	58.6	40.5	67.1	68.7	36.1	20.2	34.1	46.98 [4]
- Tuned / Total (%)	0.10	0.18	0.09	0.09	0.10	0.10	0.19	0.19	0.13
VPT-Deep [28]	68.5	60.0	46.5	72.8	73.6	47.9	32.9	37.8	54.98 [8]
- Tuned / Total (%)	0.54	2.11	1.07	0.54	0.12	0.55	2.12	2.11	1.14
E2VPT [17]	71.7	61.2	47.9	75.8	80.8	48.1	31.7	41.9	57.39 [8]
- Tuned / Total (%)	0.34	0.65	0.44	0.36	0.10	0.38	1.14	0.66	0.51
VAPT (Ours)	74.8 ± (1.70)	63.6 ± (0.36)	50.0 ± (0.74)	77.2 ± (0.72)	86.1 ± (0.24)	48.3 ± (0.89)	33.8 ± (0.95)	40.9 ± (2.29)	59.34 [8]
- Tuned / Total (%)	0.20	0.39	0.31	0.38	0.08	0.35	0.60	0.75	0.38

Furthermore, our sharing mechanism for the feature projector not only reduces the number of parameters but also facilitates knowledge transfer between layers, leading to improved performance. Overall, combining all components yielded the best performance, with an average accuracy of 72.91% on VTAB-1K.

Detailed analysis of the channel-wise convolution layer. We evaluated the effectiveness of our channel-wise convolution layer by comparing its performance with that of a standard convolution layer. We also explored alternative strategies for modeling spatial relationships, including an average pooling layer [37]. Notably, average pooling can be considered a special case of our channel-wise convolution layer, where the kernel weights are fixed rather than learned. The comparative results are presented in Table 16. Our channel-wise convolution layer not only reduces the number of parameters relative to a standard convolution layer but also mitigates overfitting, thereby improving overall performance. Furthermore, it surpasses the average pooling layer; for instance, on VTAB-1K *Structured*, we achieve a 0.93% performance gain. This improvement is attributed to the flexibility of our channel-wise convolution layer compared to average pooling.

Robustness to different hyperparameters. We systematically evaluate the influence of key hyperparameters, including prompt length N_p , kernel size K , and hidden dimension r , by conducting experiments on three representative VTAB-1K tasks: Sun397 (*Natural*), Retinopathy (*Specialized*), and Clevr/distance (*Structured*). The results are shown in Figure 7, Figure 8, and Figure 9. As depicted, the optimal hyperparameters vary across tasks. Nevertheless, VAPT consistently achieves higher performance than VPT across a range of hyperparameters. Notably, even with only a single prompt, VAPT maintains its advantage over VPT.

Linear activation in the feature projector. As shown in Appendix B, VAPT preserves its optimal

Table 8: **FGVC Per-Task Results for ViT-B/16 Supervised Pre-trained on ImageNet-21K.** “Number of Wins” in [.] denotes comparisons relative to full fine-tuning. “Tuned/Total” is the percentage of parameters tuned for each task. The highest accuracy among all approaches except Full is highlighted in **bold**.

ViT-B/16 [8] (85.8M)	FGVC [5]					Mean
	CUB-200-2011	NAbirds	Oxford Flowers	Stanford Dogs	Stanford Cars	
Full [26]	87.3	82.7	98.8	89.4	84.5	88.54
Linear [26]	85.3	75.9	97.9	86.2	51.3	79.32 [0]
Partial-1 [74]	85.6	77.8	98.2	85.5	66.2	82.63 [0]
MLP-2 [3]	85.7	77.2	98.2	85.4	54.9	80.28 [0]
MLP-3 [3]	85.1	77.3	97.9	84.9	53.8	79.80 [0]
MLP-5 [3]	84.2	76.7	97.6	84.8	50.2	78.71 [0]
MLP-9 [3]	83.2	76.0	96.2	83.7	47.6	77.31 [0]
Sidetune [76]	84.7	75.8	96.9	85.8	48.6	78.35 [0]
Bias [56]	88.4	84.2	98.8	91.2	79.4	88.41 [3]
Adapter-256 [2]	87.2	84.3	98.5	89.9	68.6	85.70 [2]
Adapter-64 [2]	87.1	84.3	98.5	89.8	68.6	85.67 [2]
Adapter-8 [2]	87.3	84.3	98.4	88.8	68.4	85.46 [1]
VPT-Shallow [28]	86.7	78.8	98.4	90.7	68.7	84.62 [1]
- Tuned / Total (%)	0.31	0.54	0.23	0.20	0.26	0.31
VPT-Deep [28]	88.5	84.2	99.0	90.2	83.6	89.11 [4]
- Tuned / Total (%)	0.29	1.02	0.14	1.17	2.27	0.98
E2VPT [17]	89.1	84.6	99.1	90.5	82.8	89.22 [4]
- Tuned / Total (%)	0.32	0.65	0.15	0.88	1.27	0.65
VAPT (Ours)	89.7 \pm (0.12)	84.6 \pm (0.06)	99.1 \pm (0.04)	91.7 \pm (0.05)	82.8 \pm (0.53)	89.58 [4]
- Tuned / Total (%)	0.36	0.79	0.19	0.53	2.04	0.78

Table 9: **VTAB-1K Natural Per-Task Results for ViT-B/16 Pre-trained on MAE [20].** “Number of Wins” in [.] denotes comparisons relative to full fine-tuning. “Tuned/Total” is the percentage of parameters tuned for each task. The highest accuracy among all approaches is highlighted in **bold**.

ViT-B/16 [8] (85.8M)	VTAB-1K [75] Natural [7]							Mean
	CIFAR-100	Caltech101	DTD	Flowers102	Pets	SVHN	Sun397	
Full [26]	24.6	84.2	56.9	72.7	74.4	86.6	15.8	59.31
VAPT (Ours)	34.4	89.7	63.1	74.2	73.8	55.1	24.3	59.23 [5]
- Tuned / Total (%)	0.17	0.16	0.10	0.13	0.07	0.12	0.40	0.16

sample efficiency even when the activation function σ in the feature projector (see equation (11)) is replaced by a linear identity function. To substantiate this theoretical result, we report the corresponding performance in Table 17, where σ is removed. The results demonstrates that the linear version of VAPT remains competitive with the non-linear variant. Notably, it still outperforms VPT by a substantial margin (e.g., 4.30% on the VTAB-1K *Structured* task), confirming both the theoretical and empirical robustness of our approach.

Table 10: **VTAB-1K Specialized** Per-Task Results for ViT-B/16 Pre-trained on MAE [20]. “Number of Wins” in [·] denotes comparisons relative to full fine-tuning. “Tuned/Total” is the percentage of parameters tuned for each task. The highest accuracy among all approaches is highlighted in **bold**.

ViT-B/16 [8] (85.8M)	VTAB-1K [75] Specialized [4]				Mean
	Patch	Camelyon	EuroSAT	Resisc45	
Full [26]	81.8	94.0	72.3	70.6	79.68
VAPT (Ours)	78.9	91.6	78.7	73.7	80.73 [2]
- Tuned / Total (%)	0.36	0.31	0.15	0.03	0.21

Table 11: **VTAB-1K Structured** Per-Task Results for ViT-B/16 Pre-trained on MAE [20]. “Number of Wins” in [·] denotes comparisons relative to full fine-tuning. “Tuned/Total” is the percentage of parameters tuned for each task. The highest accuracy among all approaches is highlighted in **bold**.

ViT-Base/16 [8] (85.8M)	VTAB-1K [75] Structured [8]								Mean
	Clevr/ count	Clevr/ distance	DMLab	KITTI/ distance	dSprites/ location	dSprites/ orientation	SmallNORB/ azimuth	SmallNORB/ elevation	
Full [26]	67.0	59.8	45.2	75.3	72.5	47.5	30.2	33.0	53.82
VAPT (Ours)	57.9	57.1	37.3	68.2	82.6	11.5	21.6	41.7	47.24 [2]
- Tuned / Total (%)	0.18	0.65	0.33	0.35	0.09	0.36	0.66	0.67	0.41

Table 12: **VTAB-1K Natural** Per-Task Results for ViT-B/16 Pre-trained on MoCo v3 [4]. “Number of Wins” in [·] denotes comparisons relative to full fine-tuning. “Tuned/Total” is the percentage of parameters tuned for each task. The highest accuracy among all approaches is highlighted in **bold**.

ViT-B/16 [8] (85.8M)	VTAB-1K [75] Natural [7]							Mean
	CIFAR-100	Caltech101	DTD	Flowers102	Pets	SVHN	Sun397	
Full [26]	57.6	91.0	64.6	91.6	79.9	89.8	29.1	71.95
VAPT (Ours)	74.5	92.0	69.5	93.2	88.2	84.6	41.8	77.69 [6]
- Tuned / Total (%)	0.15	0.20	0.09	0.34	0.09	0.10	0.40	0.20

E.5 Computational Cost

One primary concern when designing prompts as adaptive functions of the input is the associated computational overhead. Although VAPT outperforms VPT, one notable advantage of VPT is its simplicity, as its prompts remain fixed regardless of the input. To examine the trade-offs, we compare both the performance and computational cost of the two methods. Table 18 reports these costs measured in FLOPs (GFLOPs) and MACs (GMACs) for VAPT and VPT across five FGVC datasets. VAPT incurs only a slight increase in computational demands, with FLOPs rising by 0.18% for

Table 13: **VTAB-1K Specialized Per-Task Results for ViT-B/16 Pre-trained on MoCo v3 [4]**. “Number of Wins” in [.] denotes comparisons relative to full fine-tuning. “Tuned/Total” is the percentage of parameters tuned for each task. The highest accuracy among all approaches is highlighted in **bold**.

ViT-B/16 [8] (85.8M)	VTAB-1K [75] Specialized [4]				Mean
	Patch	Camelyon	EuroSAT	Resisc45	
Full [26]	85.1	96.4	83.1	74.2	84.72
VAPT (Ours)	80.6	95.9	83.9	75.4	83.95 [2]
- Tuned / Total (%)	0.36	0.34	0.11	0.03	0.21

Table 14: **VTAB-1K Structured Per-Task Results for ViT-B/16 Pre-trained on MoCo v3 [4]**. “Number of Wins” in [.] denotes comparisons relative to full fine-tuning. “Tuned/Total” is the percentage of parameters tuned for each task. The highest accuracy among all approaches is highlighted in **bold**.

ViT-Base/16 [8] (85.8M)	VTAB-1K [75] Structured [8]								Mean
	Clevr/ count	Clevr/ distance	DMLab	KITTI/ distance	dSprites/ location	dSprites/ orientation	SmallNORB/ azimuth	SmallNORB/ elevation	
Full [26]	55.2	56.9	44.6	77.9	63.8	49.0	31.5	36.9	51.98
VAPT (Ours)	74.2	65.3	48.4	73.8	88.0	51.4	32.5	52.3	60.74 [7]
- Tuned / Total (%)	0.20	0.69	0.05	0.36	0.08	0.20	0.66	0.65	0.36

Table 15: **Impact of Different Components in VAPT**. Experiments were conducted on the VTAB-1K benchmark. We used ViT-B/16 Supervised Pre-trained on ImageNet-21K as the backbone. “Tuned/Total” is the percentage of parameters tuned for each task. **Bold** highlights the best results.

Channel-wise	Feature projector	Sharing Projector	Components	Tuned / Total(%)	VTAB-1K [75]			Mean	Total
					Natural	Specialized	Structured		
✓	✓	✓		0.27	81.43	85.13	59.34	72.91	
	✓	✓		0.34	80.47	84.63	58.13	71.94	
✓				0.26	79.43	83.60	57.72	71.17	
✓	✓			0.42	80.85	85.10	59.04	72.56	

Stanford Cars and between 0.06% and 0.59% across other datasets. A similar pattern holds for MACs. These modest increases are outweighed by the significant performance gains, and it is noteworthy that VAPT also employs fewer parameters than VPT. Overall, these findings highlight the efficiency of VAPT, delivering robust performance improvements at a minimal additional computational cost.

Table 16: **Detailed Analysis of Channel-wise Convolution.** Experiments were conducted on the VTAB-1K benchmark. We used ViT-B/16 Supervised Pre-trained on ImageNet-21K as the backbone. “Tuned/Total” is the percentage of parameters tuned for each task. **Bold** highlights the best results.

Method	Tuned / Total(%)	VTAB-1K [75]			Mean Total
		Natural	Specialized	Structured	
Channel-wise Convolution	0.27	81.43	85.13	59.34	72.91
Standard Convolution	0.33	80.79	84.81	58.37	72.20
Average Pooling	0.27	81.30	85.02	58.41	72.45

Table 17: **Linear activation in the feature projector.** Experiments were conducted on the VTAB-1K benchmark. We used ViT-B/16 Supervised Pre-trained on ImageNet-21K as the backbone. “Tuned/Total” is the percentage of parameters tuned for each task. **Bold** highlights the best results.

Method	Tuned / Total(%)	VTAB-1K [75]			Mean Total
		Natural	Specialized	Structured	
VPT	0.69	78.48	82.43	54.98	69.43
VAPT _{linear}	0.27	80.89	84.93	59.28	72.64
VAPT _{non-linear}	0.27	81.43	85.13	59.34	72.91

E.6 Interpretative Visualizations

To facilitate a deeper understanding of our method, we provide visualization inspections to support the advantages of VAPT. Specifically, we use GradCAM [58] to generate attention maps by computing the gradients of a target concept with respect to the model’s final layer. Figure 10 presents examples from five VTAB-1K datasets, namely Sun397, SVHN, Resisc45, Clevr/count, and KITTI/distance, comparing heatmaps generated by VAPT and VPT. These visualizations enable us to examine which regions of the input data each technique prompts the model to focus on. We observe that VAPT can localize relevant image regions more accurately than VPT. For instance, in the Sun397 dataset, while VPT struggles to capture the complete structure of an object, VAPT succeeds in identifying and highlighting its key features. This enhanced localization indicates VAPT’s stronger ability to capture salient visual patterns. Consequently, VAPT not only improves upon VPT’s performance but also enhances the interpretability of the model by providing more coherent and precise visual explanations.

Table 18: **Comparison of FLOPs and MACs for VAPT and VPT.** The experiments were conducted on FGVC benchmark. We used ViT-B/16 Supervised Pre-trained on ImageNet-21K as the backbone.

Metric	Method	Stanford Cars	CUB-200-2011	Oxford Flowers	NABirds	Stanford Dogs
FLOPs (GFLOPS)	VAPT	73.67 (↑ 0.18%)	37.04 (↑ 0.11%)	36.10 (↑ 0.08%)	44.61 (↑ 0.31%)	54.30 (↑ 0.59%)
	VPT	73.54	37.00	36.07	44.47	53.98
MACs (GMACs)	VAPT	36.80 (↑ 0.16%)	18.51 (↑ 0.11%)	18.03 (↑ 0.06%)	22.29 (↑ 0.32%)	27.13 (↑ 0.59%)
	VPT	36.74	18.49	18.02	22.22	26.97

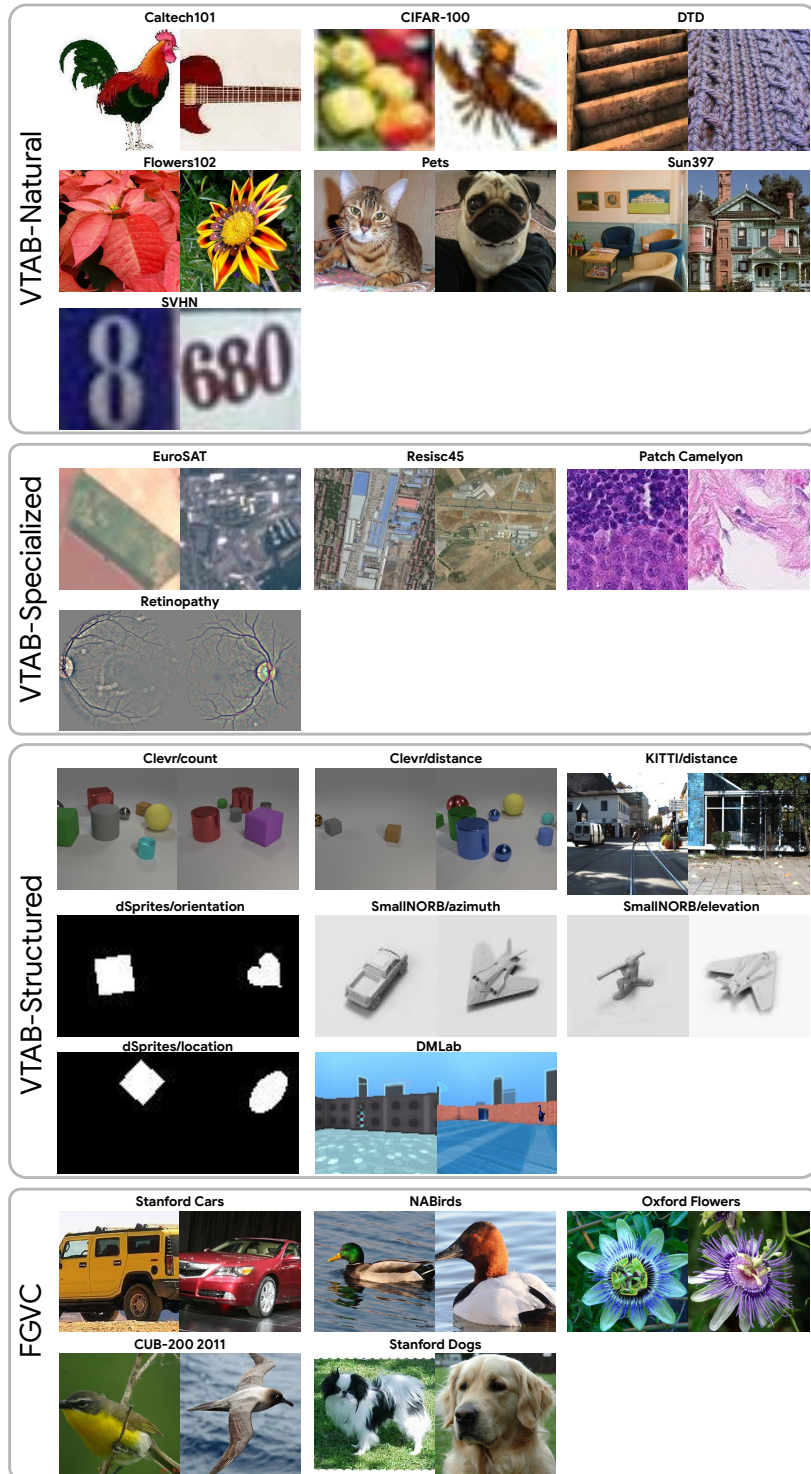


Figure 5: Dataset examples for all classification tasks evaluated

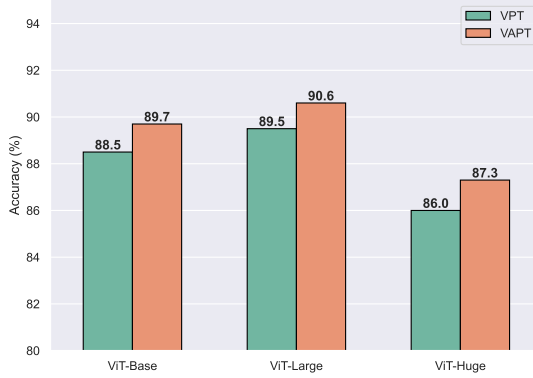


Figure 6: Comparison of VAPT and VPT across different backbone scales.

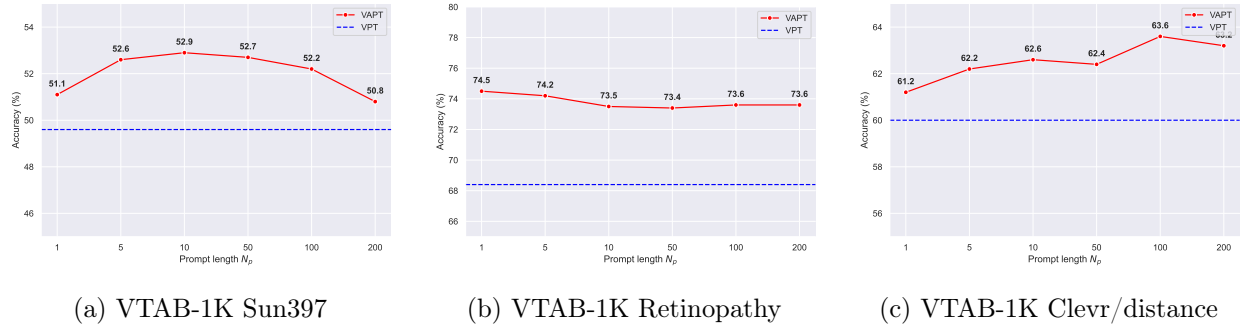


Figure 7: Ablation on prompt length N_p . Results are reported on 3 datasets, each corresponding to a distinct VTAB subgroup. The dashed line indicates the best results of VPT.

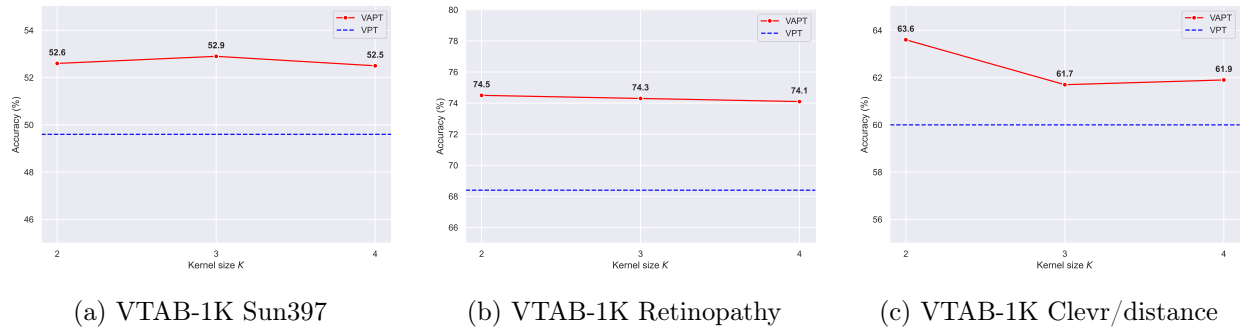


Figure 8: Ablation on kernel size K . Results are reported on 3 datasets, each corresponding to a distinct VTAB subgroup. The dashed line indicates the best results of VPT.

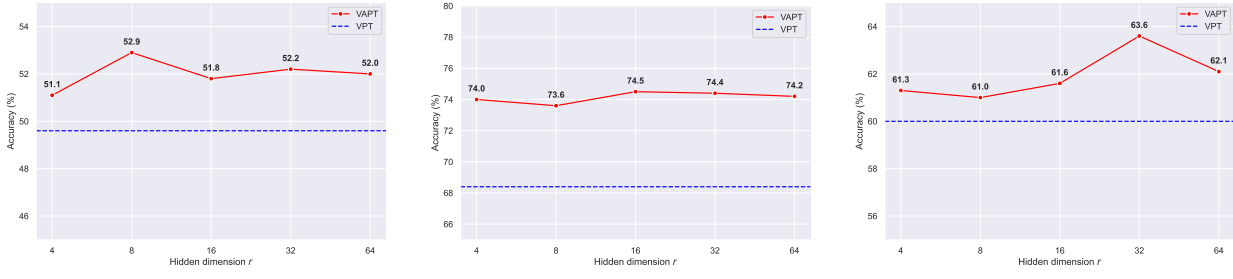


Figure 9: Ablation on hidden dimension r . Results are reported on 3 datasets, each corresponding to a distinct VTAB subgroup. The dashed line indicates the best results of VPT.

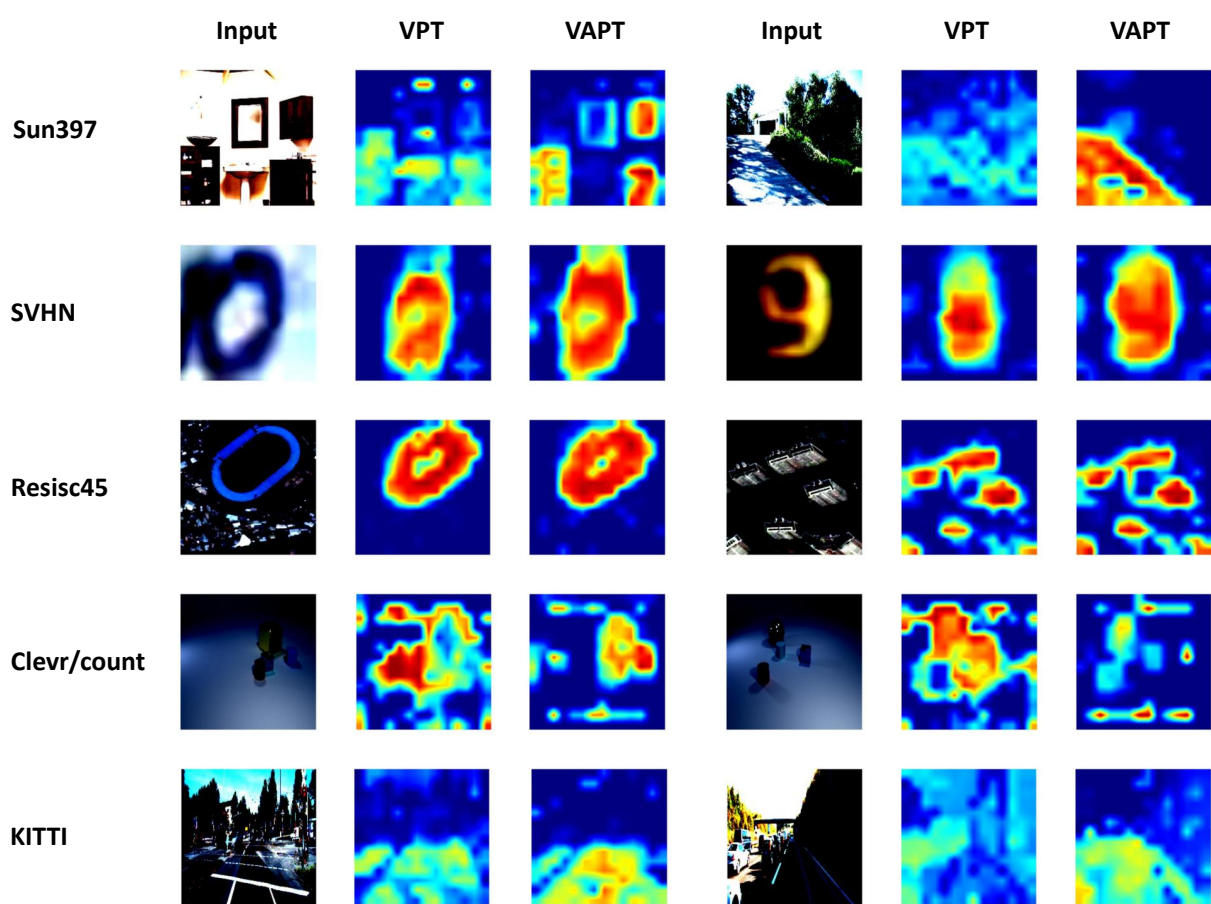


Figure 10: GradCAM visualization of VPT and VAPT on five VTAB-1K datasets. Red regions indicate areas of higher class activation. From left to right: the input image after standard data augmentation, the GradCAM output from VPT, and the GradCAM output from VAPT.

References

- [1] C. Beattie, J. Z. Leibo, D. Teplyashin, T. Ward, M. Wainwright, H. Küttler, A. Lefrancq, S. Green, V. Valdés, A. Sadik, et al. Deepmind lab. *arXiv preprint arXiv:1612.03801*, 2016. (Cited on page 40.)
- [2] H. Cai, C. Gan, L. Zhu, and S. Han. Tinytl: Reduce memory, not parameters for efficient on-device learning. *Advances in Neural Information Processing Systems*, 33:11285–11297, 2020. (Cited on pages 1, 11, 12, 39, 41, 42, 43, and 44.)
- [3] X. Chen, H. Fan, R. Girshick, and K. He. Improved baselines with momentum contrastive learning. *arXiv preprint arXiv:2003.04297*, 2020. (Cited on pages 11, 41, 42, 43, and 44.)
- [4] X. Chen, S. Xie, and K. He. An empirical study of training self-supervised vision transformers. In *Proceedings of the IEEE/CVF international conference on computer vision*, pages 9640–9649, 2021. (Cited on pages 2, 11, 12, 39, 40, 41, 45, and 46.)
- [5] G. Cheng, J. Han, and X. Lu. Remote sensing image scene classification: Benchmark and state of the art. *Proceedings of the IEEE*, 105(10):1865–1883, 2017. (Cited on page 40.)
- [6] M. Cimpoi, S. Maji, I. Kokkinos, S. Mohamed, and A. Vedaldi. Describing textures in the wild. In *Proceedings of the IEEE conference on computer vision and pattern recognition*, pages 3606–3613, 2014. (Cited on page 40.)
- [7] J. Deng, W. Dong, R. Socher, L.-J. Li, K. Li, and L. Fei-Fei. Imagenet: A large-scale hierarchical image database. In *2009 IEEE Conference on Computer Vision and Pattern Recognition*. IEEE, 2009. (Cited on pages 11 and 40.)
- [8] A. Dosovitskiy. An image is worth 16x16 words: Transformers for image recognition at scale. *arXiv preprint arXiv:2010.11929*, 2020. (Cited on pages 1, 3, 11, 39, 40, 41, 42, 43, 44, 45, and 46.)
- [9] N. Du, Y. Huang, A. M. Dai, S. Tong, D. Lepikhin, Y. Xu, M. Krikun, Y. Zhou, A. W. Yu, O. Firat, et al. Glam: Efficient scaling of language models with mixture-of-experts. In *International Conference on Machine Learning*, pages 5547–5569. PMLR, 2022. (Cited on page 39.)
- [10] S. d’Ascoli, H. Touvron, M. L. Leavitt, A. S. Morcos, G. Biroli, and L. Sagun. Convit: Improving vision transformers with soft convolutional inductive biases. In *International conference on machine learning*, pages 2286–2296. PMLR, 2021. (Cited on page 12.)
- [11] D. Eigen, M. Ranzato, and I. Sutskever. Learning factored representations in a deep mixture of experts. In *ICLR Workshops*, 2014. (Cited on page 38.)
- [12] W. Fedus, B. Zoph, and N. Shazeer. Switch transformers: Scaling to trillion parameter models with simple and efficient sparsity. *Journal of Machine Learning Research*, 23(120):1–39, 2022. (Cited on page 39.)
- [13] L. Fei-Fei, R. Fergus, and P. Perona. One-shot learning of object categories. *IEEE transactions on pattern analysis and machine intelligence*, 28(4):594–611, 2006. (Cited on page 40.)

[14] T. Gebru, J. Krause, Y. Wang, D. Chen, J. Deng, and L. Fei-Fei. Fine-grained car detection for visual census estimation. In *Proceedings of the AAAI Conference on Artificial Intelligence*, volume 31, 2017. (Cited on pages 11 and 40.)

[15] A. Geiger, P. Lenz, C. Stiller, and R. Urtasun. Vision meets robotics: The kitti dataset. *The International Journal of Robotics Research*, 32(11), 2013. (Cited on page 40.)

[16] B. Graham. Kaggle diabetic retinopathy detection competition report. *University of Warwick*, 22(9), 2015. (Cited on page 40.)

[17] C. Han, Q. Wang, Y. Cui, Z. Cao, W. Wang, S. Qi, and D. Liu. E[^] 2vpt: An effective and efficient approach for visual prompt tuning. *arXiv preprint arXiv:2307.13770*, 2023. (Cited on pages 11, 39, 41, 42, 43, and 44.)

[18] C. Han, Q. Wang, Y. Cui, W. Wang, L. Huang, S. Qi, and D. Liu. Facing the elephant in the room: Visual prompt tuning or full finetuning? *arXiv preprint arXiv:2401.12902*, 2024. (Cited on page 39.)

[19] J. He, C. Zhou, X. Ma, T. Berg-Kirkpatrick, and G. Neubig. Towards a unified view of parameter-efficient transfer learning. *arXiv preprint arXiv:2110.04366*, 2021. (Cited on page 39.)

[20] K. He, X. Chen, S. Xie, Y. Li, P. Dollár, and R. Girshick. Masked autoencoders are scalable vision learners. In *Proceedings of the IEEE/CVF conference on computer vision and pattern recognition*, pages 16000–16009, 2022. (Cited on pages 2, 11, 12, 39, 40, 41, 44, and 45.)

[21] X. He, C. Li, P. Zhang, J. Yang, and X. E. Wang. Parameter-efficient model adaptation for vision transformers. In *Proceedings of the AAAI Conference on Artificial Intelligence*, volume 37, pages 817–825, 2023. (Cited on page 39.)

[22] P. Helber, B. Bischke, A. Dengel, and D. Borth. Eurosat: A novel dataset and deep learning benchmark for land use and land cover classification. *IEEE Journal of Selected Topics in Applied Earth Observations and Remote Sensing*, 12(7):2217–2226, 2019. (Cited on page 40.)

[23] N. Ho, C.-Y. Yang, and M. I. Jordan. Convergence rates for gaussian mixtures of experts. *Journal of Machine Learning Research*, 23(323):1–81, 2022. (Cited on page 39.)

[24] N. Houlsby, A. Giurgiu, S. Jastrzebski, B. Morrone, Q. De Laroussilhe, A. Gesmundo, M. Attariyan, and S. Gelly. Parameter-efficient transfer learning for nlp. In *International conference on machine learning*, pages 2790–2799. PMLR, 2019. (Cited on page 39.)

[25] E. J. Hu, Y. Shen, P. Wallis, Z. Allen-Zhu, Y. Li, S. Wang, L. Wang, and W. Chen. Lora: Low-rank adaptation of large language models. *arXiv preprint arXiv:2106.09685*, 2021. (Cited on pages 1, 11, and 39.)

[26] E. Iofinova, A. Peste, M. Kurtz, and D. Alistarh. How well do sparse imagenet models transfer? In *Proceedings of the IEEE/CVF Conference on Computer Vision and Pattern Recognition*, pages 12266–12276, 2022. (Cited on pages 1, 11, 12, 41, 42, 43, 44, 45, and 46.)

[27] R. A. Jacobs, M. I. Jordan, S. J. Nowlan, and G. E. Hinton. Adaptive mixtures of local experts. *Neural Computation*, 3, 1991. (Cited on pages 1, 4, and 38.)

[28] M. Jia, L. Tang, B.-C. Chen, C. Cardie, S. Belongie, B. Hariharan, and S.-N. Lim. Visual prompt tuning. In *European Conference on Computer Vision*, pages 709–727. Springer, 2022. (Cited on pages 1, 3, 11, 12, 39, 40, 41, 42, 43, and 44.)

[29] J. Johnson, B. Hariharan, L. Van Der Maaten, L. Fei-Fei, C. Lawrence Zitnick, and R. Girshick. Clevr: A diagnostic dataset for compositional language and elementary visual reasoning. In *Proceedings of the IEEE conference on computer vision and pattern recognition*, pages 2901–2910, 2017. (Cited on page 40.)

[30] M. I. Jordan and R. A. Jacobs. Hierarchical mixtures of experts and the em algorithm. *Neural computation*, 6(2):181–214, 1994. (Cited on pages 4 and 38.)

[31] A. Khosla, N. Jayadevaprakash, B. Yao, and F.-F. Li. Novel dataset for fine-grained image categorization: Stanford dogs. In *Proc. CVPR workshop on fine-grained visual categorization (FGVC)*, volume 2. Citeseer, 2011. (Cited on pages 2, 11, 12, 13, and 40.)

[32] A. Kirillov, E. Mintun, N. Ravi, H. Mao, C. Rolland, L. Gustafson, T. Xiao, S. Whitehead, A. C. Berg, W.-Y. Lo, et al. Segment anything. In *Proceedings of the IEEE/CVF International Conference on Computer Vision*, pages 4015–4026, 2023. (Cited on pages 1 and 39.)

[33] A. Krizhevsky, G. Hinton, et al. Learning multiple layers of features from tiny images. 2009. (Cited on page 40.)

[34] M. Le, T. N. Luu, A. N. The, T.-T. Le, T. Nguyen, T. T. Nguyen, L. N. Van, and T. H. Nguyen. Adaptive prompting for continual relation extraction: A within-task variance perspective. In *Proceedings of the AAAI Conference on Artificial Intelligence*, volume 39, 2025. (Cited on pages 2 and 39.)

[35] M. Le, A. Nguyen, H. Nguyen, T. Nguyen, T. Pham, L. Van Ngo, and N. Ho. Mixture of experts meets prompt-based continual learning. *Advances in Neural Information Processing Systems*, 38, 2024. (Cited on pages 1, 4, 9, and 39.)

[36] M. Le, C. Nguyen, H. Nguyen, Q. Tran, T. Le, and N. Ho. Revisiting prefix-tuning: Statistical benefits of reparameterization among prompts. In *The Thirteenth International Conference on Learning Representations*, 2025. (Cited on pages 2, 4, 9, and 39.)

[37] Y. LeCun, L. Bottou, Y. Bengio, and P. Haffner. Gradient-based learning applied to document recognition. *Proceedings of the IEEE*, 86(11):2278–2324, 1998. (Cited on page 43.)

[38] Y. LeCun, F. J. Huang, and L. Bottou. Learning methods for generic object recognition with invariance to pose and lighting. In *Proceedings of the 2004 IEEE Computer Society Conference on Computer Vision and Pattern Recognition, 2004. CVPR 2004.*, volume 2, pages II–104. IEEE, 2004. (Cited on page 40.)

[39] J. Lei Ba, J. R. Kiros, and G. E. Hinton. Layer normalization. *ArXiv e-prints*, pages arXiv–1607, 2016. (Cited on page 8.)

[40] B. Lester, R. Al-Rfou, and N. Constant. The power of scale for parameter-efficient prompt tuning. *arXiv preprint arXiv:2104.08691*, 2021. (Cited on page 39.)

[41] Z. Liu, Y. Lin, Y. Cao, H. Hu, Y. Wei, Z. Zhang, S. Lin, and B. Guo. Swin transformer: Hierarchical vision transformer using shifted windows. In *Proceedings of the IEEE/CVF international conference on computer vision*, pages 10012–10022, 2021. (Cited on page 39.)

[42] D. Mahajan, R. Girshick, V. Ramanathan, K. He, M. Paluri, Y. Li, A. Bharambe, and L. Van Der Maaten. Exploring the limits of weakly supervised pretraining. In *Proceedings of the European conference on computer vision (ECCV)*, pages 181–196, 2018. (Cited on pages 39 and 40.)

[43] T. Manole and N. Ho. Refined convergence rates for maximum likelihood estimation under finite mixture models. In *Proceedings of the 39th International Conference on Machine Learning*, volume 162 of *Proceedings of Machine Learning Research*, pages 14979–15006. PMLR, 17–23 Jul 2022. (Cited on page 9.)

[44] L. Matthey, I. Higgins, D. Hassabis, and A. Lerchner. dsprites: Disentanglement testing sprites dataset, 2017. (Cited on page 40.)

[45] Y. Netzer, T. Wang, A. Coates, A. Bissacco, B. Wu, A. Y. Ng, et al. Reading digits in natural images with unsupervised feature learning. In *NIPS workshop on deep learning and unsupervised feature learning*, volume 2011, page 4. Granada, 2011. (Cited on page 40.)

[46] H. Nguyen, P. Akbarian, and N. Ho. Is temperature sample efficient for softmax Gaussian mixture of experts? In *Proceedings of the ICML*, 2024. (Cited on page 39.)

[47] H. Nguyen, N. Ho, and A. Rinaldo. On least square estimation in softmax gating mixture of experts. In *Proceedings of the ICML*, 2024. (Cited on page 39.)

[48] H. Nguyen, N. Ho, and A. Rinaldo. Sigmoid gating is more sample efficient than softmax gating in mixture of experts. In *Advances in Neural Information Processing Systems*, 2024. (Cited on page 39.)

[49] H. Nguyen, T. Nguyen, and N. Ho. Demystifying softmax gating function in gaussian mixture of experts. *Advances in Neural Information Processing Systems*, 36:4624–4652, 2023. (Cited on page 39.)

[50] M.-E. Nilsback and A. Zisserman. Automated flower classification over a large number of classes. In *2008 Sixth Indian Conference on Computer Vision, Graphics & Image Processing*. IEEE, 2008. (Cited on pages 11 and 40.)

[51] S. Oymak, A. S. Rawat, M. Soltanolkotabi, and C. Thrampoulidis. On the role of attention in prompt-tuning. In *International Conference on Machine Learning*, pages 26724–26768. PMLR, 2023. (Cited on page 1.)

[52] O. M. Parkhi, A. Vedaldi, A. Zisserman, and C. Jawahar. Cats and dogs. In *2012 IEEE conference on computer vision and pattern recognition*, pages 3498–3505. IEEE, 2012. (Cited on page 40.)

[53] A. Paszke, S. Gross, F. Massa, A. Lerer, J. Bradbury, G. Chanan, T. Killeen, Z. Lin, N. Gimelshein, L. Antiga, et al. Pytorch: An imperative style, high-performance deep learning library. *Advances in neural information processing systems*, 32, 2019. (Cited on page 41.)

[54] A. Petrov, P. H. Torr, and A. Bibi. When do prompting and prefix-tuning work? a theory of capabilities and limitations. *arXiv preprint arXiv:2310.19698*, 2023. (Cited on pages 1, 5, and 39.)

[55] A. Radford, J. W. Kim, C. Hallacy, A. Ramesh, G. Goh, S. Agarwal, G. Sastry, A. Askell, P. Mishkin, J. Clark, et al. Learning transferable visual models from natural language supervision. In *International conference on machine learning*, pages 8748–8763. PMLR, 2021. (Cited on page 1.)

[56] S.-A. Rebuffi, H. Bilen, and A. Vedaldi. Learning multiple visual domains with residual adapters. *Advances in neural information processing systems*, 30, 2017. (Cited on pages 11, 12, 39, 41, 42, 43, and 44.)

[57] C. Riquelme, J. Puigcerver, B. Mustafa, M. Neumann, R. Jenatton, A. Susano Pinto, D. Keysers, and N. Houlsby. Scaling vision with sparse mixture of experts. *Advances in Neural Information Processing Systems*, 34:8583–8595, 2021. (Cited on page 39.)

[58] R. R. Selvaraju, M. Cogswell, A. Das, R. Vedantam, D. Parikh, and D. Batra. Grad-cam: Visual explanations from deep networks via gradient-based localization. In *Proceedings of the IEEE international conference on computer vision*, pages 618–626, 2017. (Cited on page 47.)

[59] N. Shazeer, A. Mirhoseini, K. Maziarz, A. Davis, Q. Le, G. Hinton, and J. Dean. Outrageously large neural networks: The sparsely-gated mixture-of-experts layer. In *International Conference on Learning Representations (ICLR)*, 2017. (Cited on pages 1, 5, and 38.)

[60] S. Shen, Z. Yao, C. Li, T. Darrell, K. Keutzer, and Y. He. Scaling vision-language models with sparse mixture of experts. *arXiv preprint arXiv:2303.07226*, 2023. (Cited on page 39.)

[61] K. Sohn, H. Chang, J. Lezama, L. Polania, H. Zhang, Y. Hao, I. Essa, and L. Jiang. Visual prompt tuning for generative transfer learning. In *Proceedings of the IEEE/CVF Conference on Computer Vision and Pattern Recognition*, pages 19840–19851, 2023. (Cited on page 39.)

[62] S. van de Geer. *Empirical processes in M-estimation*. Cambridge University Press, 2000. (Cited on pages 9 and 27.)

[63] G. Van Horn, S. Branson, R. Farrell, S. Haber, J. Barry, P. Ipeirotis, P. Perona, and S. Belongie. Building a bird recognition app and large scale dataset with citizen scientists: The fine print in fine-grained dataset collection. In *Proceedings of the IEEE Conference on Computer Vision and Pattern Recognition*, 2015. (Cited on pages 11 and 40.)

[64] A. Vaswani. Attention is all you need. *Advances in Neural Information Processing Systems*, 2017. (Cited on page 1.)

[65] B. S. Veeling, J. Linmans, J. Winkens, T. Cohen, and M. Welling. Rotation equivariant cnns for digital pathology. In *Medical Image Computing and Computer Assisted Intervention–MICCAI 2018: 21st International Conference, Granada, Spain, September 16–20, 2018, Proceedings, Part II* 11, pages 210–218. Springer, 2018. (Cited on page 40.)

[66] C. Wah, S. Branson, P. Welinder, P. Perona, and S. Belongie. The caltech-ucsd birds-200-2011 dataset. 2011. (Cited on pages 11, 40, and 42.)

[67] Y. Wang, J. Chauhan, W. Wang, and C.-J. Hsieh. Universality and limitations of prompt tuning. *Advances in Neural Information Processing Systems*, 36, 2024. (Cited on page 1.)

[68] J. Xiao, J. Hays, K. A. Ehinger, A. Oliva, and A. Torralba. Sun database: Large-scale scene recognition from abbey to zoo. In *2010 IEEE computer society conference on computer vision and pattern recognition*, pages 3485–3492. IEEE, 2010. (Cited on page 40.)

[69] Y. Xin, S. Luo, H. Zhou, J. Du, X. Liu, Y. Fan, Q. Li, and Y. Du. Parameter-efficient fine-tuning for pre-trained vision models: A survey. *arXiv preprint arXiv:2402.02242*, 2024. (Cited on page 39.)

[70] L. Xu, M. Jordan, and G. E. Hinton. An alternative model for mixtures of experts. *Advances in neural information processing systems*, 7, 1994. (Cited on page 38.)

[71] H. Yao, R. Zhang, and C. Xu. Visual-language prompt tuning with knowledge-guided context optimization. In *Proceedings of the IEEE/CVF conference on computer vision and pattern recognition*, pages 6757–6767, 2023. (Cited on page 39.)

[72] Y. Yao, A. Zhang, Z. Zhang, Z. Liu, T.-S. Chua, and M. Sun. Cpt: Colorful prompt tuning for pre-trained vision-language models. *AI Open*, 5:30–38, 2024. (Cited on page 39.)

[73] S. Yoo, E. Kim, D. Jung, J. Lee, and S. Yoon. Improving visual prompt tuning for self-supervised vision transformers. In *International Conference on Machine Learning*, pages 40075–40092. PMLR, 2023. (Cited on page 12.)

[74] J. Yosinski, J. Clune, Y. Bengio, and H. Lipson. How transferable are features in deep neural networks? *Advances in neural information processing systems*, 27, 2014. (Cited on pages 11, 12, 41, 42, 43, and 44.)

[75] X. Zhai, J. Puigcerver, A. Kolesnikov, P. Ruyssen, C. Riquelme, M. Lucic, J. Djolonga, A. S. Pinto, M. Neumann, A. Dosovitskiy, et al. A large-scale study of representation learning with the visual task adaptation benchmark. *arXiv preprint arXiv:1910.04867*, 2019. (Cited on pages 11, 12, 40, 41, 42, 43, 44, 45, 46, and 47.)

[76] J. O. Zhang, A. Sax, A. Zamir, L. Guibas, and J. Malik. Side-tuning: a baseline for network adaptation via additive side networks. In *Computer Vision–ECCV 2020: 16th European Conference, Glasgow, UK, August 23–28, 2020, Proceedings, Part III 16*, pages 698–714. Springer, 2020. (Cited on pages 1, 11, 39, 41, 42, 43, and 44.)

[77] Y. Zhou, N. Du, Y. Huang, D. Peng, C. Lan, D. Huang, S. Shakeri, D. So, A. M. Dai, Y. Lu, et al. Brainformers: Trading simplicity for efficiency. In *International Conference on Machine Learning*, pages 42531–42542. PMLR, 2023. (Cited on page 39.)